JOHANNES GUTENBERG UNIVERSITÄT MAINZ

Radiolabelling, *in vitro* and *in vivo* evaluation of metal-labelled biomolecules for PET imaging

Dissertation

zur Erlangung des Grades

"Doktor der Naturwissenschaften"

im Promotionsfach Chemie

am Fachbereich Chemie, Pharmazie und Geowissenschaften
der Johannes Gutenberg-Universität
in Mainz

Ana de la Fuente Joaniquet

Geboren in Barcelona

Mainz, 2016

Dekan: Prof. Dr. Schneider

Tag der mündlichen Prüfung: 24.06.2016

“I hereby declare, that I wrote the dissertation submitted without any unauthorized external assistance and used only sources acknowledged in the work. All textual passages, which are appropriated verbatim or paraphrased from published and unpublished texts as well as all information obtained from oral sources are duly indicated and listed in accordance with bibliographical rules. In carrying out this research, I complied with the rules of standard scientific practice as formulated in the statutes of Johannes Gutenberg-University Mainz to insure standard scientific practice.”

Ana de la Fuente Joaniquet

A mi padre,

José

"Caminante, no hay camino,
se hace camino al andar"

"Wayfarer, there is no way,
way is made by going farther"

Antonio Machado (1875-1939)

Abstract

Radiopharmaceuticals are a convenient tool in nuclear medicine for diagnosis and treatment of different pathologies. Their application is of great interest in oncology and infectious diseases therefore investigations on the development of nanoparticles for such purposes are under focus. Their characteristics need to be studied before application as many therapeutic drugs suffer from a poor balance between efficacy and toxicity. Nuclear medicine imaging techniques such as PET are being valuable (pre)clinical tools to non-invasively assess drug performance in pharmaceutical research providing understanding into structure-property relationships *in vivo* towards optimization to more effective drug delivery.

In this study, different metal radioisotopes have been conjugated to diverse biomolecules such as antibodies, small based peptides molecules or polymer based micelles in order investigate their efficiency as disease imaging targets. Hence, versatile radiolabelling strategies were developed according to the requirements of each biomolecule and subsequent evaluations *in vitro* and *in vivo* were performed.

Zusammenfassung

In der Nuklearmedizin werden Radiopharmaka für die Diagnose und Therapie verschiedener Erkrankungen verwendet. Von besonderem Interesse ist ihre Anwendung in der Onkologie, infolgedessen steht die Entwicklung von Nanopartikeln für diese Verwendungen im Forschungsfokus.

Um das meist schlechte Verhältnis von Wirksamkeit zu Toxizität, welches bei vielen Therapeutika vorliegt, zu verbessern, müssen die entwickelten Nanopartikel intensiv hinsichtlich dieser Eigenschaft getestet werden. Nuklearmedizinische Techniken wie die Positronen-Emissions-Tomographie (PET) sind geeignete (prä)klinische Werkzeuge, um die Wirksamkeit von neuen Medikamenten nicht-invasiv zu ermitteln. Die hierdurch gewonnen Erkenntnisse zu den Struktur-Eigenschaft-Beziehungen *in vivo* können direkt in der Medikamentenentwicklung eingesetzt werden um den Wirkstofftransport zu optimieren.

In dieser Arbeit wurden verschiedene medizinisch relevante Strukturen, wie Antikörper, Peptide und Polymermizellen, mit verschiedenen Radiometallisotopen markiert und hinsichtlich ihrer Wirksamkeit als molekulare Marker von Erkrankungen untersucht. Es wurden, basierend auf den chemischen Eigenschaften der zu markierenden Strukturen, verschiedene Radiomarkierungsstrategien entwickelt und die markierten Verbindungen *in vitro* und *in vivo* evaluiert.

Table of contents

1 Introduction

Current (chemo)therapeutic drugs often suffer from a narrow therapeutic index, which is the range of dose at which a medication is effective with minimized side effects [1]. To achieve a therapeutic concentration, in many cases large quantities of the drug have to be administered leading to adverse effects accompanying therapy. Consequently, efforts towards improved drug delivery have been carried out over the past decades leading to a new field of medical and scientific research termed “nanomedicine” using nanoscale carriers selectively delivering bioactive substances to diseased sites [2].

In terms of improvement of the poor balance between efficacy and toxicity, the combination of biomolecules with radioisotopes gave rise to nuclear medicine, which allows for treatment and/or diagnosis of a variety of diseases in a non-invasive way. In addition, it is a valuable tool in pharmaceutical research as nuclear imaging techniques like positron emission tomography (PET) can assess, *in vivo*, the performance of the drug identifying how properties such as binding affinity, size, charge or hydrophilicity affect to in the *in vivo* distribution of the nanoparticle.

1.1 NANOMEDICINE

Nanomedicine formulations aim to improve the biodistribution and the target site accumulation of (chemo)therapeutic agents with the ultimate goal of improving quality of life. They can be made of materials of diverse chemical nature, including for example: liposomes, polymers, micelles and antibodies [3,4]. One of the greatest advantages of nanoparticles is the ability to generate particles functionalized with a wide variety of targeting ligands and physicochemical properties, which permit the creation of agents that are specifically tailored for a desired application [5].

1.1.1 Biological rationale using nanomedicines

Biological barriers as well as obstacles such as sequestration by the mononuclear phagocyte system may end to nonspecific distribution of nanotherapeutics [6]. Advances in pharmacy, medicine, chemistry, biology and material sciences have led to an improvement in overcoming such limitations by adjusting the particle size, the hydrophilicity or the charge and the possibility to be multifunctionalised. To minimize clearance by the immune systems, to be visualized or to reach specific cells are some of the features achievable by functionalization. The inclusion of a targeting vector leads to two general concepts - “active” and/or “passive” targeting - when guiding drugs to pathological sites.

“Passive targeting”, which is utilized by most of the systems (particularly liposomes, polymers and micelles), is based on the inherent tendency of macromolecules to accumulate in tumor tissue. Maeda and co-workers demonstrated the potential for accumulation of long circulating nanoparticles in tumor sites through extravasation of blood vessels [7]. Compared to healthy tissue, tumors are characterized by abnormalities like a damaged lymphatic drainage and a fast and defective formation of new blood vessels (angiogenesis) creating, consequently, large gaps between endothelial cells and tumor blood vessels. This fact is exploited to target solid tumors with macromolecules, as they are able to extravasate tumor tissues and be retained. This passive accumulation in pathological tumor tissue has been termed “enhanced permeability and retention (EPR) effect” [8,9] (Fig. 1).

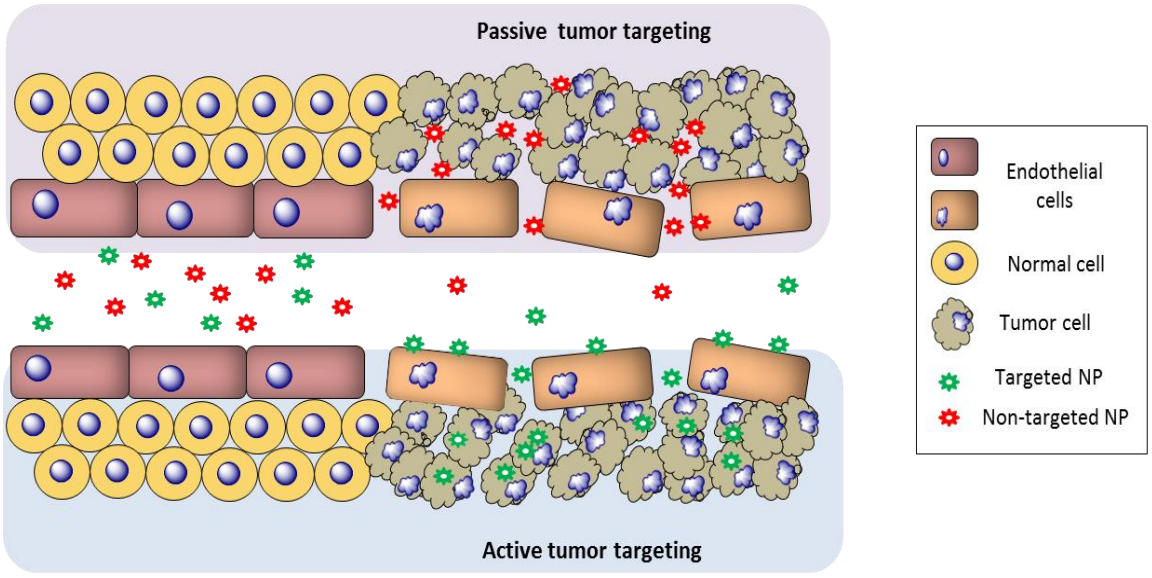

Figure 1: Active and passive targeting of nanoparticles

On the other hand, the concept of the "magic bullet" introduced by Paul Ehrich in 1903, has influenced research efforts to develop site-directed delivery strategies for drugs. This strategy is referred to as "active targeting" [10,11]. Active drug targeting relies on the use of antibodies, peptides, sugar moieties or blood cells to improve drug concentration at the diseased site thus maximizing therapeutic response [12]. In oncology, targeting not only tumor tissue but the receptors overexpressed by specific tumor cells or angiogenic endothelial cells can eradicate tumor vessels and deprive tumor cells from oxygen and nutrients hence reduce tumor grow [13]. In addition, some targeted nanoparticles can also be internalized by tumor cells *via* receptor-mediated endocytosis/phagocytosis, resulting in elevated concentration in tumor tissue.

1.1.1.1 Polymer based therapeutics

The use of polymers in the design for therapeutic agents has been widely investigated for several years [14]. It was in 1975 when Helmut Ringsdorf first proposed the concept of polymer–drug conjugation, a rational for pharmacologically active polymers [15]. The model compound consists of a biocompatible backbone where three main components are bound: (1) a solubilizer that ensures water solubility, (2) a drug, normally attached *via* a linker and (3) a targeting moiety that guides to a desired physiological destination (Fig. 2). This structure enables a better control of the drug delivery and improved drug availability to the targeted tissue. The possibility to tailor synthetic polymers in terms of molecular weight, architecture and size and the extensive array of functionalization options, that can be used to create versatile multifunctional systems for medical purposes, has resulted in a huge class of polymer based drug delivery systems [16, 17].

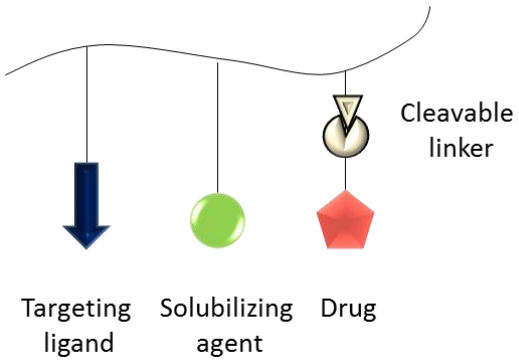

Figure 2: Model of a pharmacologically active polymer as envisioned by H. Ringsdorf.

Interdisciplinary research including polymer chemistry, medicine, cell biology and pharmaceutical sciences began to design biologically active polymeric drugs. Since then, drug delivery systems such as polymeric micelles, polymer–drug conjugates and polymer–peptide/protein conjugates have been elaborated. Such multicomponent polymer-based drugs and delivery systems have been termed as "polymer-therapeutics" [18].

To be efficient as transport vehicle, the polymer system requires being water soluble, non-immunogenic, non-toxic and should provide the possibility to achieve high drug payloads. Poly-*N*-(2-hydroxypropyl)methacrylamide (pHPMA), polyethylene glycol (PEG) and polyglutamic acid (PGA) fulfil these requirements and have the most widely investigated chemistries and the clinically most relevant polymeric backbones [14,17,19,20].

HPMA based polymeric therapeutics

It was in the late 1970s when Kopecek and colleagues first synthetized polymer-drug conjugates based on N-(2-hydroxypropyl)methacrylamide (HPMA), which was already known to be non-immunogenic, non-toxic and to reside in the circulation well [21]. Other appealing properties of HPMA are the possibility of controlled synthesis and the multiple pendant side chains to carry drug residue payload. The success of HPMA polymers as drug carriers was achieved during the early 1990s when it was evaluated in clinical trials for therapeutic validation [22]. Up to now six HPMA anticancer conjugates have progressed into clinic using doxorubicin, paclitaxel, camptothecin and platinates as therapeutic agents being able to improve the balance between the efficacy and the toxicity of chemotherapy [23,24]. Careful control of the reaction conditions to regulate polymerization kinetics allows to synthetize HPMA precursors of relatively narrow molecular weight distribution.

The first HPMA conjugates in clinical trials were synthesized mostly *via* free radical polymerization (PM) technique, but the fast chain growth and the presence of the rapid irreversible termination limits the degree of control over polymer molecular weight distribution and polymer structure [2,21,25]. This route appeared to be rather difficult concerning clinical requirements such as careful characterization, reproducibility, purification and precision. To overcome these drawbacks, new methods were developed based on either reversible deactivation of polymer radicals or a degenerative transfer process. Controlled radical polymerizations such as nitroxide-mediated polymerization (NMP), atom transfer radical polymerization (ATRP) or reversible addition-fragmentation chain transfer polymerization (RAFT) represent key strategies for the preparation of polymers with narrow molecular weight

distributions. Among them, RAFT is one of the most utilized methods as it can be used with a large variety of monomers, it is tolerant to a wide range of functional groups and reaction conditions and does not require any heavy metal catalyst as in ATRP [2,26].

Thus, RAFT polymerization offers the possibility to synthesize reactive block copolymers, which can be first precisely characterized and afterwards functionalized by polymer analogous reactions [27]. In addition, by combining RAFT with copolymers and especially block copolymers with activated ester units attached to the polymer backbone, a high variability can be achieved in terms of introducing functionality. This approach has been successfully applied for the synthesis of multifunctional HPMA-based polymers [2,21,28,29]. Figure 3 shows the schematic synthetic route underlying this concept. Starting from a reactive ester monomer PFPMA (pentafluorophenyl methacrylate), a PFPMA-homopolymer is synthesized which later can be derivatized using primary amines by polymer analogous reaction. This synthetic route enables the introduction of various functionalities that in a further step will allow facile attachment of imaging or therapeutic probes for example *via* amide bonds [2].

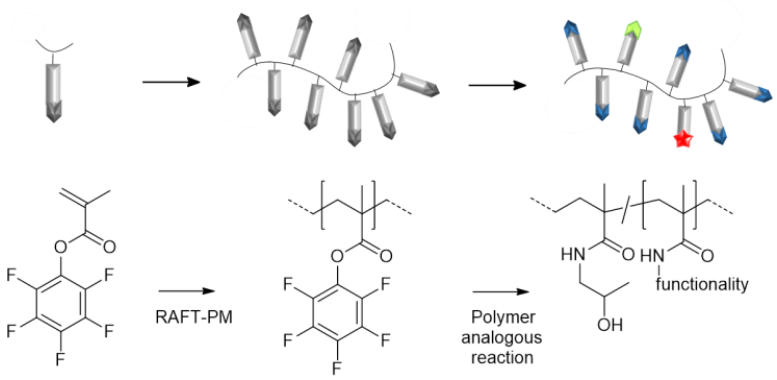

Figure 3: Schematic synthesis of functional HPMA polymers using RAFT polymerization technique and reactive ester approach [2].

HPMA can be modified with hydrophobic moieties that will serve as a micellar core in which hydrophobic drugs can be solubilized and retained while hydrophilic HPMA constitutes the micellar stealth corona. Lauryl methacrylate (LMA) hydrophobic moieties have been conjugated to HPMA thus forming amphiphilic HPMA-LMA copolymers that self-assemble forming aggregates and/or micellar structures. Such structures have been widely investigated and have shown promising results as a drug delivery system due to its capacity of loading drugs into their core and its longer circulation times when compared to homopolymers, which is translated in higher tumor accumulation [30-33]. Additional incorporation of PEG moieties (Fig. 4) reduces the

uptake of the NP by the reticuloendothelial system (RES) and increases circulation time on top of diminishing aggregation between the particles and association with serum and tissue proteins [34].

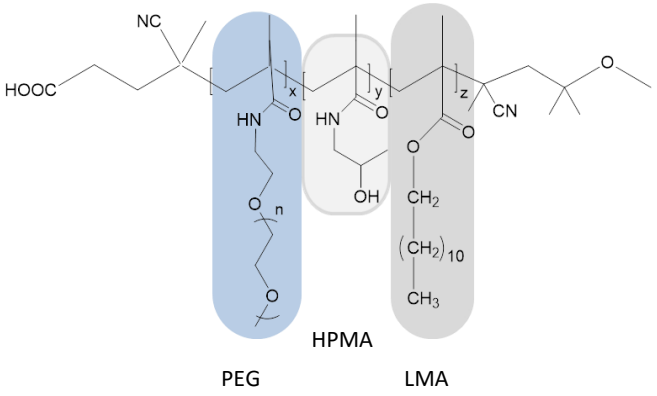

Figure 4: HPMA polymer backbone with PEG and LMA moieties

1.1.1.2 Active targeting agents

Key molecules involved in proliferation, cell death, angiogenesis, invasion or metastasis have been discovered thanks to recent advances in molecular and cellular biology [34]. The identification of such biomarkers helps to understand their mechanism of action and therefore to design molecules that specifically target a certain antigen or receptor aiming to improve target site accumulation and/or target cell uptake. Antibodies and small molecules are examples of structures that have demonstrated such abilities [35].

Antibodies are large Y-shaped proteins produced by the immune system that identify and neutralize foreign objects like bacteria and viruses. A variety of antibodies (Mw 150 kDa) as well as antibody fragments and engineered variants, like minibodies, affibodies or nanobodies with Mw ranging from 25 to 100 kDa, have been engineered. Up to date more than 30 different antibodies are approved by the US Food and Drug Administration and much others are currently under preclinical investigation [34, 36].

Typically, the advantage of monoclonal antibodies (mAbs) in cancer treatment is based on their capability to bind antigens expressed on the tumour-cell surface with highly selectivity [37].
Of special interest are mAb approved for clinical use for targeting solid tumors such as: trastuzumab, cetuximab, panitumumab and bevacizumab. They interfere with signal

transduction pathways by targeting growth factors or their receptors, the key drivers of tumor growth and survival, thus avoiding neovascularization and therefore reducing the tumor's accessibility to oxygen and nutrients. These "solid tumor mAbs" are, in general, most effective when combined with chemo- or radiotherapy [34].

In contrast, small molecular weight compounds differ from the antibodies by having small sizes, low production costs and improved stability. These advantages translate into simple pre-formulation conjugation strategies and simple synthesis. In fact, the main challenge with small molecules is the identification of new ligands with high affinity for the substrates of interest [38]. Moreover, the difference in molecular size of small-molecules might be translated into more efficient tissue penetration, tumor internalization and retention and blood clearance when compared to antibodies [37].

Early examples of small molecules utilized as a targeting tumour ligands are carbohydrate moieties (mannose, glucose, galactose and their derivatives) or folic acid with high affinity and specificity for folate receptors frequently over-expressed on the surface of a variety of human tumors [38-40]. The gain of knowledge in cell biology, chemistry and pharmacy has led to the development of a wide array of small molecules with high specificity for a certain receptor. A result of such advances, for example, is the discovery of an integral transmembrane protein as an efficient prostate cancer biomarker. This protein, named Prostate Specific Membrane Antigen (PSMA), has demonstrated to be more effective than the initial target used for prostate cancer biomarkers, the secretory protein Prostate Specific Antigen (PSA) which high levels do not always correlate with disease [41, 42]. The discovery of the highly over-expressed PSMA in the tumor cells of nearly all kinds of prostate cancer as suitable target site lead, in parallel to the development and clinical utilization of PSMA-specific mAbs, to the development of an array of small molecules with high affinity to PSMA (Fig. 5). Small molecules such as ^{68}Ga-PSMA-11, ^{68}Ga-,^{177}Lu-PSMA-617, ^{18}F-DCFBC or ^{131}I-MIP-1095 have shown high potential for detection and treatment of prostate tumor lesions [43].

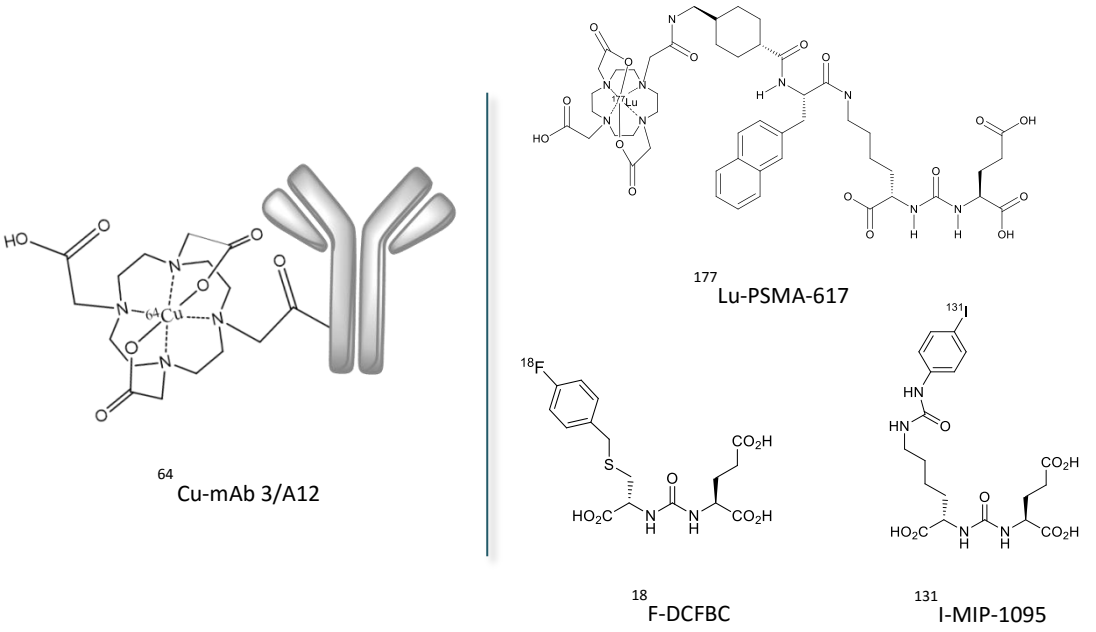

Figure 5: Comparison of antibody (> 1 x 10^5 g/mol) and small compounds (< 2 x 10^3 g/mol) exemplified for prostate cancer-based molecules.

1.2 NUCLEAR MEDICINE

The discovery of X-rays in 1895 by Wilhelm Conrad Roentgen and of radioactivity by Henri Becquerel (Nobel Prize in physics 1903, proportionately M. Curie) together with the work of George de Hevesy on the use of isotopes as tracers in the study of chemical processes (Nobel Prize in chemistry; 1943) paved the way of nuclear medicine [44-46]. Nuclear medicine takes advantage of the decay properties of radioisotopes and uses small amounts (nano- to picomols) of radioactive material to diagnose (e.g. brain, kidneys) and treat a variety of pathologies.

In contrast to other imaging techniques such as computed tomography (CT), ultrasound (US) or magnetic resonance imaging (MRI), the nuclear imaging techniques “single-photon emission computed tomography” (SPECT) and “positron-emission tomography” (PET) present (1) higher sensitivity and specificity, (2) are able to detect changes at cellular and subcellular levels in living subjects, (3) present no limit to tissue penetration in any organ allow for (4) dynamic images and (5) quantification of compound distribution [5,47]. These advantages make SPECT and PET important tools in accurate and early diagnosis. The basis of PET and SPECT techniques relies on the use of radionuclides emitting photons (directly or indirectly), with enough energy to penetrate the body and to be detected externally [48]. PET presents higher spatial and temporal

resolution in comparison to SPECT, thus allowing for more precise localization with a lower dose of injected compound [49,50].

To improve the diagnostic potential and spatial resolution, synergistic combinations such as PET/MRI or PET/CT and SPECT/CT are available. Those multimodality imaging devices combine the potentials of both morphological and molecular imaging, providing detection of pathophysiological changes in early disease phases at high structural resolution.

1.2.1 PET

Positron emission tomography is a nuclear imaging technique that can dynamically image to trace amounts of positron-emitting radionuclide-labelled radiopharmaceuticals *in vivo* [51].

Fundamentals

All positron emitters are proton-rich nuclides that in order to stabilize transform a proton into a neutron by the conversion of an up-quark into a down-quark. This process is accompanied by the emission of a positron (β^+), which is the antimatter of an electron, and a neutrino (ν) (eq. 1). In such transformation the daughter nucleus (Y) has the same mass number than the parent nuclide (X), but the atomic number is reduced by one (eq. 2).

$$ {}^{1}_{1}\mathrm{p} \rightarrow {}^{1}_{0}\mathrm{n} + {}^{1}_{0}\beta^{+} + {}^{0}_{0}\nu_{\mathrm{e}} \qquad \text{(eq. 1)} $$

$$ {}^{\mathrm{A}}_{\mathrm{Z}}X_{N} \rightarrow {}_{Z-1}{}^{\mathrm{A}}Y_{N+1} + {}^{1}_{0}\beta^{+} + {}^{0}_{0}\nu_{\mathrm{e}} \qquad \text{(eq. 2)} $$

After emission from the nucleus, the positron travels a short distance while losing kinetic energy due to interactions with the surrounding matter (i.e., tissue) until it annihilates with an electron, producing a metastable intermediate species, the positronium (Ps) and emitting gamma rays [52]. The positronium can exist in two states: para-positronium, which occurs when positron and electron have antiparallel spins (singlet) or ortho-positronium, when both particles have parallel spin (triplet) [53].

When the positron and electron collide at absolute rest energy (E_{kin}= 0), the para-Ps is formed and transforms with a lifetime of 1.25 x 10^{-10} s into the diagnostically useful two gamma rays emitted in opposite directions (180°) with equal kinetic energy of 511 keV each. The ortho-Ps

decays after a lifetime of 1.4 x 10^{-7} s into three gamma rays. The sum of E_{kin} always equals to 1.022 MeV [54].

Table 1: Comparison between ortho- and para-Ps

	ortho-Ps	para-Ps
Status	triplet	singlet
Impulse (J)	1	0
Life-time (free Ps)	1.4 x 10^{-7} s	1.25 x 10^{-10} s
Annihilation	$E_{\gamma1} + E_{\gamma2} + E_{\gamma3}$ = 1.02 MeV	2 x 0,511 keV = 1.02 MeV
Angle	static	180°

PET-technique

PET scanners typically consist of rings of 511 keV-sensitive scintillation detectors, with up to 25.000 individual scintillation elements made of NaI, bismuth germinate (BGO) or lutetium orthosilicate (LSO). The opposing PET detectors register the arrival of the annihilation photons as an event if they are detected within a narrow time frame (3-15 ns). This requirement of detecting both the photons within a time window is the fundamental basis of coincidence detection called electronic collimation [53]. PET scans thus consist of the collection of large numbers of coincidence events that later on, by using mathematical reconstruction methods and appropriate correction factors for phenomena such as gamma ray attenuation and scatter, provide information about the quantity and location of the positrons in the body (Fig. 6). Detection resolution is significantly dependent on the width of the crystal elements, but also on the range of the positron and the noncollinearity of the two gamma rays [51].

One of the main drawbacks of PET is the lack of a clear anatomical reference frame that may hamper to accurately localize anatomic structures or lesions that exhibit abnormal radiotracer accumulation. This can be solved by combining PET with anatomical imaging techniques such as CT or MRT.

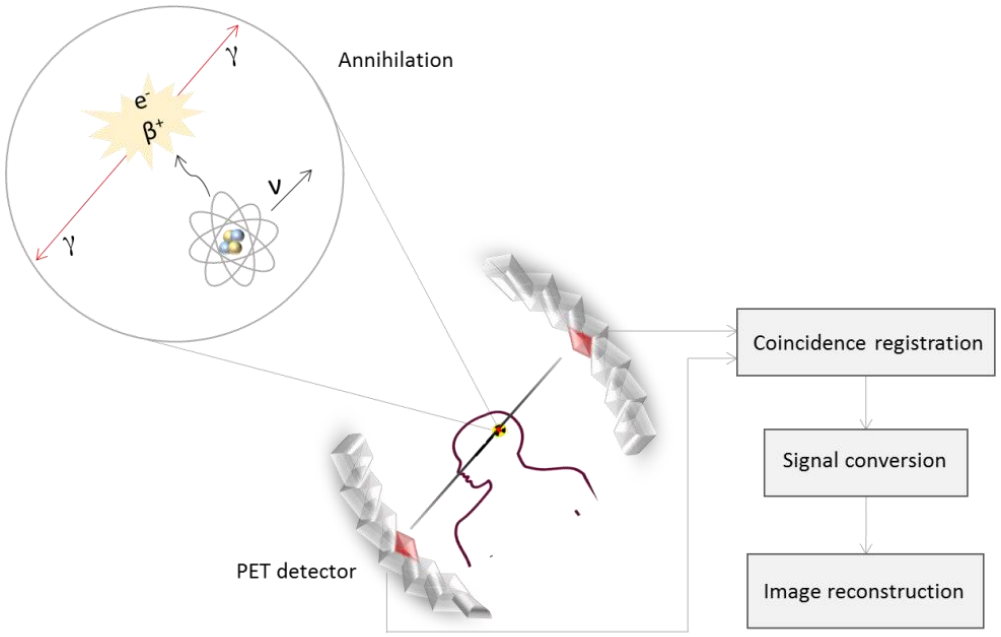

Figure 6: Schematic illustration of the principle behind PET technique.

1.2.2 Radiometals for diagnosis

The choice of radionuclides for medical purposes depends largely in its nuclear properties (t ½, type of radiation, energy, presence or lack of other particular emissions) as well as cost and availability.

Radiometals have become a fundamental component of many pharmaceuticals for diagnostic nuclear medicine applications because they offer many advantages over organic radioisotopes (^{18}F, ^{11}C, ^{15}O, ^{17}N) [55]. Metal radionuclides present: (1) fast radiolabelling reactions with simple purification procedures, (2) lower cost and easier access of certain radiometals *via* radionuclide generators, (3) broad opportunities for design and development of new target-specific radiotracers able to change the biodistribution of the radiopharmaceutical by modifying the coordination environment of the radiometal with a variety of chelators, (4) the possibility to better match the biological half-life of the targeting vector thanks to the wider variety of metallic radionuclides and (5) the availability for some radionuclides of automatized synthesis "kits" allowing rapid labelling and to finally (6) switch between diagnostic and therapeutic options [57]. Table 2 summarizes the nuclear characteristics of selected PET nuclides appropriated for molecular imaging by means of positron emission tomography.

Table 2: Nuclear characteristics of selected PET nuclides appropriated for molecular imaging

Nuclide	$t_{1/2}$	Decay [%]	$E_{\beta+}$ max [MeV]	Production
^{18}F	109.7 min	β^+ (97)	0.635	$^{18}O(p,n)^{18}F$
^{44}Sc	3.97 h	β^+ (94)	1.474	$^{44}Ti/^{44}Sc$ generator
^{68}Ga	67.7 min	β^+ (89) EC(11)	1.899	$^{68}Ge/^{68}Ga$ generator
^{124}I	4.2 h	β^+ (23) EC (77)	2.138	$^{124}Te(p,n)^{124}I$ $^{124}Te(d,2n)^{124}I$
^{64}Cu	12.7 h	β^+ (17) EC (44)	0.653	$^{64}Ni(p,n)^{64}Cu$
^{90}Nb	14.6 h	β^+ (53) EC (77)	1.500	$^{90}Zr(p,n)^{90}Nb$
^{86}Y	14.7 h	β^+ (33) EC (66)	3.141	$^{86}Sr(p,n)^{86}Y$
^{74}Br	16.2 h	β^+ (55) EC (45)	3.941	$^{76}Se(p,n)^{76}Br$
^{89}Zr	3.3 d	β^+ (23) EC (77)	0.901	$^{89}Y(p,n)^{89}Zr$

For SPECT imaging, ^{99m}Tc remains the most widely used radiometal due to its optimal nuclear properties and easy availability at low cost. The cyclotron-produced ^{111}In is also important for SPECT imaging and it is often used as imaging surrogate for the therapeutic radionuclide ^{90}Y [58].

1.2.2.1 Generator-produced PET radioisotopes

The use of short-living radionuclides has grown considerably as large doses can be administrated to the patient with minimal radiation dosage and at the same time to generate images with high quality [59]. This fact has led to the development of radionuclide generators, which provide high specific activity, no-carrier added (n.c.a) identity and a convenient alternative to accelerators or reactors and eventually on-line medical application [60]. In a generator, the long-living parent nuclide is allowed to decay to its short-living daughter that can be chemically separated with low effort. The chemical properties of both radionuclides must be different thus affording a good separation in which the daughter nuclide is obtained in a pure radionuclidic and radiochemical

form [61]. Radionuclide generator systems provide both diagnostic and therapeutic radionuclides for application in nuclear medicine. In spite of many parent/daughters pairs, only a small number are currently in routine clinical and research use as generator systems [62].

^{68}Ge/^{68}Ga generator

^{68}Ga decays with a half-life of 67.71 min to stable ^{68}Zn by positron emission (89%) and with a maximum positron energy of 1.89 MeV (Fig. 7). Such decay characteristics in addition to its cyclotron-independent availability *via* the ^{68}Ge/^{68}Ga generator and its well-known coordination chemistry, make ^{68}Ga a radionuclide of great interest for nuclear medicine [63].

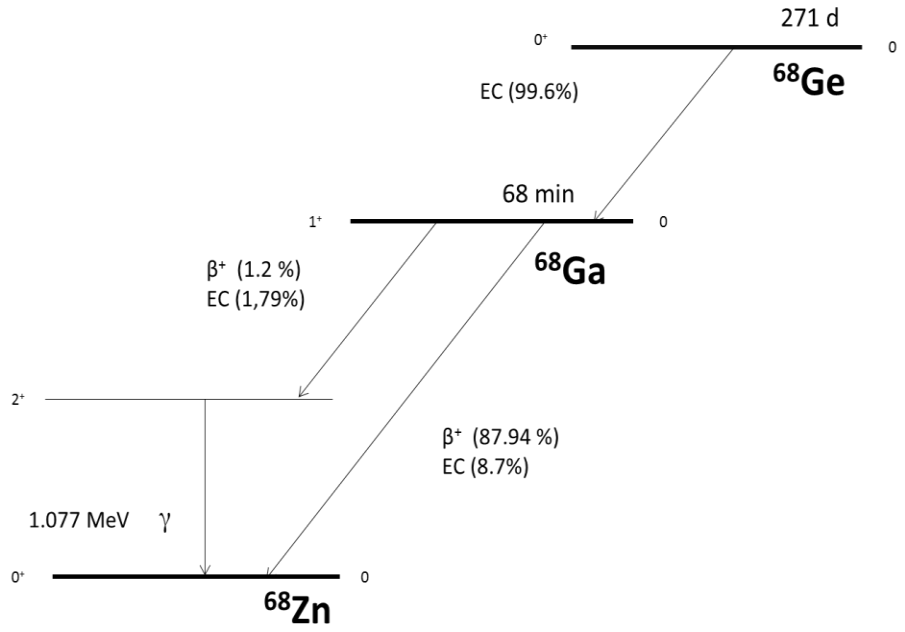

Figure 7: Decay scheme of ^{68}Ge and ^{68}Ga

The production of the parent radionuclide ^{68}Ge (t ½ = 271 d), can be achieved *via* different nuclear reaction pathways, being the (p,2n) reaction to Ga_2O_3 targets the most relevant [64]. After separation from the irradiated target, ^{68}Ge is strongly absorbed to a solid support, such as metal oxides or organic resins, from which the short-living daughter nuclide ^{68}Ga can be selectively eluted.

Nowadays commercially available generators use TiO_2, SnO_2 or polymer matrices to immobilise ^{68}Ge. ^{68}Ga is quantitatively eluted using a low concentrated HCl solution, but the conditions in

which is obtained are not suitable for direct labelling of radiopharmaceuticals. The eluate has large volumes, an acidic pH, a breakthrough of ^{68}Ge that increases with time or frequency of use, and impurities such as stable Zn(II) generated by the decay of ^{68}Ga, Ti(IV) as a constituent of the column material, and Fe(III) as a general impurity. Thus, a post-processing is recommended to pre-concentrate and purify the initial generator eluate [65, 66].

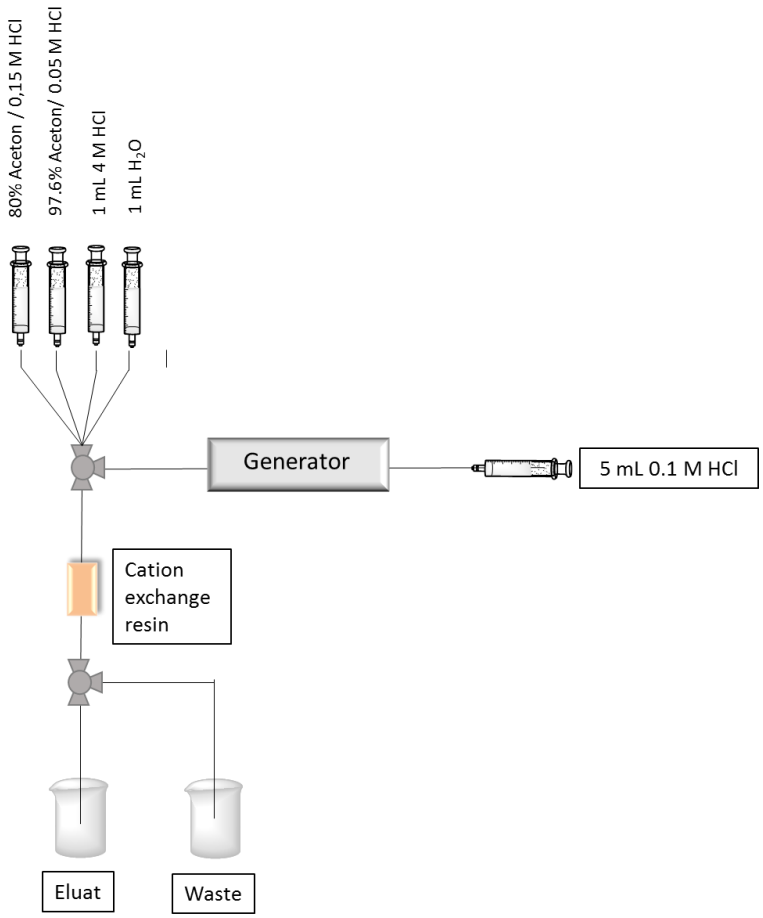

Figure 8: ^{68}Ga generator with cation exchanger applying the acetone post-processing

A number of methods for post-processing of the eluate including fractionation, anion or cation exchange purification and combination of both have been developed. The one, first developed by Zhernosekov *et al.*, is the most effective method [66]. These systems have been also implemented into fully automated modules allowing generator elution, post-processing radiolabelling and formulation, complying with regulatory demands [67]. Figure 8 shows an elution scheme of ^{68}Ga generator with cation post-processing using acetone/HCl solutions for desorption of ^{68}Ga.

^{44}Ti/^{44}Sc generator

^{44}Sc has a half-life of 3.97 hours, a high positron branching of 94.27% and mean β^+ energy of 632 keV. It is of high interest for application in nuclear medicine (Fig. 9). ^{44}Sc is obtained *via* a radionuclide generator or, alternatively, it can be produced in a cyclotron through the irradiation of ^{44}Ca target with protons (^{44}Ca(p,n)^{44}Sc)[68].

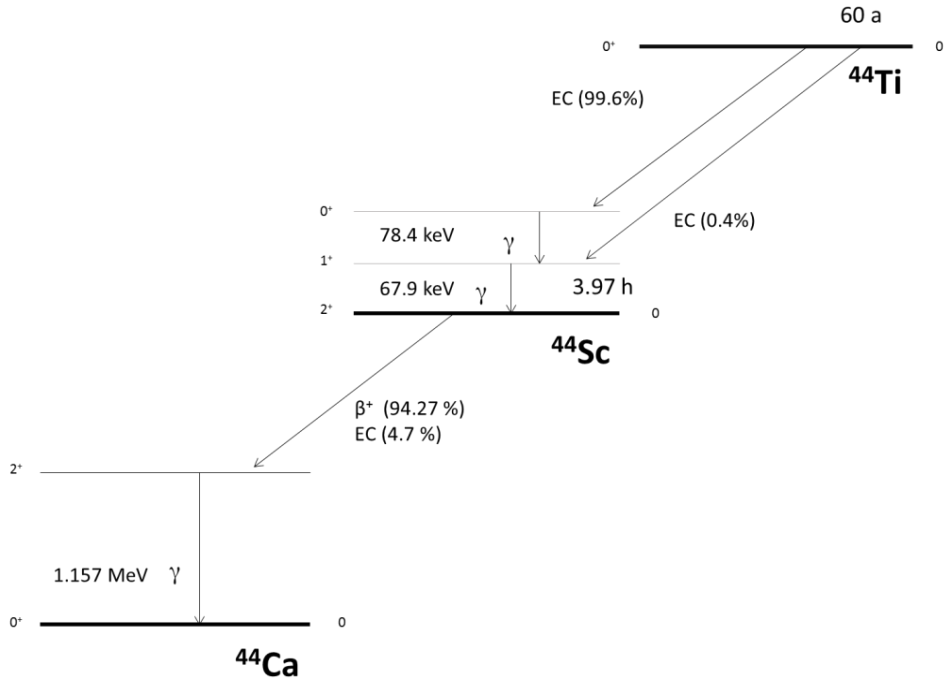

Figure 9: Decay scheme of ^{44}Ti/^{44}Sc

During the 1960s and 1970s, several radiochemical studies were carried out in order to design a ^{44}Ti/^{44}Sc generator [69-71]. But it was recently when for the first time a ^{44}Ti/^{44}Sc generator was described involving pharmaceutical aspects [72]. In this generator an anion-exchange resin is used to fix the parent nuclide ^{44}Ti (t ½ = 60 years), previously produced *via* ^{45}Sc(p,2n)^{44}Ti nuclear reaction, which transforms directly into the ground state of ^{44}Sc *via* electron capture. Elution of the generator with 20 mL of a 0.07 M HCl/ 0.005 M $H_2C_2O_4$ mixture provides 180 MBq ^{44}Sc with a ^{44}Ti breakthrough of 90 Bq which corresponds to an excellent separation factor of 2 x 10^6. During the elution, ^{44}Sc is online trapped on a cation exchange resin and will be later desorbed with 3 mL of 0.25 M ammonium acetate (NH_4OAc) buffer, pH= 4.0 with a high recovery yield (>85%) (Fig. 10) [73]. The use of this post-processing minimizes contamination with foreign ions,

optimizes the pH and reduces the volume of ^{44}Sc eluate for subsequent labelling of targeting vectors, thus ensuring the safe production of ^{44}Sc radiopharmaceuticals [74].

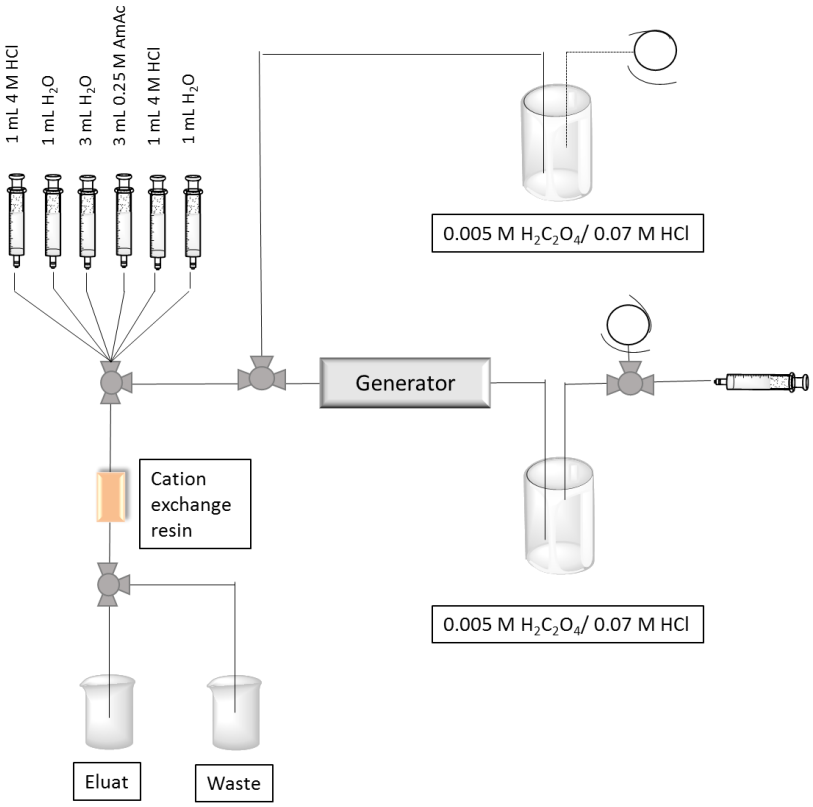

Figure 10: Scheme of ^{44}Ti/^{44}Sc generator

Owing to the long half-life of ^{44}Ti, the generator can be used for several years. Therefore it must be ensured that the generator *parameters remain constant. In practise, the distribution of ^{44}Ti has to remain as stable as possible* on the anion exchanger even after many elutions. Therefore the generator is eluted after the elution ^{44}Sc one more time. This second elution runs in the opposite direction and is essential for the shelf-life of the generator [72].

1.2.1.2 Production of non-standard PET isotopes

New radionuclides which can be routinely used for diagnosis or for evaluation of therapy would be valuable additions to the already available radionuclides used in nuclear medicine (standard nuclides). There is a big potential for production and development of new radiopharmaceuticals

using PET radionuclides with cyclotrons in the energy range of 10–20 MeV present in several medical centers [75].

Besides availability *via* generators, positron emitters are produced in charged-particle accelerators *via* bombardment of the target with high energy protons, deuterons, ^{3}He or α particles [76]. Due to the limited number of ^{3}He and α particle accelerators as well as the low production yield of these reactions, the most common method is currently the irradiation with protons in cyclotrons with low energy (up to 20 MeV) [50].

Irradiation

Several parameters that play a key role in the production of non-standard PET radionuclides need to be taken into account in order to achieve high production yields, which can be defined as the amount of activity (MBq) that can be produced at a defined energy per one μA for 1 hour irradiation time [49,77,78]. Such considerations are:

(1) Natural isotopic composition of the target: It should be high enough to produce the desired nuclide and minimize side reactions. To reduce contamination, isotopic enrichment of the target (up to 99.9%) can be applied, which will reduce co-production of other radionuclides but will increase the production cost.

(2) A high cross section value of the nuclear reaction is desired.

(3) Irradiation parameters: Energy of incident particles (MeV), beam intensity (μA), time of irradiation (h) and thickness of target material (mm).

(4) Melting point of the target material: An increase in current will create additional heating on the target surface, which a cooling system is called to reduce. Some target materials with “low” melting points can limit production yield or increase irradiation time by restriction of particle intensity.

Separation and purification

After irradiation, the micro-amount of product in the no-carrier added (n.c.a) state should be isolated from a macro-amount of target material [49,79]. In a first step, a crude separation allows isolation of the bulk amount of the target material [80]. Following gentle separation steps, afford additional separation and preconditioning of the radionuclide for further labelling (volume, media and purity) [81].

It is important that in the final sample there are neither tracers of aggressive media used for separation which are not comparable with an animal or human application nor other radioisotopes that can create additional dose burden for the patients and sufficiently decrease quality of imaging.

Non-standard PET isotope ^{90}Nb

Driven by the increasing availability of preclinical and clinical PET scanners, the use of non-standard PET nuclides has been growing in the past decade. Largely complementary to the roles of standard PET nuclides such as ^{18}F, ^{11}C or ^{68}Ga, non-standard PET nuclides enable the novel design and synthesis of a wider range of PET tracers to probe a variety of biological events [82]. Examples are ^{86}Y, ^{64}Cu or ^{89}Zr with high increase in its application during the last few years. Another non-standard positron-emitter is ^{90}Nb, whose decay characteristics make it promising for quantitative investigations on biological processes with slow distribution kinetics. It has a half-life of 14.6 hours and decays with a positron branching of 53% and a relatively low β^+-energy of E_{mean} = 0.66 MeV and E_{max} = 1.5 MeV [83].

^{90}Nb can be produced *via* several reactions by irradiation of ^{90}Zr, ^{93}Nb and ^{nat}Y targets with accelerated protons, deuterons, ^{3}He or alpha particles. The (p,n)-reactions lead to higher production yields over the other processes without requirement of high energy flux, therefore being the most advantageous route for production of ^{90}Nb. Results of cross section measurements demonstrate that ^{90}Nb can be produced efficiently and in high radionuclidic purity by means of the (p, n)-process on enriched ^{90}Zr with maximum proton energies of about 17 MeV [83,84].

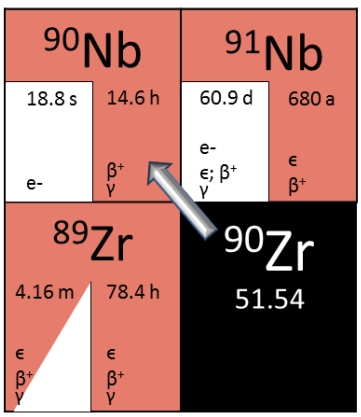

Figure 11: fragment of the chart of nuclides showing the production route to obtain ^{90}Nb

1.2.3 Radiometals for therapy

Radionuclide therapy can selectively deliver therapeutic radiation doses in targeted tissues. The basis for successful radionuclide therapy is an efficient concentration and prolonged retention of the radiopharmaceutical on the disease site with as little harm as possible to the nearby healthy tissue. This effect is determined by the total absorbed radiation dose and the sensitivity of the lesion to radiation [85].

The type of particle radiation for targeted radionuclide therapy (β^-, α, Auger electrons) which causes biological damage as well as the energy and half-life, the blood clearance, the specific activity and production feasibility are factors to be considered to identify an appropriate radionuclide [86,87]. Among various radionuclides the generator produced ^{90}Y (high energy betta emitter) and the reactor-produced ^{177}Lu (low energy beta emitter) are the most commonly used depending on the tumor size and location [88]. ^{177}Lu- or ^{90}Y-labelled octreotides (DOTATOC, DOTATATE) for example, have shown to be an appropriate treatment option for patients suffering from neuroendocrine tumors.
Other examples of β^- emitting nuclides are ^{188}Re und ^{169}Er, used ^{89}Sr used in nuclear medicine for example as palliative therapy for bone metastasis, and α-emitters such as e.g. ^{223}Ra and ^{255}Ac.

1.2.4 Labelling strategies for radiometals

The use of radiometals for labelling biomolecules generally requires bifunctional chelators (BFC), which strongly bind and stabilize the metal cation at one terminus and contain a functional group for covalent linkage to the biomolecule at the second terminus. Radiometal-based radiopharmaceuticals can be described as a four component structure: Biomolecule as a carrier, BFC, a linker moiety that connects these two functional components, and the radiometal (Fig. 12).

Selection of appropriate BFC and optimization of its labelling efficiency is an important step of the development of radiopharmaceuticals and its choice is mainly determined by the co-ordination chemistry of the metallic radionuclide.
The optimal BFC should ideally form a complex that is thermodynamically stable and kinetically inert to prevent ligand exchange or hydrolysis *in vivo,* to afford rapid complexation kinetics, to be selective to the radiometal of interest over other metals and to provide versatile conjugation chemistry [57].

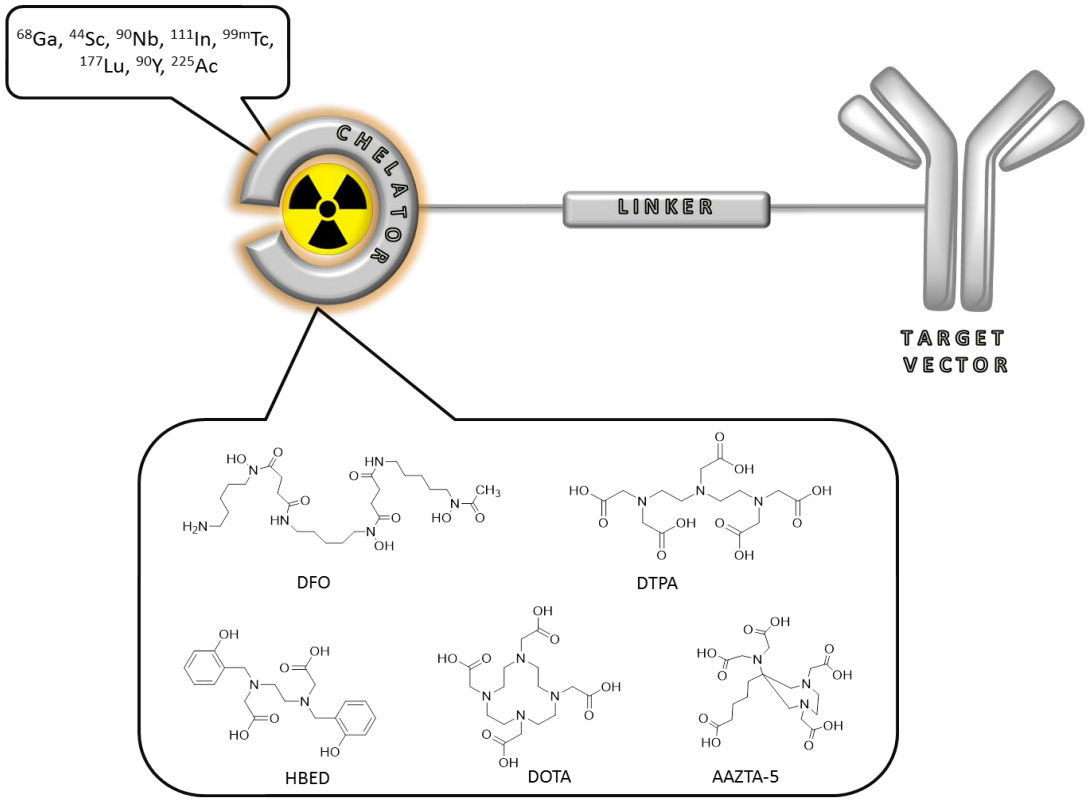

Figure 12: Construction of a metal-based radiopharmaceutical: a bifunctional chelator complex the radiometal and is bound *via* a linker to the targeting vector (exemplified for a monoclonal antibody).

There is also considerable interest in the development of chelators which are able to label quantitatively at room temperature and at milder pH due to the sensibility of some biomolecules (e.g. antibodies) to high temperatures and acidic pH. In general acyclic chelators (e.g. HBED, DFO, DTPA) present lower kinetic stability than macrocyclic ones (e.g. DOTA, NOTA, NODAGA) [58]. But, on the other hand, the metal-ligand complex formation with acyclic chelators occurs faster and normally under milder conditions, being an advantage especially for short living nuclides [88].

In spite that the use of a BFC is the most applied strategy for labelling a biomolecule with a radiometal, a BFC is not always required. Some chelating agents such as tropolone, hexamethyl-propylene-amine oxime (HMPAO) or 8-hydroxyquinoleine (oxine) have been widely used for radiolabelling of white blood cells for imaging of infection or inflammatory diseases. The complexes that such chelating agents form with some radiometals like ^{99m}Tc [89] or ^{111}In [90], normally in a ratio 3:1, are small and hydrophobic enough to be able to passively penetrate the cell membrane and once inside the cell be retained in the cytoplasm. Another example of radiolabelling of metals without utilizing BFC that has been reported is the direct labelling of antibodies [91-93]. In this case the radiometal is coordinated with donor groups (mainly

sulfhydryl groups found in cysteine residues) present in the antibody structure. This coordination presents strong bonds between the Ab and the radionuclide resistant to transchelation, but at the same time it can change sufficiently the structure and influence on further behaviour of biomolecules.

1.3 THERANOSTICS

The combination of both diagnostic and therapy gives rise to the concept of *theranostics*. In the context of nuclear medicine, it refers to the use of molecular targeting vectors labelled either with diagnostic radionuclides or with therapeutic radionuclides for detection and treatment respectively of a particular disease specifically targeted by the vector [94].

Beyond simply therapeutic functionality, theranostic materials provide a platform to integrate both therapeutic and diagnostic agents thus facilitating simultaneous and synergistic diagnosis and therapies [95]. In theranostic strategies, patients are pre-selected on the basis of initial target site accumulation studies using a diagnostic radionuclide-labelled tracer to perform initial low dose imaging to evaluate the maximum tolerated dose, followed by subsequent radiotherapy with the same precursor coupled to a therapeutic radionuclide [13]. By use of theranostic radionuclides, both applications are accessible with minimal change in the pharmacokinetics. An example is the use of ^{68}Ga-PSMA-617 for diagnosis and ^{177}Lu-PSMA-617 for treatment of neuroendocrine tumors [94].

1.3.1 Radiometals for theranostics

In order to predict the biodistribution and delivered dose of the radiotherapeutic tracer with the aim to minimize undesirable side effects, dosimetry studies are required. Dosimetry allows follow-up of personalized treatment utilizing an imaging analogue of the therapeutic pharmaceutical compound. The imaging probe quantifies the absorbed dose delivered in a specific site, offering accurate monitoring and planning of the patient's response to therapy. Finally, the efficiency of the therapy is evaluated in a post-therapeutic control [96].

The optimal condition for theranostic application is to use isotopes of the same element since they present the same electronic structure and, consequently, the chemical, biochemical and pharmacologic characteristics of the diagnostic and therapeutic entities are identical. An

example is the yttrium pair $^{90}Y/^{86}Y$ [97]. However, for most of the radionuclide pairs a lot of important information (e.g. long-term distribution) is not available due to the different half-lives of the two radionuclides. Such difference is exemplified by the diagnostic nuclide ^{62}Cu (t ½ = 9.74 min) *vs.* its therapeutic pair ^{67}Cu (t ½ = 2.58 d) [98]. Alternatively, another diagnostic radionuclide from a chemical element different to the therapeutic one may be used. In this case, however, pharmacological studies need to ensure that the analogy in chemistry reflects a similarity in pharmacology for the two different radiolabelled compounds. Trivalent radionuclides are of special interest due to their similar chemistry, this fact has focused the development of such metals for their application in nuclear medicine. The PET isotopes ^{68}Ga and ^{44}Sc and eventually ^{110m}In provide valuable information on labelled radiopharmaceuticals with trivalent β^- emitters such as ^{90}Y, ^{153}Sm and ^{177}Lu, sufficiently reflecting the biological parameters such as e.g. the *in vitro* binding affinities of the original therapeutics [99]. The radiation exposure in a particular tissue can be determined by equation 3.

$$\overline{D}_{t \leftarrow s} = S_{t \leftarrow s}\, \tilde{A}_s \qquad \text{(eq. 3)}$$

With $\overline{D}$ = mean absorbed dose, s = source organ, t = target organ, S = mean absorbed dose of the target organ when the unit dose is homogeneously distributed in the source organ, $\tilde{A}$ = time integral of the accumulated activity.

For the time integral, the accumulated activity is:

$$\tilde{A}_s = \int A_s(t)\, dt \qquad \text{(eq. 4)}$$

$$\tilde{A}_s = \int A_s\, e^{-(\lambda_{phys} + \lambda_{biol})\, t}\, dt \qquad \text{(eq. 5)}$$

Where A_s= activity, λ_{phys} = physical component and λ_{biol} the biological component and finally equation 6 is obtained.

$$\overline{D}_{t \leftarrow s} = S_{t \leftarrow s} \int A_s\, e^{-(\lambda_{phys} + \lambda_{biol})\, t}\, dt \qquad \text{(eq. 6)}$$

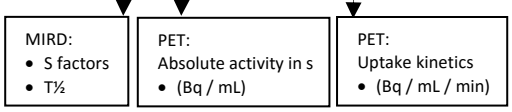

This equation was developed by the Medical Internal Radiation Dose (MIRD) committee of the Society of Nuclear Medicine and Molecular Imaging (SNMMI) and states that for determining the absorbed dose in the patient both the physical as well as the biological component must be considered [100].

The dosimetric properties are unique for each radionuclide according to their decay parameters such as half-life, type, abundance and energy of emissions, and these values are tabulated (S-factors). However, the residence times of the labelled compounds should be measured experimentally. Adequate positron emitters, covering at least the relevant initial uptake kinetics, are ideal to determine these biological kinetic processes.
For the calculation of radiation doses of specific radiotherapeutics, the biological residence data derived for the PET surrogate tracer may be used, while the S-factors of the therapeutic nuclide are employed.

Table 3: Radiometals for theranostic applications (PET/therapy) [96].

Therapeutic nuclide		**Diagnostic nuclide**		
Nuclide	$t_{1/2}$	Nuclide	$t_{1/2}$	β^+_{branch} [%]
Isotope pair				
^{47}Sc	3.34 d	^{47}Sc	3.93 h	94
^{67}Cu	2.58 d	^{62}Cu	9.74 min	97
^{90}Y	2.67 d	^{86}Y	14.74 h	33
Non-isotopic substituents				
^{90}Y	2.67 d	^{68}Ga	67.71 min	89
^{153}Sm	1.95 d	^{44}Sc	3.93 min	94
^{177}Lu	6.67 d	^{110m}In	1.15 h	62
^{273}Bi	45.6 min			
^{225}Ac	10.0 d			

If the positron emitter and the therapeutic nuclide are representing isotopes of the same element, equation 6 is valid. However, if the PET nuclide represents a nuclide of another chemical element, the biological parameters of the two pharmaceuticals may differ to a specific degree. In this case, another factor may be introduced considering these deviations [96,99]. In table 3 some radionuclides applied in PET and therapy for theranostic purposes are enumerated.

REFERENCES

[1] Tamargo J, Le Heuzey JV, Mabo P. Narrow therapeutic index drugs: a clinical pharmacological consideration to flecainide. *Eur J Clin Pharmacol* **2015**; 71: 549–567.

[2] Moderegger D, PhD thesis, Johannes Gutenberg-Universität, Mainz, **2012**, 227 pp.

[3] Lammers T, et al. Theranostic nanomedicine. *Acc chem res* **2011**; 10: 1029-1038.

[4] Duncan R, Gaspar R. Nanomedicine(s) under the microscope. *Mol Pharmaceutics* **2011**; 8: 2101–2141.

[5] Branco De barros AL, Ferreira Soares DC. Theranostic Nanoparticles: Imaging and therapy combined. *J Mol Pharm Org Process Res* **2014;** 2: e113

[6] Blanco E, Shen H, Ferrari M. Principles of nanoparticle design for overcoming biological barriers to drug delivery. *Nat Biotechnol* **2015;** 33: 941-951.

[7] Matsumura Y, Maeda HA. A new concept for macromolecular therapeutics in cancer chemotherapy: mechanism of tumoritropic acumulation of proteins and the antitumor agent. *Cancer res* **1986**; 46: 6387-6392.

[8] Fang J Nakamura H, Maeda H. The EPR effect: Unique features of tumor blood vessels for drug delivery, factors involved, and limitations and augmentation of the effect. *Adv Drug Deliv Rev* **2011;** 63: 136-151.

[9] Greish K. Enhanced permeability and retention (EPR) effect for anticancer nanomedicine drug targeting. *Methods Mol Biol* **2010;** 624: 25-37.

[10] K Strebhardt K, Ullrich A. Paul Ehrlich´s magic bullet concept: 100 years of progress. *Nat Rev Cancer* **2008**; 8: 473–480.

[11] Breimer D. D., Future challenges for drug delivery research. *Adv Drug Deliv Rev* **1998**; 33: 265–268.

[12] Fernandez-Fernandez A, Manchanda R, McGoron AJ. Theranostic applications of nanomaterials in cancer: Drug delivery, image-guided therapy and multifunctional platforms. *Appl Biochem Biotechnol* **2011**; 167: 1628-1651.

[13] Rizzo LY, et al. Nanotheranostics and Image-guided Drug Delivery: current concept and future direction. *Curr Opin Biotechnol* **2013**; 4: 1-8.

[14] Larson N, Ghamdehari H. Polymeric conjugates for drug delivery. *Chem mater* **2012;** 24: 840-853.

[15] Ringsdorf H. Journal of Polymer Science: Polymer Symposia **1975**; 51: 135-153.

[16] Fox ME, Szoka FC, Fréchet JMJ. Soluble polymer carriers for the treatment of cancer *Acc Chem Res* **2009**; 42: 1141-1151.

[17] Duncan R. The dawning era of polymer therapeutics. *Nat Rev Drug Discov* **2003**; 2: 347-360.

[18] Duncan R. Polymer therapeutics as nanomedicines: new perspectives. *Curr Opin Biotechnol* **2011**; 22: 492–501.

[19] Duncan R. Polymeric conjugates for drug delivery. *Adv Drug Deliv Rev* **2009**; 61: 1131-1148.

[20] Dumitriu S, Popa V. Polymeric Biomaterials, 3rd ed, vol. 2, Taylor & Francis, USA, **2013.**

[21] Kopeček J, Bažilová H. Poly[*N*-(2-hydroxypropyl)methacrylamide]-I. Radical polymerization and copolymerization. *Eur Polym J* **1973**; 9: 7-14.

[22] Kopeček J. Polymer-drug conjugates: origins, progress to date and future directions. *Adv Drug Deliver Rev* **2013**; 65: 49-59.

[23] Lammers T. Improving efficacy of combined modality anticancer therapy using HPMA copolymer-based nanomedicine formulations. *Adv Drug Deliver Rev* **2010***;* 62: 203-230

[24] Duncan R. Vicent MJ. Do HPMA copolymer conjugates have a future as clinically useful nanomedicines? A critical overview of current status and future opportunities. *Adv Drug Deliver Rev* **2010**; 62: 272-282.

[25] Moad G, et al. Living free radical polymerization with reversible addition – fragmentation chain transfer (the life of RAFT). *Polym Intern* **2000**; 49: 993-1001.

[26] Scales CW, Vasilieva YA, Convertine AJ, Lowe AB, McCormick CL. Direct, Controlled Synthesis of the Nonimmunogenic, Hydrophilic Polymer, Poly(N -(2-hydroxypropyl)methacrylamide) via RAFT in Aqueous Media. *Biomacromolecules* **2005;** 6: 1846–1850.

[27] Eberhardt M, Mruk R, Zentel, R. Theato, P. Postpolymerization modification of poly(pentafluorophenyl methacrylate): synthesis of a diverse water-soluble polymer library. *Eur Polym J* **2005**; *41*: 1569.

[28] Barz M, et al. From Defined Reactive Diblock Copolymers to Functional HPMA-Based Self-Assembled Nanoaggregates. *Biomacromolecules* **2008**; 9: 3114–3118.

[29] Allmeroth M, et al. Modifying the Body Distribution of HPMA-Based Copolymers by Molecular Weight and Aggregate Formation. *Biomacromolecules* **2011**; 12: 2841–2849.

[30] Talelli M, et al. Micelles based on HPMA copolymers. *Adv Drug Deliv Rev* **2010**; 62: 231-239.

[31] Barz M, et al. The uptake of N-(2-hydroxypropyl)-methacrylamide based homo, random and block copolymers by human multi-drug resistant breast adenocarcinomacells. *Biomaterials* **2009**; 29: 5682-5690.

[32] Hemmelmann M, et al. Amphiphilic HPMA–LMA copolymers increase the transport of Rhodamine 123 across a BBB model without harming its barrier integrity. *J Control Rel* **2012**; 163: 170-177.

[33] Hemmelmann M, et al. Radioactive Labeling of Defined HPMA-Based Polymeric Structures Using [18F]FETos for In Vivo Imaging by Positron Emission Tomography. . *Biomacromolecules* **2012**; 13: 4065-4074.

[34] Jockerst JV, Lobovkina T, Zare RN, Gambhir SS. Nanoparticle PEGylation for imaging and therapy. *Nanomedicine* **2011**; 6: 715-728

[35] Van Dongen GA, et al. Immuno-PET: A Navigator in Monoclonal Antibody Development and Applications. *Oncologist* **2007**; 12: 1379–1389.

[36] Wang M, et al. Targeting the Urokinase Plasminogen Activator Receptor with Synthetic Self-Assembly Nanoparticles. *Bioconj Chemistry:* **2009***;* 20: 32-40.

[37] U. S. Food and Drug Administration, U. S. Department of Health and Human Services. [Website] *Available, from: http://www.fda.gov*

[38] Imai K, Takaoka A. Comparing antibody and small-molecule therapies for cancer. *Nature Rev* **2006**; 6: 714-727.

[39] Bertrand N, et al. Cancer nanotechnology: the impact of passive and active targeting in the era of modern cancer biology. *Adv Drug Deliv Rev* **2014;** 66: 2–25.

[40] Zhang H, Ma Y, Sun XL. Recent developments in carbohydrate-decorated targeted drug/gene delivery. *Med Res Rev **2010**; 30: 270-89*

[41] Li X, Zhou H, Yang L, Du G, Pai-Panandiker AS, Huang X, Yan B. Enhancement of cell recognition in vitro by dual-ligand cancer targeting gold nanoparticles*. Biomaterials **2011**; 32: 2540-2545.*

[42] Chang SS. Overview of Prostate-Specific Membrane Antigen*. Rev Urol* **2004**; 6: 13-18.

[43] Hillier et al. Preclinical Evaluation of Novel Glutamate-Urea-Lysine Analogs that Target Prostate Specific Membrane Antigen as Molecular Imaging Pharmaceuticals for Prostate Cancer. *Cancer Res* **2009**; 69: 6932–6940.

[44] Eder M, et al. PSMA as a target for radiolabelled small molecules. *Eur J Nucl Med Mol Imaging* **2013;** 40: 819–823.

[45] Bequerel A. *Nobel Lect.* **1903**, 52–70.

[46] Hevesy GD. The Absorption and Translocation of Lead by Plants, A Contribution to the Application of the Method of Radioactive Indicators in the Investigation of the Change of Substance in Plants. *Biochem J* **1923**; 17: 439–445.

[47] De Hevesy G. Nobel Lect. **1944**.

[48] Kim EE, Jackson EF. Molecular Imaging in Oncology: PET, MRI, and MRS. Springer-Verlag Berlin-Heidelberg 1999.

[49] Cutler CS, et al. Radiometals for Combined Imaging and Therapy. *Chem Rev* **2013**; 113: 858-883.

[50] Radchenko V. PhD thesis, Johannes Gutenberg-Universität, Mainz, **2013**, 159 pp.

[51] Mc Ardle BA, Dowsley TF, deKemp RA, Wells GA, Beanlands RS. Does rubidium-82 PET have superior accuracy to SPECT perfusion imaging for the diagnosis of obstructive coronary disease?: A systematic review and meta-analysis. *J Am Coll Cardiol* **2012;** 60: 1828-37.

[52] Cherry SR. Fundamentals of positron emission tomograpgy. *J Clin Pharmacol* **2001**; 41: 482-491.

[53] Basu S, et al. Special Techniques and Technical Advances in PET/Computed Tomographic Imaging. *Ann NY Acad Sci* **2011**; 1228: 1-18.

[54] Bailey DL, Karp JS, Surti, S. Positron emission tomography: basic science and clinical practice. Springer-Verlag London Ltd. Chapter: physics and instrumentation in PET. **2003:** 41-67.

[55] Ache H. Angew. Chemie des positrons und positroniums. Chemie **1972**, 84, 234–255.

[56] Carroll V, Demoin DW, Hoffman TJ, Jurisson SS. Inorganic chemistry in nuclear imaging and radiotherapy: current and future directions. Radiochi Acta 2012; 100: 635-667

[57] Zeglis BM, et al. Underscoring the Influence of Inorganic Chemistry on Nuclear Imaging with Radiometals. *Inorg Chem* **2014**; 53: 1880–1899

[58] Bhattacharyya S, Dixit, M. Metallic radionuclides in the development of diagnostic and therapeutic radiopharmaceuticals. *Dalton Trans* **2011**; 40: 6112–6128.

[59] Gopal B. Saha **2010**. Fundamentals of Nuclear Pharmacy pp 67-82

[60] Production of long lived parent radionuclides for generators: ^{68}Ge, ^{82}Sr, ^{90}Sr and ^{188}W. Vienna : International Atomic Energy Agency, 2010.

[61] Rösch F, Baum RP. Generator-based PET radiopharmaceuticals for molecular imaging of tumours: on the way to THERANOSTICS. *Dalton Trans* **2011**; 40: 6104-6111.

[62] Rösch F, Knapp FF. Radionuclide generators. **2010**. Handbook of nuclear chemistry

[63] Maecke HR, André JP. Ernst Schering Res Found Workshop. **2007**; 62: 215-42.

[64] Rösch F, Riss JR. The Renaissance of the 68Ge/68Ga Radionuclide Generator Initiates New Developments in ^{68}Ga Radiopharmaceutical Chemistry. *Curr Top Med Chem* **2010;** 10:1633-1668.

[65] Rösch F. Past, present and future of ^{68}Ge/^{68}Ga generators. *Appl Radiat Isot* **2013**; 76: 24-30.

[66] Zhernosekov K, et al. Processing of generator-produced ^{68}Ga for medical application. *J Nucl Med* **2007**; 48: 1741–1748

[67] K. Eigner Henke. Production of gallium-68 for PET-diagnostics using "ionic" ^{68}Ge/^{68}Ga radionuclide generator. Nuclear Physics Institute Řež Czech Republic. Biennial report **2007-2008.**

[68] Krajewski S. Cyclotron production of ^{44}Sc for clinical application. *Radiochim Acta* **2013**; 101: 333–338.

[69] Rösch F. Scandium-44: benefits of a long-lived PET radionuclide available from the ^{44}Ti/^{44}Sc generator system. *Curr Radiopharm* **2012**; 5: 187-201

[70] Greene MW, Hillman M. A scandium generator. *Int J Appl Radiat Isot* **1967;** 18: 540–541

[71] Mirza MY, Aziz A. A scandium generator. *Radiochim. Acta* **1969**; 11: 43–44.

[72] Filosofov DV, Loktionova NS, Rösch F. A ^{44}Ti/^{44}Sc radionuclide generator for potential application of ^{44}Sc-based PET-radiopharmaceuticals. *Radiochim Acta* **2010**; 98: 149–156.

[73] Prusynski M, et al. Post-elution processing of ^{44}Ti/^{44}Sc generator-derived ^{44}Sc for clinical application. *Appl Rad Isot* **2010**; 68: 1636-1641

[74] Pruszynski M, Majkowska-Pilip A, Loktionova NS, Eppard E, Rösch F. Radiolabeling of DOTATOC with the long-lived positron emitter 44Sc. *Appl Rad Isot* **2012**; 70: 974–979.

[75] Cyclotron Produced Radionuclides: Emerging Positron Emitters for Medical Applications: ^{64}Cu and ^{124}I. **2016** *IAEA Radioisotopes and radiopharmaceuticals* reports No 1.

[76] Qaim SM. New trends in nuclear data research for medical radionuclide production. *Radiochim. Acta* **2013**; 101: 473–480.

[77] Qaim SM. Decay data and production yields of some non-standard positron emitters used in PET. *J Nucl Med Mol Imaging* **2008**; 52(2); 111-120.

[78] Cyclotron produced radionuclides: physical characteristics and production methods. Technical reports series No. 468, *International Atomic Energy Agency, Vienna,* **2009**

[79] Jahn M, Radchenko V, Filosofov D, Hauser H, Eisenhut M, Jennewein M, Rösch F. Separation and purification of no carrier added arsenic from bulk amounts of germanium being adequate to radiopharmaceutical labeling chemistry. *Radiochim Acta* **2010**; 98: 807-812.

[80] Radchenko V, Filosofov D, Bochko OK, Lebedev NA, Rakhimov AV, Hauser H, Eisenhut M, Aksenov NV, Bozhikov GA, Ponsard B, Roesch F. Separation of Nb-90 from zirconium target for application in immuno-PET. *Radiochim Acta* **2014**; (5): 433–442

[81] Bunney R, Ballou NE, Pascual J, Foti S. Quantitative Radiochemical Analysis by ion Exchange Anion Exchange Behavior of Several Metal Ions in Hydrochloric, Nitric, and Sulfuric Acid Solutions. *Anal Chem* **1959**; 31: 324-326

[82] Hao G, Singh AN, Liu W, Sun X. PET with non-standard nuclides. *Curr Top Med Chem* **2010**;10:1096-112.

[83] Busse S, Rösch F, Qaim SM. Cross section data for the production of the positron emitting niobium isotope 90Nb via the ^{90}Zr(p, n)-reaction. *Radiochim Acta* **2002**;90:1-5.

[84] Radchenko V, Hauser H, Eisenhut M, Vugts DJ, van Dongen GA, Roesch F. ^{90}Nb: a potential PET nuclide: production and labeling of monoclonal antibodies. *Radiochim. Acta* **2012;** 100: 857-863.

[85] Hoefnagel C. Radionuclide cancer therapy. *Annals of nuclear medicine* **1989**; 12: 61-70.

[86] Advancing Nuclear Medicine Through Innovation. **2007** ISBN: 0-309-11068-8, 176 pp.

[87] Liu S. Bifunctional Coupling Agents for Radiolabeling of Biomolecules and Target Specific Delivery of Metallic Radionuclides. *Adv Drug Del Rev* **2008**; 60: 1347-1370

[88] Stavroula S. Radionuclide carriers for targeting of cancer. *Int J Nanomedicine* **2008;** 3: 181–199.

[89] Aydın F, Cengiz AK, Güngör F. Tc-99m Labeled HMPAO white Blood Cell Scintigraphy in Pediatric Patients. *Mol Imaging Radionucl Ther* **2012;** 21: 13–18.

[90] Roca M, de Vries EFJ, Jamar F, Israel O, Signore A. Guidelines for the labelling of leucocytes with ^{111}In-oxine. *Eur J Nucl Med Mol Imaging* **2010;** 37: 835–841.

[91] Griffiths GL, David M. Goldenberg, Knapp FF, Callahan AP, Chang CH, Hansen HJ. Direct Radiolabeling of Monoclonal Antibodies with Generator-produced Rhenium-188 for Radioimmunotherapy: Labeling and Animal Biodistribution Studies. *Cancer Res* **1991** 51; 4594-4602.

[92] Direct labeling of antibodies and other protein with metal ions. Patent **US 5460785 A** U.S. Pat. No. 4, 424, 200, entitled Method for Radiolabelling

[93] Garron JY, Moinereau M, Pasqualini R, Saccavini JC. Direct ^{99m}Tc labeling of monoclonal antibodies: radiolabeling and in vitro stability. *Int J Rad Appl Instrum* **1991**; 18: 695-703.

[94] Baum RP, Kulkarni HR. THERANOSTICS: From Molecular Imaging Using Ga-68 Labeled Tracers and PET/CT to Personalized Radionuclide Therapy - The Bad Berka Experience. *Theranostics* **2012**; 2: 437–447.

[95] Peng H, et al. Polymeric multifunctional nanomaterials for theranostics. *J Mater Chem* **2015**; 3: 6856-6870

[96] Eppard E. PhD thesis, Johannes Gutenberg-Universität, Mainz, **2013**, 189 pp.

[97] Bockisch A. Matched pairs for radionuclide-based imaging and therapy. *Eur J Nucl Med Mol Imaging* **2011;** 38: 1-3.

[98] Cutler CS, Hennkens HM, Sisay N, Hucleier-Markai, Jurisson SS. Radiometals for combined Imaging and Therapy. *Chem Rev* **2013;** 113: 858-883.

[99] Rösch F, Baum RP. Generator-based PET radiopharmaceuticals for molecular imaging of tumours: on the way to THERANOSTICS. *Dalton Trans* **2011;** 40: 6104-6111.

[100] Bolch *et al*. A Generalized Schema for Radiopharmaceutical Dosimetry Standardization of Nomenclature. *J Nucl Med* **2009**; 50:477–484.

2 OBJECTIVES AND OUTLINE

PET is a powerful non-invasive imaging technique of metabolic processes *in vivo*. It is widely used in the clinics for detection of several pathologies including areas such as oncology or cardiology, aiming to set up a personalized treatment plan for best therapeutical response rates.

A big array of nanoparticles is used to treat different diseases and investigations keep ongoing towards their improvement. In this sense PET is an important tool as well in research. It can provide information about specific characteristics such as charge, hydrophilic-lipophilic balance or flexibility affecting the *in vivo* performance of carrier systems, which is essential to optimize and further functionalize carrier systems to guide the way to new generation nanomedicines.

In this work different nanoparticles have been radiolabelled and evaluated systematically with the objective to improve their pharmacology as theranostic agents for further possible applications in nuclear medicine. Due to their different pysico-chemical characteristics various radioisotopes have been employed to match their physical half-life with the biological half-life of the nanoparticles.

Aspect 1. Optimization of HPMA-based nanoparticles for theranostic applications

Among polymer-based carrier systems, HPMA is a promising biocompatible polymer that has demonstrated to accumulate in tumor tissue by means of the EPR effect [1]. Moreover, its polymerization *via* RAFT offers the possibility to synthetize well defined structures and a facile introduction of several functionalities.

In nuclear medicine both metal and organic radioisotopes can be employed. However, radiometals offer the advantage of providing higher radiolabelling yields in contrast to organic isotopes. In addition, some radiometals of them are easy available *via* generators. Nevertheless, the labelling of nanoparticles with a radiometal requires a bifunctional chelate that is previously attached to the nanoparticle. The modification of nanoparticles with chelates may alter their biological functions. Part of this work aimed to achieve quantitative radiolabelling yields by modifying as less as possible the HPMA-based nanocarriers.

Thus, different HPMA-linker-DOTA polymer conjugates were synthetized aiming to identify the less amount of chelate needed to still provide a quantitative radiochemical yield.
As chelate, DOTA was chosen owing to its capacity to form stable complexes with a variety of radiometals including both diagnostic and therapeutic nuclides. To facilitate the introduction of the chelate in the polymeric structure, various DOTA-linker systems with different linker structure (alkyl chains or alkoxy) and length (1-12 carbon atoms) were synthesized and later coupled in a polymer-analogous reaction to the HPMA backbone. Subsequent labellings with ^{68}Ga, ^{44}Sc and ^{177}Lu as well as *in vitro* evaluations were performed. Finally the conjugates with the highest stability should be evaluated *in vivo.*

On the other hand, exploiting the capacity of amphiphilic polymers to self-assemble forming micelles and spontaneously incorporate hydrophobic drugs into their core, a novel strategy to radiolabel micelles was investigated. The strategy provides a fast and quantitative labelling with a radiometal without previous modification of the polymer structure with a chelate. The key point is the use of hydrophobic chelating agents that will be incorporated in the hydrophobic core of the micelles. Three different structures of HPMA-LMA based polymer (random, block and PEGylated-block) were radiolabelled using such strategy and their stability was analysed *in vitro*. The polymer architecture that presented highest stability *in vitro* was further evaluated *in vivo* in healthy mice.

Aspect 2. Formulation and evaluation of a novel radiopharmaceutical for diagnosis of prostate cancer lesions

Prostate cancer is the second most common cancer and the sixth leading cause of cancer death in men worldwide [2]. Big efforts are being made to develop theranostic drugs for its efficient diagnosis and treatment. In nuclear medicine, ^{177}Lu-labelled DKFZ-617 has recently entered into the clinics and has demonstrated successful response against prostate cancer lesions.

Nevertheless, there is no accurate dosimetry study on this radiopharmaceutical after 5 h p.i [3]. Dosimetry calculations are an important step on the way to personalized medicine. A pre-therapy study is necessary to evaluate the response to the therapeutic drug as well as the received dose in tumor and non-tumor tissues.

^{68}Ga-DKFZ-617 is up-to-date the analogue of ^{177}Lu-PSMA-617 for imaging of prostate cancer. ^{68}Ga has a significate importance in current clinical practice due to its favourable decay characteristics and its cyclotron independence production *via* the ^{68}Ge/^{68}Ga generator. However, its short physical half-life of 68 min does not allow follow up at late time points.

In this context, ^{44}Sc presents an alternative owing to its decay characteristics (t ½ = 3.97 h and positron branching = 94.27%) and its generator and cyclotron availability. With a half-life 4 times longer than ^{68}Ga, ^{44}Sc provides an extended frame time for *in vivo* follow up, consequently being more suitable for dosimetry calculations on ^{177}Lu analogues.

In this work we propose ^{44}Sc-DKFZ-617 as a PET imaging agent for prostate cancer lesions. In order to be used as imaging agent in the clinics, a fast an efficient labelling needs to be achieved. Stability in physiological conditions should be ensured and affinity and internalization values of the novel imaging radiopharmaceutical to prostate cancer cells should not differ from the therapeutical radiopharmaceutical values. A detailed evaluation of DKFZ-617 with ^{44}Sc has been completed and successful results have led to human *in vivo* evaluation in a patient suffering from prostate cancer.

Aspect 3. Evaluation of ^{90}Nb as potential PET isotope

With rising interest on using antibodies or antibody fragments for tumor imaging and therapy, radionuclides with long and intermediate half-life are on demand. However, the lack of nuclides that in addition have decay characteristics suitable for nuclear imaging has motivated the present work.

^{90}Nb is a potential radionuclide for application in *immuno*-PET thanks to its decay parameters (t ½ = 14.6 h, positron branching of 53%, E_{β^+} mean = 0.66 MeV). Production and separation of ^{90}Nb from irradiated target has been recently developed [4,5] but strategies for *in vivo* application need further investigation.

In this study ^{95}Nb (t ½ = 35 d) has been used as analogue of ^{90}Nb, to develop a labelling protocol of antibodies for later evaluation *in vivo*. *Nb isotopes were obtained by irradiation of ^{nat}Zr. ^{95}Nb

was produced *via* the ^{nat}Zr(n, γ)-reaction in a reactor and ^{90}Nb *via* the ^{90}Zr(p,n)-reaction in a cyclotron. $^{90/95}$Nb was recovered from irradiated target in a multistep separation that afforded the desired niobium isotope in conditions suitable for direct labelling (pH, volume, specific activity). The monoclonal antibodies bevacizumab and citubximab were modified with DFO chelate, which has shown to form stable complexes with niobium. High *in vitro* stability of purified *Nb-mAb lead to *in vivo* evaluation of ^{95}Nb-mAb in healthy and tumor bearing mice.

References

[1] M. Allmeroth *et al*. PEGylation of HPMA-based block copolymers enhances tumor accumulation in vivo: A quantitative study using radiolabeling and positron emission tomography. *J Control Rel* **2013;** 172: 77–85.

[2] Jemal A, Bray F, Center MM, Ferlay J, Ward E, Forman D. Global cancer statistics. *Cancer J Clin* **2011**; 61: 69–90.

[3] Ali Afshar-Oromieh. The novel theranostic PSMA-ligand PSMA-617 in the diagnosis of prostate cancer by PET/CT: biodistribution in humans, radiation dosimetry and first evaluation of tumor lesions. *J Nucl Med* **2015;** 56: 1697-1705

[4] Busse S, Rösch F, Qaim SM. Cross section data for the production of the positron emitting niobium isotope ^{90}Nb via the ^{90}Zr (p, n)-reaction. *Radiochim Acta* **2002**; 90: 1-5.

[5] Busse S, Brockmann J, Roesch F. Radiochemical separation of no-carrier-added radioniobium from zirconium targets for application of ^{90}Nb-labelled compounds. *Radiochim Acta* **2002**; 90: 411-415.

3 MANUSCRIPTS

This work is based on the following manuscripts:

(I) E. Eppard, A. de la Fuente, N. Mohr, M. Allmeroth, R. Zentel, F. Rösch. Labeling of HPMA-based polymer-conjugates with metallic radionuclides for theranostic applications

(II) A. de la Fuente, S. Kramer, N. Mohr, S. Pektor, N. Bausbacher, R. Zentel, F. Rösch. ^{68}Ga-oxine: A novel strategy of in situ radiolabelling of HPMA-based micelles.

(III) A. de la Fuente, E. Eppard, M. Benesova, F. Roesch, M. Essler, K. Kopka. ^{44}Sc-PSMA-617 for dosimetry of prostate cancer.

(IV) V. Radchenko, P. Bouziotis, T. Tsotakos, M. Paravatou-Petsotas, A. de la Fuente, G. Loudos, A.L. Harris, S. Xanthopoulos, D. Filosofov, H. Hauser, M. Eisenhut, B. Ponsard, F. Roesch. Labeling and preliminary in vivo assessment of niobium-labeled radioactive species: A proof-of-concept study. Nuclear Medicine and Biology **2016;** 43: 280–287.

(V) A. de la Fuente, V. Radchenko, T. Tsotakos, C. Tsoukalas, M. Paravatou-Petsotas, A. L. Harris, U. Köster, F. Rösch*, P. Bouziotis. Conjugation, labelling and *in vitro/in vivo* assessment of an anti-VEGF monoclonal antibody labelled with niobium isotopes. Submitted *Nucl Med Biol*

3.1 Labeling of HPMA-based polymer-conjugates with metallic radionuclides for theranostic applications

Labeling of HPMA-based polymer-conjugates with metallic radionuclides for theranostic applications

E. Eppard[1], A. de la Fuente[1], N. Mohr[2], M. Allmeroth[C], R.Zentel[2], F. Rösch[1*]

[1] Institute of Nuclear Chemistry, Johannes Gutenberg-University, Fritz-Straßmann-Weg 2, 55128 Mainz, Germany

[2] Institute of Organic Chemistry, Johannes Gutenberg-University, Duesbergweg 10-14, 55128 Mainz, Germany

ABSTRACT

Nanomaterials play a key role in medicine as drug carrier systems aiming to improve lack of selectivity of utilized anticancer drugs. In this work, diverse DOTA-linker systems were conjugated in different amounts to HPMA homopolymer aiming to identify the fewer amount and the optimal DOTA-linker structure that provides quantitative labeling yields. PET and therapeutic nuclides were employed for labelling and *in vitro* stability and *in vivo* evaluations were performed

Methods:

HPMA homopolymers were modified with different DOTA-linker systems following RAFT technique. Radiolabelling were performed with ^{68}Ga, ^{44}Sc and ^{177}Lu and influence of linker structure and amount incorporated was evaluated. *In vitro* stability of labelled polymers was studied in different media: 0.9 % NaCl, human serum (HSA), metal cations (Fe^{3+}, Mg^{2+}, Ca^{2+}) and competing ligands (EDTA, DTPA). Final proof-of-principle *in vivo* evaluation of one of the conjugates was performed in tumor bearing rat.

Results:

Complex formation depends on the incorporation rate of DOTA and minimum of 1.6 % DOTA is enough to obtain labeling yields >90 % after 20 min. Alkoxy linkers generally exhibit lower labeling yields than alkane linkers despite of similarly chain length and DOTA incorporation. A short linker is enough to provide quantitative radiolabeling yields. High stability in all examined solutions was presented for all conjugates. Accumulation in tumor site was observed for the first *in vivo* evaluation in tumor-bearing rat.

Conclusions:

This study confirms the principle applicability of HPMA-conjugates for labeling with different radionuclides with established radiolabeling chemistry. Introducing as less than only c.a 1.5% of DOTA chelator using a short linker chain, which facilitates the synthesis and efficiency of the polymer conjugates, allows introduction of both diagnosis and therapeutic radiometals.

KEYWORDS: HPMA-DOTA-conjugates; theranostic; ^{68}Ga; ^{44}Sc; PET

1 INTRODUCTION

One of the major problems in current chemotherapy is the lack of selectivity of the utilized anticancer drugs. Most of these agents (e.g. doxorubicin, cisplatin) are compounds of low molecular weight (< 800 g/mol), which inhibit cell growth by affecting DNA duplication and cell division. As a result of affecting not only cancer cells, but basically all cells with high proliferation rates, conventional chemotherapeutic drugs suffer from a narrow therapeutic index. The therapeutic index of a drug can be improved by increasing the accumulation at the target site. In this context nanomaterials moved in the focus of drug development as drug carrier systems. The particles are too big to overcome the tight junctions of healthy tissue (normally 2-4 nm) and the renal threshold (5-7 nm). In addition, nanomaterials are a convenient base to combine imaging agents and drugs within one formulation. Due to the particle size (< 100 nm) nanomaterials often can prolongate pharmacokinetics and may passively and/or actively invade and accumulate in tumor tissue. Consequently, an increase in circulation time is induced and bioavailability while affection of healthy tissue is minimized. For the first investigations radionuclides of choice are ^{68}Ga and ^{44}Sc, two generator produced positron emitters. These two nuclides, with half-lives of 67.71 min (^{68}Ga) and 3.97 h (^{44}Sc), are suitable to investigate processes such as EPR mediated accumulation of nanoparticles in tumor tissue. Long-term investigation of pharmacokinetics could also be accessible using radionuclides with longer physical half-life like ^{64}Cu, or utilizing other imaging techniques like MRI (Gd) or SPECT (^{111}In). For the controlled incorporation of a metallic radionuclide, highly efficient binding ligands such as DOTA (1,4,7,10-tetraazacyclododdecane-tetraaceticacid) are necessary. DOTA was chosen as chelator to enable the introduction of several imaging and therapeutic nuclides and consequently different imaging techniques (MRI, PET, SPECT) could be applied. The chelator was coupled to the polymer using three different linkers, an alkane chain with two, six and twelve carbons, and two different alkoxy chains, in order to evaluate the influence of the DOTA morphology on the radiolabeling efficacy. Incorporation rate of the chelator was also varied.

1.1 Imaging

In medicine, nanomaterials are primary designed to improve the therapeutic index of systemically administered drugs. To enable pharmacokinetic analyses, it is useful to quantitatively determine circulation time and biodistribution in real-time. This approach is in particular important if the assay can be performed *in vivo*, i.e. with a living object. For this purpose, nanomaterials have been co-loaded with imaging agents. Imaging agents applied to

SPECT (Single Photon Emission Computed Tomography) and PET (Positron Emission Tomography) utilize photon-radiation emitted from the corresponding radionuclides (Tab. 1).

Table 1: Commonly used isotopes for non-invasive imaging of nanomaterials [1-6].

Isotope	Emission	Half-life	E_{max} (γ) [keV]
^{131}I	γ (81.2 %)	8.0 d	284, 364, 637
^{67}Ga	γ	78.3 h	93, 184, 300, 393
^{111}In	Auger, γ	67.2 h	171, 245
^{123}I	Auger, γ	13.2 h	159
^{99m}Tc	γ	6.0 h	140
^{18}F	β^+	1.83 h	511
^{64}Cu	β^+	12.7 h	511
^{188}Re	γ (15 %), β	16.9 h	155

Apart from only two exceptions (iodine and fluorine) all of the dedicated radioisotopes are metals. For radiolabeling with metallic radionuclides like ^{67}Ga, ^{64}Cu or ^{111}In it is indispensable to either covalently attach or to load a chelating function to the nanomaterial. The chelate should be able to form stable complexes with the utilized radionuclide (Fig. 1). Those chelators can be bifunctionally coupled to the nanoparticle *via* versatile linker systems.

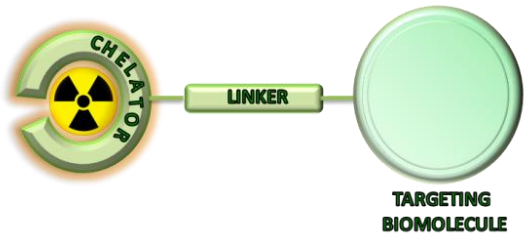

Figure 1: Chelator attached to a nanoparticle over a linker structure, which is coupled to a coupling functionality of the chelator and the targeting vector that can be a nanoparticle.

By the use of suitable chelators, different metallic radionuclides can be incorporated and therefore several imaging techniques can be used by minimal alteration in pharmacokinetics. A new and extremely promising approach is on “theranostics”, i.e. to select particle-emitting radionuclides in order to add a therapeutic option. Radioisotopes like ^{67}Cu, ^{90}Y, ^{177}Lu support the therapeutic effect of the loaded drug. This combination principally allows an effective minimal-invasive diagnosis and based on that, an individualized treatment planning [7].

Among the metallic radionuclides mentioned in table 1, only ^{188}Re is available *via* ^{188}W/^{188}Re radionuclide generator. With regard to costs and availability it is desirable to take the advantage of the cyclotron independent isotopes to label nanomaterials. ^{68}Ga is a positron emitter (89 %) with a half-life of 67.71 min and average positron energy of 1.899 MeV. Its physical half-life is adequate to allow the preparation and purification of ^{68}Ga-labeled radiopharmaceuticals and for imaging biological processes with short half-life. The major advantage of ^{68}Ga is its availability via a ^{68}Ge/^{68}Ga generator system, which affords a cyclotron independent and cost-effective source of the isotope in suitable conditions for labeling after its post-processing [10-14]. Other metallic radionuclide suitable for PET imaging is ^{44}Sc (94%), which is also available *via* the ^{44}Ti/^{44}Sc generator system [8, 15]. Due to its longer physical half-life of 3.97 h, ^{44}Sc facilitates the tracking of processes with longer biological half-life than ^{68}Ga or even ^{18}F. It could be applied for more exact planning and dosimetry calculations in endoradiotherapy and also for direct matching of the β^- emitting ^{47}Sc radiopharmaceuticals [9]. According to that, the matched pair ^{44}Sc/^{47}Sc would permit coordinated dosimetry PET imaging and therapy like ^{62}Cu/^{67}Cu or ^{86}Y/^{90}Y. Contrary to ^{68}Ga and ^{44}Sc, ^{177}Lu is not suitable for PET imaging, but as a result of emitting both β^- (average energy 133.1 keV) and gamma radiation (113.0 and 208.4 keV) it can be used for therapy and SPECT imaging.

1.2 Polymeric nanoparticles

Various studies on hydrophilic polymers investigated their potential as cancer drug carrier systems. They have been used to modify proteins, liposomes or the surface of biomaterials as well as carrier systems for drugs to improve their pharmacokinetics. Since the early 1970s N-(2-hydroxypropyl)methacrylamide (HPMA) is investigated as drug delivery system based on the enhanced permeability and retention (EPR) effect. HPMA-based copolymers are hydrophilic, biocompatible and non-immunogenic [16, 17] and its selection of as drug carrier is based on detailed studies of the relationship between structure and biocompatibility hydrophilic polymers [18-24]. HPMA-copolymer conjugates have been successfully utilized in the delivery of

miscellaneous drugs (e. g. doxorubicin [25], paclitaxel [26], camptothecin [27]). Modification can be achieved through activated comonomers leading to biocompatible polymers with functionalities for polymer analoge reaction. This strategy is very flexible in the choice of ligands, type of activation and occupancy rate and was already used in various studies [28]. Reaction of a reactive ester polymer with several ligands leads to multifunctionalised copolymers which can be applied for theranostic applications.

In the present study, we aimed to synthesize "theranostic" HPMA-conjugated DOTA copolymers with alkyl- and alkoxy-linkers for labeling with metallic radionuclides for cancer PET imaging and therapy. The chelator DOTA allows the introduction of several diagnostic and therapeutic nuclides representing trivalent metals (Gd; ^{44}Sc; ^{64}Cu, ^{68}Ga, ^{111}In; ^{177}Lu; ^{90}Y) and consequential the utilization for several applications (MRI; PET; SPECT; therapy). The main objective was to show the influence of the linker (structure and length) as well as the amount of DOTA incorporated on labeling kinetics, stability and whether labeling procedures for different radionuclides can be utilized. Labeling of the synthesized DOTA-conjugated copolymers was first performed with ^{68}Ga to evaluate reaction parameters (incubation time, amount of compound, temperature, influence of organic solvent). The stability of the ^{68}Ga-labeled conjugates was analysed *in vitro* in 0.9% NaCl and human serum (HSA), as well as in the presence of different metal cations and other competing chelators, like EDTA and DTPA. Additionally, labeling with the diagnostic and therapeutic isotopes ^{44}Sc and ^{177}Lu was performed. Finally, proof-of-principle *in vivo* experiments on the pharmacology of ^{68}Ga-DOTA-HPMA derivative 31 was conducted in tumor bearing rat.

2 MATERIALS AND METHODS

All chemicals were analytical or pure reagent grade and used as received unless otherwise specified. DOTA-(^{t}Bu)$_3$ was obtained from CheMatech (Dijon, Graz). All other organic and inorganic reagents were purchased from Sigma-Aldrich and Across Organics. Deionized Milli-Q water (18.2 MΩ•cm; Millipore) was used in all organic reactions. Dioxane was distilled over a sodium/potassium composition. Lauryl methacrylate was distilled to remove the stabilizer and stored at -18 °C. 2,2'-Azo-bis-(isobutyronitrile) (AIBN) was recrystallized from diethyl ether and stored at -18 °C as well. ^{1}H-NMR spectra were obtained by a Bruker AC 300 spectrometer at 300 MHz, ^{19}F-NMR analysis was carried out with a Bruker DRX-400 at 400 MHz. The synthesized polymers were dried at 40 °C under vacuum overnight, followed by Gel Permeation Chromatography (GPC). GPC was performed in tetrahydrofuran (THF) as solvent, using following equipment: pump PU 1580, autosampler AS 1555, UV detector UV 1575 and RI detector RI 1530

from Jasco as well as a miniDAWN Tristar light scattering detector from Wyatt. Columns were used from MZ Analysentechnik, 300x8.0 mm: MZ-Gel SDplus 106 Å 5 µm, MZ-Gel SDplus 104 Å 5 µm and MZ-Gel SDplus 102 Å 5 µm. GPC data were evaluated by using the software PSS WinGPC Unity (Polymer Standard Service Mainz, Germany). The flow rate was set to 1 mL/min with a temperature of 25 °C. Commercial generators based on TiO_2 phase absorbing ^{68}Ge(IV) were obtained from Cyclotron Co. Ltd (Obninsk, Russia). Typically, batch activities of 80-150 MBq were used. ^{44}Sc was provided from a ^{44}Ti/^{44}Sc generator system developed in Mainz [8]. Batch activities of 165-180 MBq were used. ^{177}Lu was obtained from ITG (Munich, Germany) and used without further purification. Counting was performed in a borehole counter (Nuklear-Medizintechnik Dresden GmbH, Germany). Thin layer chromatography (TLC) was performed on silica-gel (silica-gel 60 F254; MERCK, Darmstadt, Germany)) coated aluminium TLC-sheets and analysed using an instant imager (Instant Imager, Canberra Packard, Schwadorf, Austria). The cation exchange resins AG 50W-X8 (- 400 mesh), AG 50W-X4 (200 – 400 mesh) and AG 50W-X8 (200 - 400 mesh) were obtained from Bio-Rad (Munich, Germany). Strata-X mini-C-18 cartridges were obtained from Phenomenex (Aschaffenburg, Germany). HiTrap™ Desalting Columns were purchased from GE-Healthcare Europe GmbH (Freiburg, Germany). TraceSelect water (Sigma-Aldrich, Germany) was used for all aqueous radiolabeling solutions.

2.1 Synthesis and characterization of HPMA-DOTA-conjugates

The HPMA-DOTA conjugates were prepared following the synthesis routes depicted in figures 2 and 3. Figure 2 shows the preparation of different DOTA-linkers that later on were conjugated to HPMA backbone in different amounts. Details on the synthesis route and characterization are added in the supplementary information.

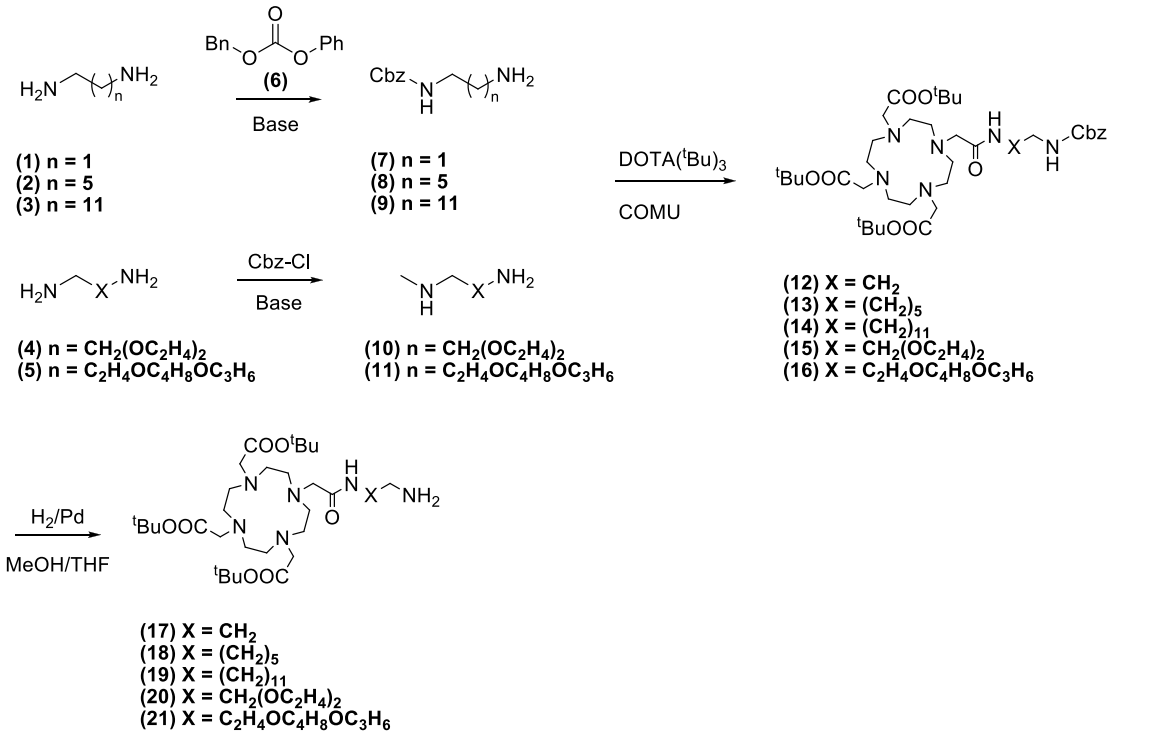

Figure 2: Synthesis of the (^{t}Bu)$_3$-DOTA ligands (17-21).

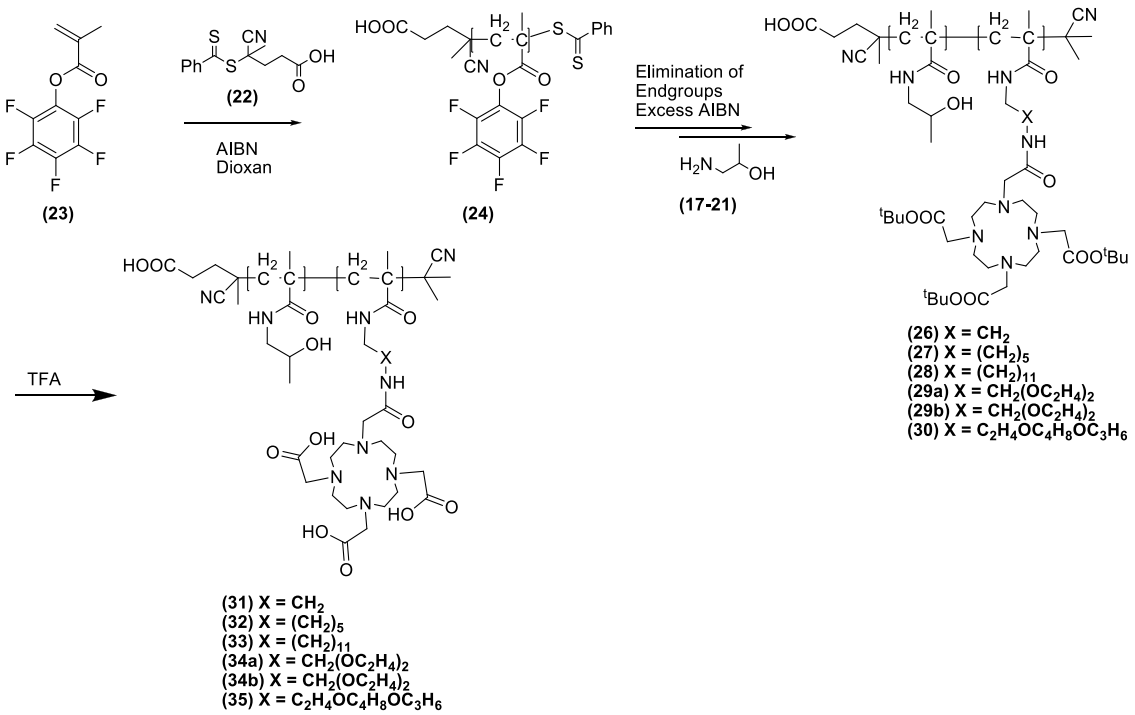

Figure 3. Synthesis of the HPMA-linker-DOTA systems (31-35)

2.2 Radiochemistry

Labeling with ^{68}Ga

Labeling of DOTA-conjugated HPMA-homopolymers was performed by mixing aliquots of polymer stock-solution (1 mg/mL in water) with post-processed ^{68}Ga eluate. Investigation of the needed amount of conjugate for labeling reaction was performed by varying time and concentration of DOTA-conjugated polymer using conjugate 31 with acetone post-processed ^{68}Ga and was adopted for all the other labeling reactions. Acetone post-processed eluate 400 µL N2 (97.56 % acetone/0.05 N HCl) containing 40-60 MBq of ^{68}Ga, was added to 3 mL 1 M NaAcetate containing the polymer and the reaction mixture was heated up to 95°C. In addition, labeling with HPMA homopolymer without DOTA-functionalization was performed under these conditions to investigate the unspecific binding. Additionally labeling with ethanol post-processed eluate was performed for conjugates (33-35). 1 mL N5 (90 % ethanol/0.9 N HCl) was added to 3 mL 1 M NaAcetate buffer containing polymer and the reaction mixture was heated up to 95°C for 30 min.

Labeling with ^{44}Sc

Labeling of DOTA-conjugated HPMA-homopolymers was performed with 250 µL polymer stock solution (1 mg/mL in water) in post-processed ^{44}Sc eluate (3 mL) and heating up to 95°C for 30 min.

Labeling with ^{177}Lu

Labeling of DOTA-conjugated HPMA-homopolymers was performed with 250 µL polymer stock-solution (1 mg/mL in water) with 150 µL 0.1 M NaAcetate buffer (pH = 8) and 100 µL ^{177}Lu, and heating up to 95°C for 30 min. The ratio polymer to ^{177}Lu was 10:1.

Purification of the labeled conjugates

The radiolabeled polymeric systems were cleaned from unreacted radiometal by Sephadex G-25 size exclusion chromatography (HiTrap™ Desalting Column, Sephadex G-25 Superfine, 0.9% NaCl, flow rate: 0.5 mL/min) leading to a pure, ^{68}Ga-labeled polymer solution ready for subsequent experiments.

Quality control

Quality control of complex formation was performed by radiothin-layer chromatography (radioTLC). The TLC plates were developed with 0.1 M citric buffer (pH = 4). Quantitative distribution of radioactivity on TLC plates was measured using an instant imager.

In vitro stability

Stability studies were performed with ^{68}Ga-labeled polymers of radiochemical purity > 98 % in physiological conditions and in presence of competing metals and chelates. Detailed set up is explained in the supplementary section.

3 RESULTS AND DISCUSSION

3.1 Organic Synthesis

For coupling reaction between the HPMA backbone and the bifunctional chelator, orthogonal amidation chemistry *via* active ester groups was selected. Synthesis of the amine terminated DOTA based ligands (17-21) from commercially available (^{t}Bu)$_3$-DOTA is depicted in figure 2. First, the commercially available α,ω-diamines (1-5) were mono-Cbz-protected. The protection was realized with benzylphenylcarbonate (6) for (1-3) [29] and with benzylchloroformate for (4-5). As reported in [34] the selectivity of the mono-Cbz-protection using (6) decreases with the length of the alkyl chain but achieves good yields for (1-3). Mono-Cbz-protection with (6) was ineffective for the alkoxy diamines (4-5) so benzylchloroformate was used instead obtaining good yields of the desired product. The following amidation of (^{t}Bu)$_3$-DOTA with (7-11) afforded the Cbz-protected (^{t}Bu)$_3$-DOTA ligands (12-16) in good yields of 66-79 %. The Cbz-protecting group was removed *via* hydrogenation to obtain the (^{t}Bu)$_3$-DOTA ligands (17-21) in almost quantitative yields (93-97 %).

The synthetic route to the HPMA-DOTA conjugates is depicted in figure 3. Starting from pentafluorophenyl methacrylate monomer (23) the precursor homopolymer (24) was synthesized according to literature [30-32]. The dithioester end group was removed by an excess of 2,2´-azo-bis-(isobutyronitrile) as described in literature [33] taking the advantage of circumventing side reactions during the next reaction steps. Functionalization of the polymeric precursor was obtained by aminolysis via the amine terminated (^{t}Bu)$_3$-DOTA ligands (17-21). The incorporation was calculated to be between 0.6 – 11 % DOTA for each conjugate. Addition of 2-

hydroxylamine lead to the polymeric structures (26-30). Entire conversion of the reactive ester groups was proved by means of ^{19}F-NMR spectroscopy, evidencing their complete disappearance of ^{19}F-signals of the polymeric backbone. In a final step the chelator was deprotected using TFA. The pure HPMA-DOTA conjugates, ready for labeling, could be obtained as white powders with good yields of 89 %, except conjugate (32), which could not be recovered from the dialysis flexible tube.

As intended, five different DOTA-conjugated polymer conjugates with relatively low polydispersity index (PDI) and therefore narrow molecular weight distribution have been achieved by RAFT polymerization and successfully functionalized in a following polymer analogous reaction. Their molecular weight average number (Mn), polydispersity index (PDI) and % of incorporated chelator are shown in table 2.

Table 2: Analytical data of the final HPMA-DOTA conjugates (31-35).

Polymer	M_n [g/mol]	PDI[a]	% DOTA[b]	Linker
(31)	15.000	1.3	11	(1)
(33)	12.000	1.2	1.6	(3)
(34a)	12.000	1.2	0.6	(4)
(34b)	12.000	1.2	1.2	(4)
(35)	13.000	1.2	3.5	(5)

[a]Determination by GPC in THF as solvent. [b]Determined by ^{1}H-NMR spectroscopy after polymer analogous reaction with 2-hydroxypropylamine.

Later on, in order to have only one variable for direct comparison (the conjugates so far presented different linker structures with different incorporation rates of DOTA), conjugate 31 was modified with different percentages of DOTA, affording the conjugates 31a-31c following the same synthesis route as described for conjugate 31 (Tab. 3).

Table 3: Analytical data of the final HPMA-DOTA conjugates (31 derivate).

Polymer	M_n [g/mol]	PDI[a]	% DOTA[b]	Linker
(31)	15.000	1.2	11	(1)
(31a)	14.000	1.2	4.8	(1)
(31b)	13.000	1.2	3.3	(1)
(31c)	13.000	1.2	1.6	(1)

[a]Determination by GPC in THF as solvent. [b]Determined by ^{1}H-NMR spectroscopy after polymer analogous reaction with 2-hydroxypropylamine.

3.2 Radiochemistry

Commonly used chelators in radiopharmacy are macrocyclic as they are able to form more stable complexes than acyclic ones. Nevertheless, DOTA derivatives generally require elevated temperatures for complex formation in contrast to acyclic chelators. Standard labeling procedures of DOTA derivatives use temperatures of about 95°C to form complexes with different radionuclides (e.g. ^{68}Ga, ^{44}Sc, ^{177}Lu), on that score, only 95°C was used as standard temperature for labeling experiments with the HPMA-DOTA conjugates. Nonspecific binding of the metal cation to nanoparticles is a basic problem in labeling those systems, investigation of nonspecific binding of ^{68}Ga to a HPMA polymer was performed with 20 nmol HPMA homopolymer without functionalization (Mn: 12.000 g/mol, 0% DOTA) utilizing the optimized protocol. The polymer presents no labeling with ^{68}Ga. Within 25 min less than 5 % of the radioactivity binds to the HPMA homopolymer (Fig. 4).

Figure 4 shows the kinetics of ^{68}Ga-(31) complexation. The accessible labeling yield is not influenced by the amount of conjugate used. Thereon, 20 nmol was used for further experiments. Labeling with generator derived and acetone post-processed ^{68}Ga in water is accomplished within 15 min at 95°C with RCY of 90 %. The complex formation is fast and efficient.

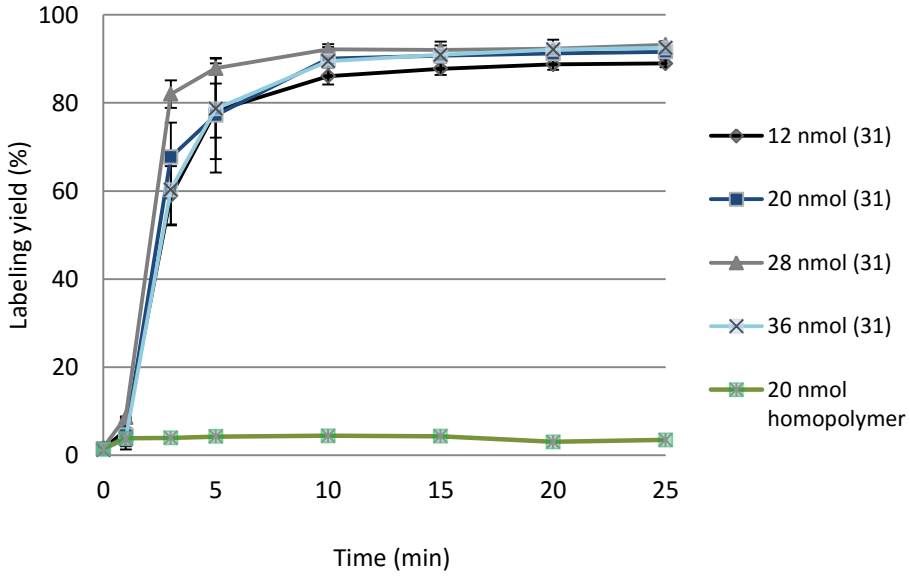

Figure 4: Comparison of the time course of ^{68}Ga complex formation with varying amount of HPMA-DOTA conjugate (31d) and polymer 20 not modified with DOTA as a control.

Labeling of all HPMA-DOTA-conjugates using the same conditions is shown in figure 5 and summarized in table 4. Within 15 min labeling yields of 44-92 % can be achieved. It was found that labeling efficiency depends on the length of the linker and the incorporation rate into polymer. Due to the short ethyl linker of (31) lower radiolabeling yields than for (33) with a dodecyl linker can be expected. This could obviously be, compensated by its high incorporation rate of 11 % DOTA. More explicit is the effect of incorporation rate for conjugates (34). 34b has twice as much DOTA incorporated (1.2%) as 34a (0.6%). Here the labeling yield lowers from 60 % for 34b to less than 5 % for 34a.

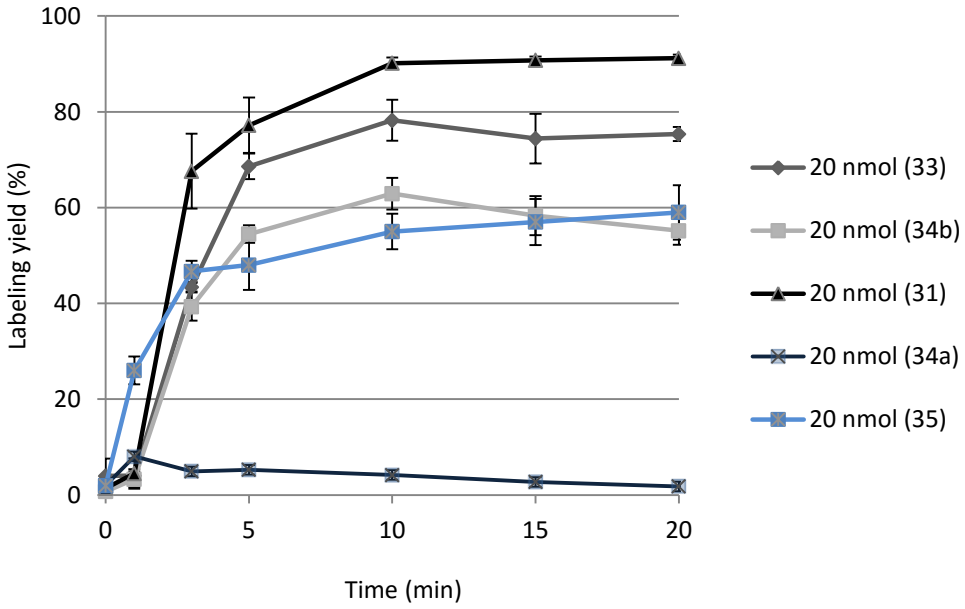

Figure 5: Labeling yield using acetone post-processed ^{68}Ga (20 nmol; 15 min; 95°C; n = 3)

Table 4: Labeling of HPMA-DOTA conjugates (31-35) using acetone and ethanol post-processed ^{68}Ga-eluate (20 nmol, 20 min, 95°C).

Polymer	Linker	% DOTA	RCY Acetone PP (%)	RCY Ethanol PP (%)
(31)	(1)	11	91 ± 1	98 ± 1
(33)	(3)	1.6	75 ± 2	97 ± 1
(34b)	(4)	1.2	55 ± 3	40 ± 8
(35)	(5)	3.5	45 ± 22	67 ± 6

Labeling is also affected by the linker structure. Conjugates (33) and (35) have the same chain length (n = 12) but differ in the structure. Conjugate (33) contain a dodecyl linker while the positions 4 and 9 are substituted with oxygen atoms in the linker chain of (35). This structural difference is reflected in the decreasing labeling yield from 75 % ((33)) to 45 % ((35)) although (33) has the lower DOTA incorporation rate (tab 2).

The influence of the DOTA incorporation rate in polymers with the same linker length is shown in figure 6. It can be observed that radiolabeling kinetics is not direct proportional to the amount of incorporated chelator. Faster radiolabeling kinetics are achieved for the polymer with lowest presence of DOTA (1.6%), followed by the polymer with higher amount of DOTA (11%). That could be explained by a possible steric interaction between chelators impeding coordination of radiometal, which will not be relevant for the polymer with highest amount of DOTA due to the compensation of total interactions with total amount of chelators. In any case, all conjugates showed quantitative radiolabeling yields after 25 min.

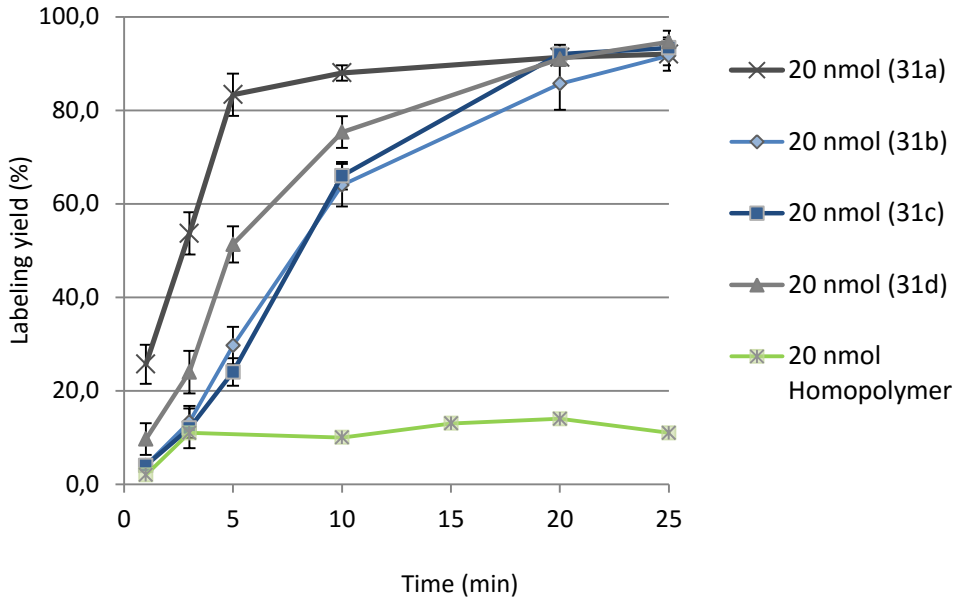

Figure 6: Radiolabeling yield of conjugates 31 utilizing acetone post-processed ^{68}Ga (20 nmol; 25 min; 95°C; n = 3).

Recently, benefit of additional use of organic solvents to facilitate more efficient radiolabeling was proven [35] and utilized in an ethanol-based post-processing [14]. It has been shown that this ethanol-based post-processing protocol increases significantly radiochemical yield even at lower temperature compared to the standard procedure for DOTATOC as model compound [14].

To take the advantage of additional ethanol, enhancing labeling yields, conjugate 33-35 were labeled utilizing this protocol too. Figure 7 shows the results of labeling conjugate (33) utilizing the two post-processing methods. Labeling with the ethanol post-processed ^{68}Ga in 1 M NaHEPES buffer leads to significantly increased yields of complex formation. The difference between both labeling procedures is accounted for 20 %. An additional advantage of the ethanol-based post-processing is the possibility to reduce the overall volume the labeling solution from 5.25 mL (acetone) to 2.25 mL (ethanol), and therefore to increase the specific activities.

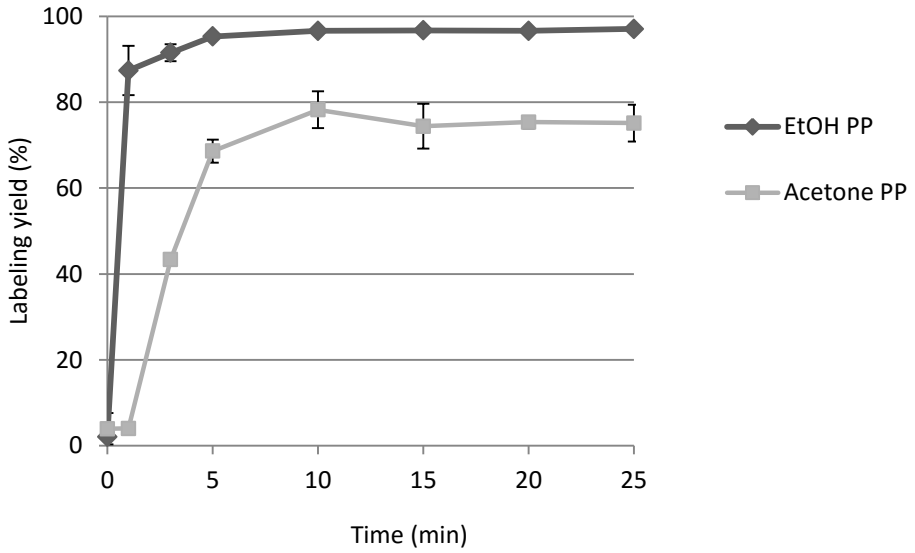

Figure 7: Comparison of labeling yields of (33) using EtOH and acetone post-processed ^{68}Ga (95°C; n = 3).

3.2.1 Purification of ^{68}Ga-labeled HPMA-DOTA-conjugates and quality control

After labeling, the polymeric systems could be purified fast and easy using Sephadex G-25 size exclusion chromatography. Over 90 % of the radiolabeled product can be collected in two fractions with radiochemical purity of >98 %. As the product is eluted from the column with 0.9 % NaCl the resulting solution could be directly used for in vivo studies.

Radiochemical analysis of complex formation with thin-layer chromatography (TLC) using 0.1 M citric buffer as mobile phase. The R_f values for free uncomplexed ^{68}Ga and labeled conjugates were determined as R_f (^{68}Ga) = 0.9 and R_f (^{68}Ga-conjugate) = 0. The R_f values for ^{44}Sc and ^{177}Lu utilizing the same method are the same as for ^{68}Ga 0.9.

3.2.2 Radiolabeling with ^{44}Sc

Scandium belongs to the transition metals group and its complex formation strongly depends on pH of aqueous solution as previously shown for ^{44}Sc-DOTATOC complex formation [31]. Utilizing the post-processing method leads to a final solution of ^{44}Sc in ammonium acetate buffer (pH 4) suitable for direct labeling [15]. Labeling with post-processed ^{44}Sc, in ammonium acetate buffer (pH 4), yields up to 95 % within 30 min for (31) (Fig. 6).

3.2.3 Radiolabeling with ^{177}Lu

Radiolabeling with ^{177}Lu is fast and efficient. Within 3 min reaction is completed and yields up to 97 % can be obtained for conjugated 31 (Fig. 8).

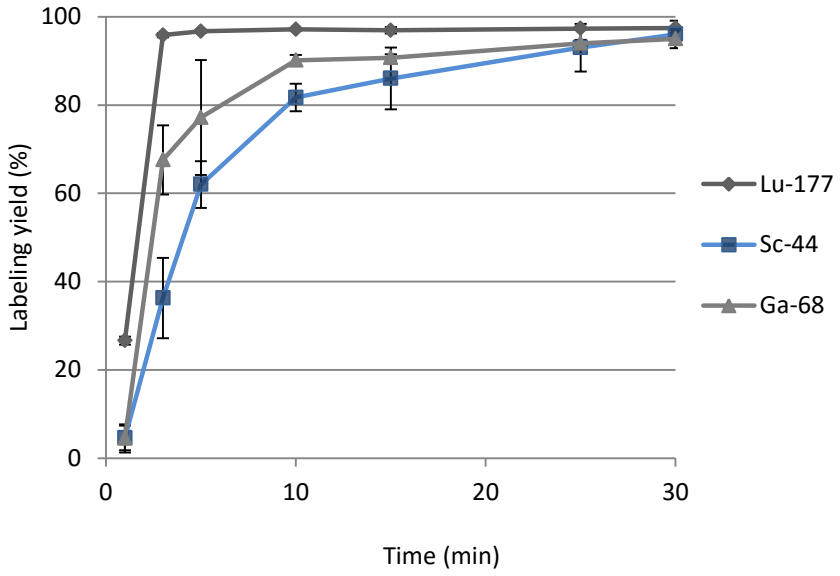

Figure 8: Labeling yields for (31) with ^{44}Sc, ^{68}Ga and ^{177}Lu (20 nmol; 30 min; 95°C; n = 3).

3.3 *In vitro* stability

Stability of the formed complex is a crucial factor in the development of new radiopharmaceuticals. It is necessary to guarantee the stability of the complex not less than two half-lives of the investigated biological process. Therefore several experiments were done to explore stability of the labeled conjugates in NaCl (used as final solvent), human serum, against transmetallation (Fe^{3+}; Ca^{2+}; Mg^{2+}) and transchelation (EDTA, DTPA).

Stability was determined for the HPMA-DOTA conjugates were first analysed in 0.9 % NaCl. The results for all conjugates are presented in figure 9. It indicates a higher stability of the labeled conjugates even after 2 h incubation at 37°C.

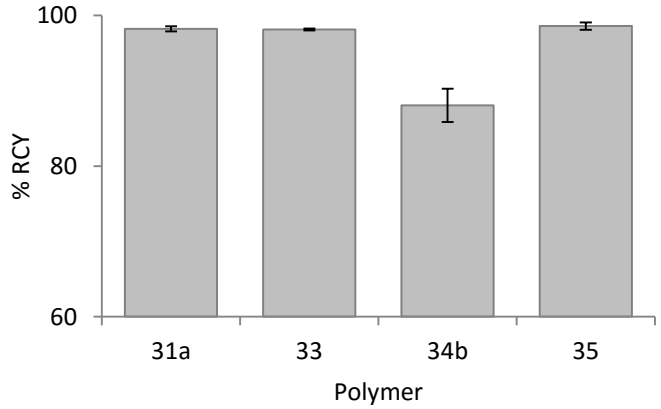

Figure 9: Stability of ^{68}Ga-labeled conjugates in 0.9 % NaCl within 120 min at 37°C (n = 3).

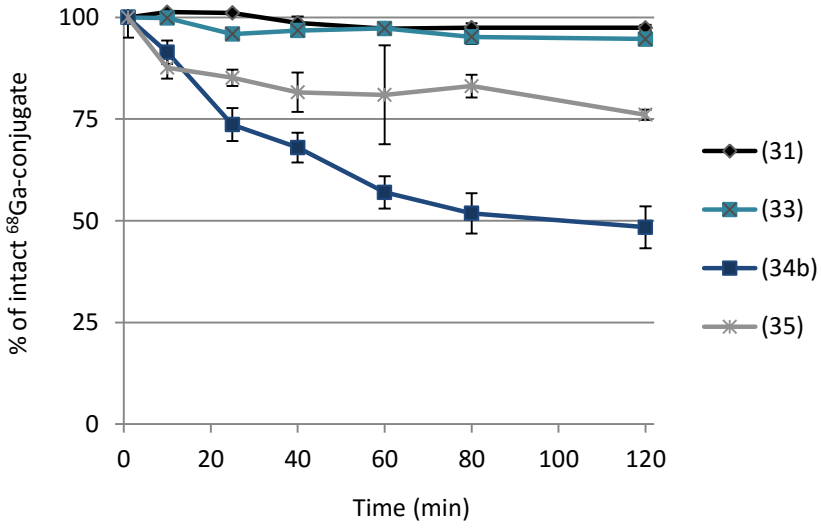

Figure 10: Stability of ^{68}Ga-labeled conjugates in HSA within 120 min at 37°C (n = 3).

In human serum the conjugates with alkyl linkers (31) and (33) indicate high stability. For both conjugates the percentage of intact ^{68}Ga-conjugate is higher than 95 %. Contrary to that the conjugates with alkoxy linker structure show higher decomposition rate that can be explained as a possible unstable complexation of Ga(III) with the oxygens present in the linker (Fig 10).

Presence of different metal cations (e.g. Fe^{3+}) in the final solution or in blood can cause transmetallation of radiolabeled conjugate and finally lead to a release of free radionuclide into solution. Therefore, it is necessary to determine prior to *in vivo* studies whether the conjugate forms stable complexes in presence of relevant metal cations or not.

Table 5: Stability of ^{68}Ga conjugates at 37°C in presence of different metal cations at 10^{-2} M concentrations (n = 3).

Conjugate	Linker	% DOTA	% of intact ^{68}Ga conjugate ± SD		
			Fe^{3+}	Mg^{2+}	Ca^{2+}
(31c)	(1)	1.6	94 ± 3	92 ± 1	92 ± 5
(33)	(3)	1.6	94 ± 9	69 ± 2	99 ± 2
(34a)	(4)	0.6	88 ± 2	80 ± 3	70 ± 1
(34b)	(4)	1.2	84 ± 2	86 ± 2	90 ± 1
(35)	(5)	3.5	74 ± 2	85 ± 1	83 ± 8

Conjugate 31 shows the highest stability against transmetallation (Tab. 5). Corresponding to the stability in HSA (34-35) are affected by addition of other metal cations. Within 120 min decomposition up to 30 % can be observed. More complex are the results for (33). This conjugate indicate high stability in experiments with HSA, Fe^{3+} and Ca^{2+} while a decomposition is observed for challenge studies against Mg^{2+}.

Similarly, stability against other complexing agents like EDTA and DTPA was investigated to check if transmetallation from HPMA-DOTA conjugate to competing ligand occurs. The results are shown in table 6.

Table 6: Stability of ^{68}Ga conjugates at 37°C in presence of EDTA or DTPA at molar ratio 100:1 of competing ligand to conjugate (n = 3) after 120 min.

Conjugate	Linker	% DOTA	% of intact ^{68}Ga conjugate ± SD	
			EDTA	DTPA
(31c)	(1)	1.6	92 ± 5	83 ± 1
(33)	(3)	1.6	90 ± 2	87 ± 1
(34a)	(4)	0.6	77 ± 2	59 ± 1
(34b)	(4)	1.2	80 ± 3	61 ± 1
(35)	(5)	3.5	78 ± 5	93 ± 1

4 CONCLUSIONS

Optimized conjugation of DOTA onto HPMA-backbone yielded several poly(HPMA)-linker-DOTA conjugates with different linker-structure and with variation of amount of DOTA. These derivatives can be labeled with various metallic radionuclides (^{68}Ga, ^{44}Sc, ^{177}Lu) linked to the HPMA-backbone. Labeling and stability of the produced conjugates were investigated in detail with the generator derived PET radionuclide ^{68}Ga.

It was observed that complex formation with ^{68}Ga depends on the incorporation rate of DOTA. A minimum of 1.6 % DOTA is enough to obtain labeling yields higher of 90 %. The linker structure also is a variable that influences on labeling efficiency. Alkoxy linker structure generally exhibit lower labeling yields than alkane linkers despite of similarly chain length and DOTA incorporation. Moreover it was observed that a short linker (two-carbon chain) is enough to provide quantitative radiolabeling yields. Another investigated effect is the radiolabeling in presence of ethanol, which is known to improve labeling efficacy. Utilizing the ethanol post-processed ^{68}Ga eluate enhances the labeling efficacy for all conjugates. In conclusion, ca. 1.5% of DOTA allow achieving quantitative radiolabeling, if the optimal conditions are applied.

These results are consistent with the transmetallation and transchelation values, where (31c) and (33) showed the highest stability against presence of other metal cations or competing ligands. The conjugates with alkoxy linker structure not only exhibit lower labeling yields, they also showed slightly lower stability even with comparable DOTA incorporation or linker length.
With regards to future *in vivo* evaluations special efforts were focused on stability studies of ^{68}Ga labeled conjugates. Only the conjugates with alkyl chains as linker structure ((31), (33)) provide high stability in all examined solutions: 0.9 % NaCl, human serum (HSA), metal cations (Fe^{3+}, Mg^{2+}, Ca^{2+}) and competing ligands (EDTA, DTPA). In addition labeling was successfully adopted for ^{44}Sc (PET imaging) and ^{177}Lu (therapy).
This study confirms the principle applicability of HPMA-conjugates for labeling with different radionuclides with established radiolabeling chemistry. Introducing as less than only 1.5% of DOTA chelator using a short linker chain, which facilitates the synthesis and efficiency of the polymer conjugates, it allows introduction of both diagnosis and therapeutic radiometals.

REFERENCES

[1] X. Ying, H. E. Wen, W. L. Wu, J. Du, J. Guo, W. Than, Y. Zhang, R. J. Li, T. Y. Yang, D. W. Shang, J. N. Lou, L. R. Zhang, Q. Zhang, Dual-targeting daunorubicin liposomes improve therapeutic efficacy of brain glioma in animals*. J. Control. Release* 141 (2010) 183-192.

[2] K. Kostarelos, D. Emfietzoglou, Liposomes as carriers of radionuclides: from imaging to therapy. J. Liposome Res. 9 (1999) 429-460.

[3] H. Hong, Y. Zhang, J. Sun, W. Cai, Molecular imaging and therapy of cancer with radiolabeled nanoparticles. Nano Today 4 (2009) 399-413.

[4] S. Sofou, Molecular imaging and therapy of cancer with radiolabeled nanoparticles. Int. *J. Nanomed.* 3 (2008) 181-199.

[5] A. J. L. Villaraza, A. Bumb, M. W. Brechbiel, Macromolecules, Dendrimers, and Nanomaterials in Magnetic Resonance Imaging: The Interplay between Size, Function, and Pharmacokinetics. 110 (2010) 2921-2959.

[6] H. Kobayashi, Y. Koyama, T. Barrett, Y. Hama, C. A. S. Regino, I. S. Shin, B.-S. Jang, N. Le, C. H. Paik, P. L. Choyke, Y. Urano, Multimodal Nanoprobes for Radionuclide and Five-Color Near-Infrared Optical Lymphatic Imaging. 1 (2007) 258-264.

[7] F. Rösch, R. P. Baum, Generator-based PET radiopharmaceuticals for molecular imaging of tumours: on the way to THERANOSTICS*. Dalton Trans.* 10 (2011) 6104-6111.

[8] D. V. Filosofov, N. S. Loktionova, F. Rösch, A ^{44}Ti/^{44}Sc radionuclide generator for potential nuclear-medical application of ^{44}Sc-based PET-radiopharmaceuticals. *Radiochim. Acta* 98 (2010) 149-156.

[9] L. F. Mausner, V. Joshi, K. L. Kolsky, G. E. Meinken, R. C. Mease, M. P. Sweet, S. C. Srivastava, Evaluation of chelating agents for radioimmunitherapy with scandium-47. *J. Nucl. Med*. 36 (1995) 104.

[10] W. A. P. Breeman, M. de Jong, E. de Blois, B. F. Bernard, M. Konijnenberg, E. P. Krenning, Radiolabelling DOTA-peptides with ^{68}Ga. *Eur J Nucl Med Mol Imaging* 32 (2005) 478-485.

[11] G.-J. Meyer, H. Mäcke, J. Schuhmacher, W. H. Knapp, M. Hofmann, ^{68}Ga-labelled DOTA-derivatised peptide ligands. Eur. *J. Nucl. Med. Mol. Imaging* 31 (2004) 1097-1104.

[12] K. P. Zhernosekov, D. V. Filosofov, R. P. Baum, P. Aschoff, H. Bihl, A. A. Razbash, M. Jahn, M. Jennewein, F. Rösch, Processing of Generator-Produced ^{68}Ga for Medical Application. *J. Nucl. Med*. 48 (2007) 1741-1748.

[13] D. Mueller, I. Klette, R. P. Baum, M. Gottschaldt, M. K. Schultz, W. A. P. Breeman, Simplified NaCl Based ^{68}Ga Concentration and Labeling Procedure for Rapid Synthesis of ^{68}Ga Radiopharmaceuticals in High Radiochemical Purity. Bioconjugate Chem. 23 (2012) 1772-1717.

[14] E. Eppard, M. Wuttke, P. L. Nicodemus, F. Rösch, Ethanol-based post-processing of generator derived ^{68}Ga towards kit-type preparation of ^{68}Ga-radiopharmaceuticals. *J Nucl Med (*2014); 55: 1023-1028

[15] M. Pruszynski, N. S. Loktionova, D. V. Filosofov, F. Rösch, Post-elution processing of ^{44}Ti/^{44}Sc generator-derived ^{44}Sc for clinical application. *Appl Rad Isotop* 2010;68: 1636-41

[16] J. Kopecek, H. Bazilova, Poly[N-(2-hydroxypropyl)methacrylamide]—I. Radical polymerization and copolymerization*. Eur. Polym J.* 9 (1973) 7-14.

[17] M. Bohdanecky, H. Bazilova, J. Kopecek, Poly[N-(2-hydroxypropyl)methacrylamide]—II. Hydrodynamic properties of diluted polymer solutions*. Eur. Polym J.* 10 (1974) 405-410.

[18] L. Sprincl, J. Vacik, J. Kopecek, D. Lim, Biological tolerance of poly(N-substituted methacrylamides*). J. Biomed. Mater. Res*. 5 (1971) 197-205.

[19] J. Kopecek, L. Sprincl, H. Bazilova, J. Vacik, Biological tolerance of poly(N-substituted methacrylamides). *J. Biomed. Mater. Res*. 7 (1973) 111-121.

[20] L. Sprincl, J. Kopecek, D. Lim, Effect of porosity of heterogeneous poly(glycol monomethacrylate) gels on the healing-in of test implants. *J. Biomed. Mater. Res.* 5 (1971) 447-458.

[21] L. Sprincl, J. Vacik, J. Kopecek, D. Lim, Biological tolerance of ionogenic hydrophilic gels. *J. Biomed. Mater. Res*. 7 (1973) 123-136.

[22] K. Ulbrich, L. Sprincl, J. Kopecek, Biocompatibility of poly(2,4-pentadiene-1ol). *J. Biomed. Mater. Res*. 8 (1974) 155-161.

[23] J. Kopecek, L. Sprincl, D. Lim, New types of synthetic infusion solutions. I. Investigation of the effect of solutions of some hydrophilic polymers on blood. *J. Biomed. Mater. Res*. 7 (1973) 179-191.

[24] J.Kopecek, L. Sprincl, Relationships between structure and biocompatibility. *Polim. Med.* 4 (1974) 109-117.

[25] P. A. Vasey, S. B. Kaye, R. Morrison, C. Twelves, P. Wilson, R. Duncan, A. H. Thomson, L. S. Murray, T. E. Hilditch, T. Murray, S. burtles, D. Fraier, E. Frigerido, J. Cassidy, Phase I Clinical and Pharmacokinetic Study of PK1 [N-(2-Hydroxypropyl)methacrylamide Copolymer Doxorubicin]: First Member of a New Class of Chemotherapeutic Agents - Drug-Polymer Conjugates*. Clin. Cancer Res.* 5 (1999) 83-94.

[26] J. M. Meerum Terwogt, W. W. ten Bokkel Huinink, J. H. M. Schellens, M. Schot, I. A. M. Mandjes, M. G. Zurlo, M. Rocchetti, H. Rosing, F. J. Koopman, J. H. Beijnen, Phase I clinical and pharmacokinetic study of PNU166945, a novel water-soluble polymer-conjugated prodrug of paclitaxel. *Anticancer Drugs* 12 (2001) 315-323.

[27] N. E. Schoemaker, C. van Kesteren, H. Rosing, S. Jansen, M. Swart, J. Lieverst, D. Fraier, M. Breda, C. Pellizzoni, R. Spinelli, M. G. Porro, J. H. Beijnen, J. H. M. Schellens, W. W. ten Bokkel Huinink, A phase I and pharmacokinetic study of MAG-CPT, a water-soluble polymer conjugate of camptothecin. Br. *J. Cancer* 87 (2002) 608-64.

[28] J. Kopecek, P. Kopecekova, T. Minko, Z.-R. Lu, HPMA copolymer-anticancer drug conjugates: design, activity, and mechanism of action. *Eur. J. Pharm. Biopharm.* 50 (2000) 61-81.

[29] M. Pittelkow, R. Lewinsky, J. B. Christensen, Selective Synthesis of Carbamate Protected Polyamines Using Alkyl Phenyl Carbonates. Synthesis 15 (2002) 2195-2202.

[30] M. Perez-Malo Cruz, F. Roesch, Improved efficacy of synthesis of ^{68}Ga radiopharmaceuticals in mixtures of aqueous solution and non-aqueous solvents. Eur. J. *Nucl. Med. Mol. Imag*. 39 (2012).

[31] M. Pruszynski, A. Majkowska-Pilip, N. S. Loktionova, E. Eppard, F. Roesch. Radiolabeling of DOTATOC with the long-lived positron emitter ^{44}Sc. *Appl. Rad. Isotop.* 70 (2012) 974-979.

Supporting Information

Labeling of HPMA-based polymer-conjugates with metallic radionuclides for theranostic applications

E. Eppard, A. de la Fuente, N. Mohr, M. Allmeroth, R. Zentel, F. Rösch

Contents

1 Experimental

I. Synthesis of Benzyl-phenyl-carbonate

Benzyl alcohol (0.64 mol, 69.21 g) and pyridine (0.79 mol, 64 mL) were mixed with 175 mL CH_2Cl_2. Within 1 h phenylchloroformate (0.64 mol, 100.21 g) was added drop wise. The reaction mixture was stirred for 3 h and then added to 250 mL H_2O. The organic phase was washed 2 x with 250 mL 2 M H_2SO_4, dried and concentrated under vacuum. Excess of benzyl alcohol was removed under vacuum and the residue dried under vacuum. The method gave 142.85 g (0.63 mol; 98 % yield) product as white solid. ^{1}H NMR (300 MHz, $CDCl_3$) δ (ppm) = 5.28 (s, 2H), 7.18 – 7.28 (m, 3H), 7.36 – 7.46 (m, 7H). MS (ESI) m/z (% rel Int) = 229.30 $[M-H]^+$, 251.35 $[M-Na]^+$

II Synthesis of mono-Cbz-protection of unprotected alkanediamines

Benzyl-phenyl-carbonate (5 mmol, 1.141 g) in 5 mL EtOH was added drop wise over a period of 1 h to a solution of α,ω-diamine (5 mmol) in 25 mL abs. EtOH at 0 °C. The reaction mixture was stirred at room temperature for 2 days, concentrated under vacuum and the residue added to 25 mL H_2O. The pH was adjusted to 3 with 4 N HCl and the aqueous phase extracted 3 x with 50 mL CH_2Cl_2. After adjusting the pH with 2 N NaOH to 11 N the aqueous phase was extracted 3x with 80 mL CH_2Cl_2. The organic phase was dried with $MgSO_4$ and evaporated under reduced pressure. The residue was then dried under vacuum to yield the product as white solid.

- Benzyl-2-aminoethylcarbamate (7)

(85 % yield). ^{1}H NMR (300 MHz, $CDCl_3$) δ (ppm) =1.43 (s, 2H), 2.75 – 2.79 (t, 2H), 3.17 – 3.21 (m, 2H), 5.08 (s, 2H), 5.44 (bs, 1H), 7.28 – 7.34 (m, 5H). MS (ESI) m/z (% rel Int) = 195.11 $[M-H]^+$, 217.10 $[M-Na]^+$

- Benzyl-6-aminohexylcarbamate (8)

(67 % yield). ^{1}H NMR (300 MHz, $CDCl_3$) δ (ppm) =1.25 (s, 2H), 1.32 – 1.50 (m, 8H), 2.65 – 2.69 (t, 2H), 3.15 – 3.20 (m, 2H), 5.09 (s, 2H), 5.44 (bs, 1H), 7.32 – 7.37 (m, 5H). MS (ESI) m/z (% rel Int) = 251.17 $[M-H]^+$, 274:20 $[M-Na]^+$

- Benzyl-12-aminododecylcarbamate (9)

(50 % yield). ^{1}H NMR (300 MHz, $CDCl_3$) δ (ppm) =1.25 (s, 16H), 1.40 – 1.50 (m, 4H), 2.67 – 2.72 (t, 2H), 3.15 – 3.22 (m, 2H), 5.09 (s, 2H), 5.44 (bs, 1H), 7.33 – 7.37 (m, 5H). MS (ESI) m/z (% rel Int) = 335.26 $[M-H]^+$, 357.26 $[M-Na]^+$

III. Synthesis of mono-Cbz-protection of unprotected alkoxydiamines

Alkoxydimamine (20 mmol) and Na_2CO_3 (2 g) were mixed in 50 mL $CHCl_3$ and cooled to 0°C. To this solution Cbz-Cl (10 mmol, 1.612 g) was added drop wise within 2 h. The mixture was stirred 2 h at 0°C, then 1 day at RT. After concentration the residue was added to 25 mL H_2O. pH was adjusted to 3 with 4 N HCl and then the mixture was extracted 3x with 50 mL CH_2Cl_2. After adjusting the pH with 2 N NaOH to 11 the aqueous phase was extracted 3x with 80 mL CH_2Cl_2. The organic phase was dried with Na_2SO_4 and concentrated under reduced pressure. The residue was dried under vacuum to yield the product as white solid.

- Benzyl-2-(2-(2-aminoethoxy)ethoxy)ethylcarbamate (10)
(47 % yield). ^{1}H NMR (300 MHz, $CDCl_3$) δ (ppm) =1.53 (s, 2H), 2.78 – 2.81 (t, 2H), 3.32 – 3.37 (m, 2H), 3.43 – 3.49 (m, 6H), 3.50 – 3.59 (m, 6H), 5.06 (s, 2H), 7.28 – 7.32 (m, 5H). MS (ESI) m/z (% rel Int) = 283.12 $[M-H]+$, 305.14 $[M-Na]^+$

- Benzyl-3-(4-(3-aminopropoxy)butoxy)propylcarbamate (11)
(39 % yield). ^{1}H NMR (300 MHz, $CDCl_3$) δ (ppm) =1.56 – 1.67 (m, 8H), 2.74 – 2.76 (m, 2H), 3.22 – 3.29 (m, 2H), 3.36 – 3.45 (m, 10H), 5.05 (s, 2H), 7.27 – 7.32 (m, 5H). MS (ESI) m/z (% rel Int) = 339.20 $[M-H]^+$, 361.24 $[M-Na]^+$

IV. Coupling of mono-Cbz-protected spacers to DOTA-$(tBu)_3$

DOTA-$(tBu)_3$ (0.035 mmol; 20 mg), mono-Cbz-protected amine (0.052 mmol) and TMP (0.08 mmol; 9 mg) were dissolved in 5 mL NMP and cooled to 0°C. COMU (0.055 mmol; 23.5 mg) was dissolved in 2 mL NMP, added drop wise to the mixture and stirred 15 min at 0°C and 2 h at RT. The mixture was then diluted with 20 mL EtOAc and extracted 3x with 20 mL 0.1 N HCl, $NaHCO_3$ and Brine. The organic phase was dried and concentrated under reduced pressure. The product was achieved as colourless oil.

-^{t}Butyl-2,2´,2´´-(10-(2-(2-(benzoyloxycarbonylamino)ethylamino)-2-oxoethyl)-1,4,7,10-tetraazacyclodo-decane-1,4,7-triyl)triacetate (12)
(75% yield). ^{1}H NMR (300 MHz, $CDCl_3$) δ (ppm) =1.45 (s, 27H), 1.63 (s, 8H), 2.50 – 3.50 (bm, 20H), 5.06 (s, 2H), 7.31 – 7.35 (m, 5H). MS (ESI) m/z (% rel Int) = 749.48 $[M-H]+$, 771.36 $[M-Na]^+$

-^{t}Butyl-2,2´,2´´-(10-(2-(6-(benzoyloxycarbonylamino)hexylamino)-2-oxoethyl)-1,4,7,10-tetraazacyclodo-decane-1,4,7-triyl)triacetate (13)

(72% yield). ^{1}H NMR (300 MHz, $CDCl_3$) δ (ppm) =1.15 – 1.30 (m, 10H), 1.33 - 153 (s, 27H), 1.98 (s, 2H) 2.32 – 3.24 (bm, 24H), 5.07 (s, 2H), 7.26 – 7.35 (m, 5H). MS (ESI) m/z (% rel Int) = 805.58 [M-H]+, 827.44 $[M-Na]^+$

-^{t}Butyl-2,2´,2´´-(10-(2-(12-(benzoyloxycarbonylamino)dodecylamino)-2-oxoethyl)-1,4,7,10-tetraazacyclo-dodecane-1,4,7-triyl)triacetate (14)
(66% yield). ^{1}H NMR (300 MHz, $CDCl_3$)) δ (ppm) =1.24 – 1.35 (m, 37H), 2.00 – 2.99 (s, 16H) 3.15 – 3.73 (bm, 10H), 5.05 (s, 2H), 7.28 – 7.39 (m, 5H). MS (ESI) m/z (% rel Int) = 889.64 $[M-H]^+$, 911.59 $[M-Na]^+$

-^{t}Butyl-2,2´,2´´-(10-(3,14-dioxo-1-phenyl-2,8,10-trioxa-4,13-diazapentadecan-15-yl)-1,4,7,10-tetraaza-cyclododecane-1,4,7-triyl)triacetate (15)
(70% yield). ^{1}H NMR (300 MHz, $CDCl_3$) δ (ppm) =1.24 – 1.35 (m, 37H), 2.00 – 2.99 (s, 16H) 3.15 – 3.73 (bm, 10H), 5.05 (s, 2H), 7.28 – 7.39 (m, 5H). MS (ESI) m/z (% rel Int) = 837.58 $[M-H]^+$, 859.50 $[M-Na]^+$

-^{t}Butyl-2,2´,2´´-(10-(3,18-dioxo-1-phenyl-2,8,13-trioxa-4,17-diazanondecan-19-yl)-1,4,7,10-tetraazacyclo-dodecane-1,4,7-triyl)triacetate (16)
(79% yield). ^{1}H NMR (300 MHz, $CDCl_3$) δ (ppm) =1.24 – 1.30 (m, 10H), 1.40 – 1.49 (s, 27H), 1.52 – 1.61 (m, 4H), 1.66 – 1.79 (m, 4H), 2.20 – 2.99 (s, 16H) 3.15 – 3.73 (bm, 20H), 5.05 (s, 2H), 7.28 – 7.39 (m, 5H). MS (ESI) m/z (% rel Int) = 893.52 [M-H]+, 915.55 $[M-Na]^+$

V. Hydrogenation

Pd/C (30 mg), 0.06 mmol of the compounds (12-16) were mixed in 5 mL THF:MeOH (1:1) and stirred for 4 h under H_2-atmosphere at RT. The mixture was passed over celite, concentrated and dried under vacuum. The product was achieved as colourless oil.

-^{t}Butyl-2,2´,2´´-(10-(2-(2-ethylamino)-2-oxoethyl)-1,4,7,10-tetraazacyclododecane-1,4,7-triyl)triacetate (17)
(96% yield). ^{1}H NMR (300 MHz, $CDCl_3$) δ (ppm) =1.45 (s, 27H), 1.63 (s, 8H), 2.50 – 3.50 (bm, 20H)

-^{t}Butyl-2,2´,2´´-(10-(2-(6-aminohexylamino)-2-oxoethyl)-1,4,7,10-tetraazacyclododecane-1,4,7-triyl)-triacetate (18)
(97% yield). ^{1}H NMR (300 MHz, $CDCl_3$) δ (ppm) =1.15 – 1.30 (m, 10H), 1.33 - 153 (s, 27H), 1.98 (s, 2H) 2.32 – 3.24 (bm, 24H)

-^{t}Butyl-2,2´,2´´-(10-(2-(12-aminododecylamino)-2-oxoethyl)-1,4,7,10-tetraazacyclododecane-1,4,7-triyl)-triacetate (19)
(93% yield). ^{1}H NMR (300 MHz, $CDCl_3$) δ (ppm) =1.24 – 1.35 (m, 37H), 2.00 – 2.99 (s, 16H) 3.15 – 3.73 (bm, 10H)

-^{t}Butyl-2,2´,2´´-(10-(2-(2-(2-(2-aminoethoxy)ethoxy)ethylamino)-2-oxoethyl)-1,4,7,10-tetraazacyclodo-decane-1,4,7-triyl)triacetate (20)
(96% yield). ^{1}H NMR (300 MHz, $CDCl_3$) δ (ppm) =1.24 – 1.35 (m, 37H), 2.00 – 2.99 (s, 16H) 3.15 – 3.73 (bm, 10H)

-^{t}Butyl-2,2´,2´´-(10-(2-(3-(4-(3-aminopropoxy)butoxy)propylamino)-2-oxoethyl)1,4,7,10-tetraazacyclo-dodecane-1,4,7-triyl)triacetate (21)
(94% yield). ^{1}H NMR (300 MHz, $CDCl_3$) δ (ppm) =1.24 – 1.30 (m, 10H), 1.40 – 1.49 (s, 27H), 1.52 – 1.61 (m, 4H), 1.66 – 1.79 (m, 4H), 2.20 – 2.99 (s, 16H) 3.15 – 3.73 (bm, 20H)

VI Synthesis of 4-Cyano-4-((thiobenzoyl)sulfanyl)pentanoic acid (CTP) (22)

4-Cyano-4-((thiobenzoyl)sulfanyl)pentanoic acid was used as chain transfer agent (CTA) and synthesized according to the literature [1].

*VII. Synthesis of p*entafluorophenyl methacrylate (PFPMA) (23)

Pentafluorophenyl methacrylate was prepared according to reference [2].

VIII. Synthesis of reactive ester homopolymers (macro-CTA) (24)

RAFT polymerization of pentafluorophenyl methacrylate with 4-cyano-4-((thiobenzoyl)sulfanyl)pentanoic acid was carried out in a schlenk tube [3, 4]. For this purpose, 4 g of PFPMA were dissolved in 5 mL of absolute dioxane, furthermore CTP and AIBN were added. The molar ratio of CTP/AIBN was chosen 1:8. After three freeze-vacuum-thaw cycles, the mixture was immersed in an oil bath at 65 °C and stirred overnight. Afterwards, the polymeric solution was precipitated three times in hexane, centrifuged and dried under vacuum at 40 °C overnight. A slightly pink powder was obtained. (52% yield). ^{1}H-NMR (300 MHz, $CDCl_3$) δ (ppm): 1.20-1.75 (br), 2.00-2.75 (br s). ^{19}F-NMR (400 MHz, $CDCl_3$) δ (ppm): -162.03 (br), -156.92 (br), -152 to -150 (br)

IX. Removal of dithioester end groups

The dithiobenzoate end group was removed using the protocol reported by Perrier et al. 2005 [5]. Therefore a 25-fold molar excess of AIBN was added to the polymer dissolved in dioxane. After 4 h of heating the solution in an oil bath at 70 °C, the polymer was precipitated twice in hexane and collected by centrifugation. The polymer was dried under vacuum overnight, a colourless powder was obtained. Yield: 75 %. Removal of the dithioester end group could be proven by UV-Vis spectroscopy.

IX. Synthesis of DOTA derivatives

For radioactive labeling of homopolymers the protocol was applied as follows. 180 mg of poly(PFPMA) homopolymer was dissolved in 2 mL of absolute dioxane. 0.11 mmol of DOTA-spacer (17-21) and 11 mg of triethylamine were diluted in abs. DMSO and added to the vessel. After stirring for 36 h at 45 °C, 45 mg of 2-hydroxypropylamine and 61 mg of Et_3N were added and the solution further stirred for 48 h. For final removal of reactive ester side groups 45 mg of 2-hydroxypropylamine were additionally added the next morning. The solution was finally prepared in a DMSO/water mixture for dialysis. After lyophilisation a white, crystalline powder could be obtained. (51%-55% yield). ^{1}H-NMR (400 MHz, d. DMSO) δ (ppm): 0.60-1.40 (br), 1.35-1.45 (s), 1.45-2.20 (br), 2.75-3.10 (br), 3.50-3.80 (br), 4.60-4.80 (br)

X. D*eprotection of homopolymers*

The polymer was dissolved in acetonitrile and TFA was added (1:1). This solution was stirred 4 h at RT. For purification dialysis over 2 days was used. The product was obtained as white powder. Yield: 89-92 %; (Exception: It was not possible to recover the purified conjugate (32) from the dialysis flexible tube) ^{1}H-NMR (400 MHz, d. DMSO) δ (ppm): 0.60-1.40 (br), 1.45-2.20 (br), 2.75-3.10 (br), 3.50-3.80 (br), 4.60-4.80 (br)

XI. *In vitro stability*

Stability studies were performed with ^{68}Ga-labeled polymers of radiochemical purity > 98 %. Stability studies in 0.9 % NaCl and human serum were performed by addition 50 µL of purified product to 500 µL of pre-warmed NaCl or human serum. Solutions were incubated for 2 h at 37 °C. Stability of ^{68}Ga-labeled product was also monitored in solutions containing different metal cations (Fe^{3+}, Ca^{2+}, Mg^{2+}) at concentration levels of 10^{-2} M each. 50 µL purified product were

added to 500 µL of an aqueous solution containing one of the metal cations. Solutions were incubated for 2 h at 37 °C. Studies with ETDA or DTPA solutions were also performed to check the stability of labeled product in presence of competing chelating ligands. The aliquot of purified product were added to DTPA or EDTA solutions in 0.9 % NaCl with a final molar ratio of 100:1. The final volume of the solution was 550 µL. Solutions were incubated for 2 h at 37 °C. From all studied solutions aliquots were taken after 1, 10, 25, 40, 60, 80 and 120 min and analysed by TLC.

2 REFERENCES

[1] E. R. G. Moad, S. H. Thang, Living Radical Polymerization by the RAFT process. *Aust. J. Chem.* 58 (2005) 379-410.

[2] M. Eberhardt, R. Mruk, R. Zentel, P. Théato, Synthesis of pentafluorophenyl(meth)acrylate polymers: New precursor polymers for the synthesis of multifunctional materials. *Eur. Polym. J.* 41(7) (2005) 1569-1575.

[3] P. Theato, Synthesis of well-defined polymeric activated esters. J. Polym. Sci., Part A: *Polym. Chem*. 46(20) (2008) 6677-6687.

[4] M. Barz, R. Luxenhofer, R. Zentel, A. V. Kabanov, The uptake of N-(2-hydroxypropyl)-methacrylamide based homo, random and block copolymers by human multi-drug resistant breast adenocarcinoma cells. *Biomat*. 30 (2009) 5682-5690.

[5] S. b. Perrier, P. Takolpuckdee, C. A. Mars, Reversible Addition-Fragmentation Chain Transfer Polymerization: End Group Modification for Functionalized Polymers and Chain Transfer Agent Recovery. *Macromol.* 38(6) (2005) 2033-2036.

3.2 ^{68}Ga-, ^{111}In-oxine: A novel strategy of *in situ* radiolabelling of HPMA-based micelles

^{68}Ga-,^{111}In-oxine: A novel strategy of *in situ* radiolabelling of HPMA-based micelles

A. de la Fuente[1], S. Kramer[2], N. Mohr[2], S. Pektor[3], N. Bausbacher[3], R. Zentel[2], F. Rösch[1]

[1] Institute of Nuclear Chemistry, Johannes Gutenberg-University, Fritz-Straßmann-Weg 2, 55128 Mainz, Germany

[2] Institute of Organic Chemistry, Johannes Gutenberg-University, Duesbergweg 10-14, 55128 Mainz, Germany

[3] Department of Nuclear Medicine, University Medical Center Johannes Gutenberg-University, Langenbeckstrasse 1, 55131 Mainz

ABSTRACT

Polymeric micelles are of increasing interest as drug delivery vehicles since they can accumulate in tumor tissue through EPR effect and be visualized no invasively by nuclear imaging techniques. A novel fast and efficient technique for radiolabelling the biocompatible HPMA-LMA based polymer with metal radionuclides was investigated. Promising *in vitro* stability results lead to *in vivo* evaluation in healthy mice.

Methods:

Different amphiphilic HPMA-LMA based polymers were synthesized by controlled radical polymerization. Hydrophobic ^{68}Ga-, ^{111}In-oxine complexes were spontaneously incorporated into the micellar core within 1 min at room temperature. Stability of purified micelles was analyzed in NaCl 0.9% and in human serum. *In vivo* behaviour of radiolabelled micelles was evaluated 1, 4 and 24 h post injection in healthy mice.

Results:

^{68}Ga- and ^{111}In-oxine complexes were formed quantitatively at 40 °C in 10 min. The incorporation rates for ^{68}Ga-^{111}In- oxine into the micellar core were 79% ± 4 for the random copolymer, 92% ± 2 for the block copolymer and 97% ± 1 for the PEGylated block copolymer. Stability in HS was of c.a 60% after 30 min for random and after 2 h for the block micelles. Stability of PEGylated block micelles was of 91% ± 3 after 2 h and 87% after 2 days; however e*x vivo* studies showed c.a 15 % stability after 24 h p.i.

Conclusions:

Fast and high incorporation of ^{68}Ga/^{111}In-oxine into the micellar core of HPMA-LMA based polymers was achieved within one minute. PEGylated block copolymer presented the highest labelling efficacy and *in vitro* stability. Unfortunately e*x vivo* evaluation in healthy mice showed low stability *in vivo* already after 1 hour post injection. Satability of such structure needs to be further investigated to build a stable entity *in vivo*.

Keywords: HPMA, micelles, PET, SPECT, ^{68}Ga, ^{111}In

1 INTRODUCTION

Recently, polymer micelles have been under focus as a versatile nanomedicine platform for drug delivery systems, particularly for anticancer applications [1]. Bader *et al.* initiated the approach of introducing block copolymer micelles as drug vehicles with the concept of mimicking lipoprotein structures [2].

Micelles are formed by self-assembly of amphiphilic copolymers, consisting of both hydrophobic and hydrophilic blocks, in aqueous solution.
Their inner hydrophobic core serves as a reservoir for hydrophobic compounds, which are either physically entrapped or chemically attached, while the hydrophilic shell is responsible for the colloidal stability and protects them against protein adsorption and opsonisation during circulation, resulting in prolonged circulation times.

The size of polymeric micelles (ranging from 200 to 10 nm) and their long circulation, allows for accumulation in pathological sites with leaky vasculature (e.g. tumors), through the enhanced permeability and retention (EPR) effect [3].
Furthermore, it has been shown that random amphiphilic copolymers are able to mediate drug delivery over biological barriers into the brain [4].
Therefore, polymeric micelles have been recognized as a desirable and attractive class of drug carriers.

To select promising candidates at an early stage of research and development, imaging approaches are essential [5]. By visualizing pharmacokinetics *in vivo*, the influence of specific characteristics such as charge or hydrophilic-lipophilic balance affecting the behaviour of carrier systems can be studied, which is necessary to optimize the preparation and formulation of carrier systems and to guide the way to a new generation of nanomedicines.

Positron emission tomography (PET) and single photon emission computed tomography (SPECT) are both non-invasive, quantitative and whole body molecular imaging techniques that provide information of the *in vivo* behaviour of the labelled biomolecule.

In order to be able to use these techniques, PET and SPECT radionuclides, as listed in table 1, are commonly used. The challenge consists in selectively incorporate them into the micelles.

Table 1: Nuclear characteristics of selected PET and SPECT nuclides for molecular imaging [6].

Nuclide	t ½	Decay (%)	Production
^{68}Ga	67.7 min	β^+ (89) EC (11)	^{68}Ge/^{68}Ga generator
^{18}F	109.7 min	β^+(89) EC(11)	^{18}O (p,n) ^{18}F
^{44}Sc	4.0 h	β^+(94)	^{44}Ti/^{44}Sc generator
^{124}I	4.2 h	β^+ (89) EC (11)	^{124}Te (p,n) ^{124}I ^{124}Te(d,2n) ^{124}I
^{64}Cu	12.7 h	β^+ (17) EC (44)	^{64}Ni (p,n)^{64}Cu
^{90}Nb	14.6 h	β^+ (53) EC (47)	^{90}Zr(p,n) ^{90}Nb
^{76}Br	16.2 h	β^+ (55) EC (45)	^{76}Se (p,n) ^{76}Br
^{99m}Tc	6.0 h	IT (100)	^{99}Mo/^{99m}Tc generator
^{111}In	2.8 d	EC (100)	^{112}Cd (p,2n) ^{111}In

The structure of the nanocarrier micellar system as well as the radiolabeling strategy need to be designed to guarantee a stable radiolabelled compound for *in vivo* applications.

The chemistry to incorporate such radionuclides can be divided into two general types depending on the characteristics of the nuclide: covalent and ionic.

In covalent chemistry, examples of such nuclides are ^{18}F, ^{11}C, ^{76}Br and $^{123/124}$I, the nuclide is incorporated as ^{11}C-carbon or radiohalogen-carbon bond. In most cases, those nuclides do not significantly alter the structure or the pharmacokinetics of the radiolabelled compound, but the chemical procedures are often lengthy, tedious and providing low yields.

In contrast, radiometals are introduced in forms of coordination chemistry. Bifunctional chelator are needed when metallic radioisotopes such as ^{68}Ga, ^{44}Sc, ^{90}Nb, ^{99m}Tc are involved. Bifunctional chelators have a metal binding moiety, which allows complexation of the radionuclide in its cavity and a chemical reactive functional group for covalent attachment to the biomolecule of interest.

For stable complexation, chelating agents based on polyamino carboxylic acids e.g. diethylene triamine pentaacetic acid (DTPA) or 1,4,7,10-tetraazacyclododecane-N,N'',N''',N''''-tetraacetic acid (DOTA) are commonly used in radiopharmacy, as they provide high thermodynamic stability of the complex. Radiolabelling typically is fast and proceeds in aqueous solution. Moreover, chemical properties of the radiolabelled product may be altered due to the prerequisite of a rather large chelating group [7].

Typically, the chelating agent itself is rather large, bulky and charged and as a result influences the particle structure and consequently its biological behaviour [8]. In this context, we have developed a novel radiolabelling strategy that applies to micelles and overcomes the drawbacks of both radiolabelling strategies. Taking profit of the micelles capacity to spontaneously incorporate hydrophobic drugs [9], a hydrophobic *Me(III)-ligand complex, has been introduced into the micellar core with no requirement of previous modification of the polymers with a chelator. Furthermore, high radiolabelling yields have been achieved in contrast to non-metallic radiolabelling strategies.

^{68}Ga-oxine has been identified as the hydrophobic *Me(III)-ligand complex. For the experiments, different structures of the well-known biocompatible HPMA polymer [10] modified with the hydrophobic moiety LMA have been studied as well as the stability of the labelled micelles in presence of human serum and NaCl 0.9%. Figure 1 schematically represents the labelling strategy.

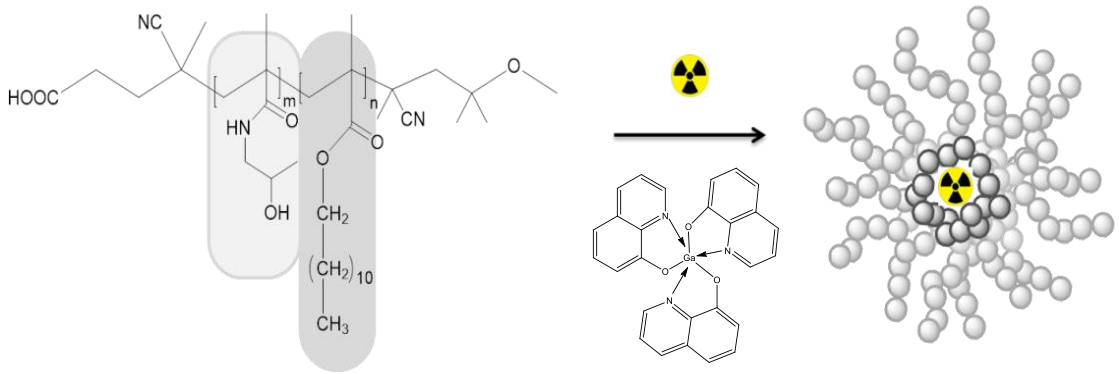

Figure 1: Illustration of the novel labelling strategy of HPMA-based micelles.

1.1 HPMA as a building block of micelle-forming copolymers

Poly[N-(2-hydroxypropyl)methacrylamide] (pHPMA) is a hydrophilic polymer currently under investigation for its use in polymer–drug conjugates. Its biocompatibility, non-immunogenicity and the possibility for functionalization are properties that resulted in broad pharmaceutical and biomedical applications, also in the micelle technology research.

Being hydrophilic, it can serve as a micellar stealth corona, while it can also be modified with hydrophobic moieties such as lauryl meta acrylate (LMA), to serve as a micellar core in which hydrophobic drugs can be solubilized and retained [3,9], therefore in the present study, HPMA was modified with hydrophobic LMA moieties and additionally, the block copolymer was modified with PEG moieties owing to its shielding efficacy and stabilization properties reducing micelles aggregation size [11] (Fig.2).

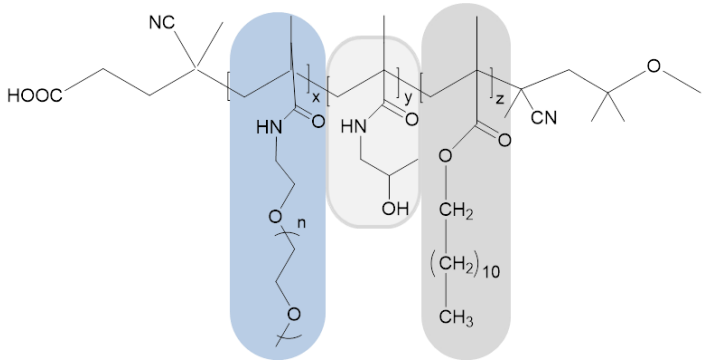

Figure 2: HPMA based polymer backbone: left PEG moiety, middle HPMA, right LMA.

As result of the influence of the additive PEG groups on the physical, chemical and biological properties of the micellar nanocarriers [3], the loading capacity and the drug release profile in presence of human serum and saline for the following three different polymeric structures (random copolymer, block copolymer, PEGylated block copolymer) were investigated using ^{68}Ga-oxine as model drug.

1.1.1 Random copolymer

Random copolymers contain many independent hydrophobic groups spread throughout the hydrophilic polymer chain, therefore in aqueous solution the structure of the micelles are not well defined as hydrophobic groups can be present in the corona (Fig. 3a).

1.1.2 Block copolymer

Block copolymers are composed of well-separated hydrophilic and hydrophobic blocks, the hydrophilic exterior provides steric stabilization/shielding and the hydrophobic core enables the facile entrapment of lipophilic drugs [12] (Fig. 3b).

1.1.3 PEGylated block copolymer

Increasing the hydrophilicity of the hydrophilic HPMA block by incorporation of highly hydrophilic PEG segments is a promising concept to decrease aggregate size by increasing steric stabilization. In addition, PEG is known for its shielding efficacy towards opsonic proteins [11] (Fig. 3c).

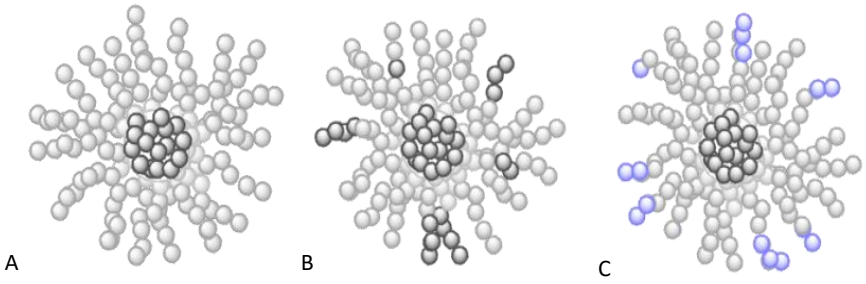

Figure 3: schematic structures of polymeric micelles formed by a) random polymer b) block copolymer c) PEGylated block copolymer

2 MATERIALS AND METHODS

2.1 Materials

All chemicals were analytical or pure reagent grade and used as received unless otherwise specified.

Deionized Milli-Q water (18.2 MΩ•cm; Millipore) was used in all organic reactions. Dioxane was distilled over a sodium/potassium composition. Lauryl methacrylate was distilled to remove the stabilizer and stored at -18 °C. 2,2'-Azo-bis-(isobutyronitrile) (AIBN) was recrystallized from diethyl ether and stored at -18 °C as well. ^{1}H-NMR spectra were obtained by a Bruker AC 300 spectrometer at 300 MHz, ^{19}F-NMR analysis was carried out with a Bruker DRX-400 at 400 MHz. All measurements were accomplished at room temperature. The synthesized polymers were

dried at 40 °C under vacuum overnight, followed by Gel Permeation Chromatography (GPC). GPC was performed in tetrahydrofuran (THF) as solvent, using following equipment: pump PU 1580, autosampler AS 1555, UV detector UV 1575 and RI detector RI 1530 from Jasco as well as a miniDAWN Tristar light scattering detector from Wyatt. Columns were used from MZ Analysentechnik, 300x8.0 mm: MZ-Gel SDplus 106 Å 5 µm, MZ-Gel SDplus 104 Å 5 µm and MZ-Gel SDplus 102 Å 5 µm. GPC data were evaluated by using the software PSS WinGPC Unity (Polymer Standard Service Mainz, Germany). The flow rate was set to 1 mL/min with a temperature of 25 °C.

Commercial generators based on TiO_2 were obtained from Cyclotron Co. Ltd (Obninsk, Russia). The cation exchange resins AG 50W-X8 (- 400 mesh), AG 50W-X4 (200 – 400 mesh) and AG 50W-X8 (200 - 400 mesh) were obtained from Bio-Rad (Munich, Germany). HiTrap™ Desalting Columns were purchased from GE-Healthcare Europe GmbH (Freiburg, Germany). TraceSelect water (Sigma-Aldrich, Germany) was used for all aqueous radiolabeling solutions.

Thin layer chromatography (TLC) was performed on silica-gel (silica-gel 60 F254; MERCK, Darmstadt, Germany)) coated aluminium TLC-sheets and instant thin layer chromatography (iTLC).They were analysed using an instant imager (Instant Imager, Canberra Packard, Schwadorf, Austria). RadioHPLC using HiTrap^{TM} column (5mL, G-25 sephadex) was used to quantify the purity of the compounds. HPLC was performed using Hitachi L–7100 pump system coupled with UV (Hitachi L–7400) and radiometric (Gamma Raytest) detectors. Isocratic elution (100% water) and flow rate of 0.2 mL/ min.

2.2 Synthesis of polymers

Synthesis and characterization of the polymers is explained in detail in the supporting section.

2.3 Synthesis of ^{nat}Ga-oxine

8-Hydroxiquinoline (3.5 eq) was dissolved in 10% acetic acid solution and $Ga(NO_3)_3$ (1 eq) was slowly added. The solution was stirred for 10 minutes and then heated up to 80°C under reflux. After few minutes pH was adjusted to 7 with concentrated NH_4OH. The yellow suspension was refluxed for 1 hour. The yellow precipitate was filtered off, washed with hot water and dried at 100°C.

2.4 Synthesis of ^{68}Ga-oxine and ^{111}In-oxine

The ^{68}Ge/^{68}Ga generator was eluted using 5 mL of 0.1 N HCl and the ^{68}Ga was online trapped on a cation exchange resin. ^{68}Ga was post-processed as previously described [13, 14]. 400 µL of the acetone post-processed ^{68}Ga eluate were added to 1 mL NaOAc 1 M solution together with 10-15 µL of oxine in ethanol (20 mg/mL). ^{111}In was obtained as $^{111}InCl_3$ in 0.02 N HCl solution from Mallinckrodt. Aliquots of these solutions were added to 1 mL of NaOAc 1 M together with 10-15 µL of oxine in ethanol (20 mg/mL). The reaction mixture was stirred for 10 minutes at room temperature for both reactions. Final pH was of 6.6-6.8. ^{68}Ga-oxine and ^{111}In-oxine were analysed by iTLC: $CHCl_3$/MeOH (95:5).

2.6 Micelle formation

Different amounts of polymer (3 mg – 7.5 mg) and of cold Ga-oxine (1.5 mg – 5.5 mg) were dissolved in 100 µL DMSO and added to the ^{68}Ga-oxine NaOAc solution. The formed solution was slowly added to 1 mL of NaCl 0.9%. The micelles were formed spontaneously within 1 minute. After micelle formation purification using Sephadex G-25 size exclusion chromatography with saline as eluent was performed. Micelle formation was analysed by TLC using citrate buffer 0.1 M pH = 4.0 as a mobile phase.

2.7 *In vitro* stability

Stability of purified micelles was tested in fresh human serum and isotonic solution, both at a 1:4 v/v dilution. The samples were incubated at 37°C and at various time points, aliquots were taken and analysed by TLC using citrate buffer 0.1 M pH 4.0 as a mobile phase.

2.8 *Ex vivo* evaluation

^{111}In-oxine-micelles (1.5 mg in 1 mL of isotonic saline) and ^{111}In-oxine (0.15 mg/mL) to serve as a control were injected i.v. in anaesthetized healthy mice (C57BL6/J, male, 6 weeks, from Janvier) *via* the retro-orbital venous plexus, with a mean activity of 1.6 ± 0.3 MBq for micelles and of 1.6 ± 0.4 MBq for the ^{111}In-oxine. After 1, 4 and 24 hours, the animals were sacrificed and different organs and blood were removed. The tissue samples were weighed and the ^{111}In-activity in the organs was directly measured in a γ-counter (2470 WIZARD2 Automatic Gamma Counter, PerkinElmer). All animal experiments had previously been approved by the regional animal

ethics committee and were conducted in accordance with the German Law for Animal Protection and the UKCCCR Guidelines [16].

2.9 *Ex vivo metabolism evaluation*

Blood samples (ca. 100 µl), collected during the biodistribution, were mixed with heparin solution (150 µl) to avoid coagulation. Blood samples were weighed and activity was measured in a γ-counter. 500 µl of PBS were added and the blood was centrifuged at 4000 rpm for 5 min in order to separate blood cells and plasma. The plasma fractions were weighed and activity was measured in a γ-counter. Proteins and micelles were precipitated by adding 200 µl of acetonitrile to the plasma fraction. To separate proteins and free polymer from plasma water the samples were centrifuged at 4000 rpm for 5 min. The supernatants were weighed followed by determination of the activity in a γ-counter. The percentage of radioactivity in the blood cells, protein plus micelles and plasma water fractions was calculated by subtracting the activities of the supernatants from the activity of the whole blood sample.

3 RESULTS

3.1 Synthesis of oxine complexes

The Ga-oxine cold complex was obtained as a yellow powder after purification by precipitation in diethyl ether. IR signal of –OH group of oxine was not detectable for the gallium complex which is an indicator of successful formation of the complex.

^{68}Ga-oxine complex was quantitatively (>96 %) formed within 15 minutes at room temperature Results were analysed by iTLC using a mixture of $CHCl_3$/MeOH (95:5) as eluent. Rf (^{68}Ga) = 0, Rf (^{68}Ga-oxine) = 0.9 [15]. Same protocol was applied to ^{111}In-oxine. The specific activity of ^{68}Ga was of 155 MBq/µmol oxine.

3.2 Synthesis of polymers

Amphiphilic p(HPMA-co-LMA) copolymers were synthesized by controlled radical polymerization with lauryl methacrylate (LMA) monomers having 20-23 mol % of hydrophobic lauryl side chains. Their molecular weight and polydispersity are shown in table 1.

Table 1. Chemical analitics of the three HPMA polymers used

Polymer	M_n PFPMA-LMA precursor	Đ	% LMA	M_n HPMA-LMA Polymer	M_n g/mol	Đ
Random	68.400 g/mol	1.2	20	44.4400 g/mol	76.300	1.4
Block	26.800 g/mol	1.3	23	17.800 g/mol	26.000	1.3
Block-PEG	26.800 g/mol	1.3	23	36.400 g/mol	46.000	1.3

3.3 Micelle formation

For all polymer systems, micelles were formed within one minute. The incorporation rates for ^{68}Ga-oxine into the micellar core were of about 79 % ± 4 for the random copolymer, 92 % ± 2 for the block copolymer and 97 % ± 1 for the PEGylated block copolymer.

For the three polymeric systems, different amounts of cold Ga-oxine, as hydrophobic excipient, were used in micelle formation in order to find the best ratio polymer/Ga-oxine that will represent the efficiency on ^{68}Ga-oxine loading. A ratio of 1/0.75 molecular weight polymer/Ga-oxine was found to be optimal for micelle stabilization.

Purification through size exclusion columns was performed for the three type of polymeric micelles affording >97 % of purified labelled micelles in all cases. NaCl 0.9 % solution was used as eluent. Results were analysed by TLC using citrate buffer 0.1 M as mobile phase (micelles Rf = 0, ^{68}Ga/^{111}In-oxine Rf = 0.9). RadioHPLC was performed with a 5 mL size exclusion column using Milli-Q water as a mobile phase at a flow rate of 0.2 ml/min. Retention time of labelled micelles was 3.8 min with 99% purity. A broad tailored signal with peak maximum at 33 min was observed for ^{68}Ga-oxine complex. Both chromatograms are shown in figure 4.

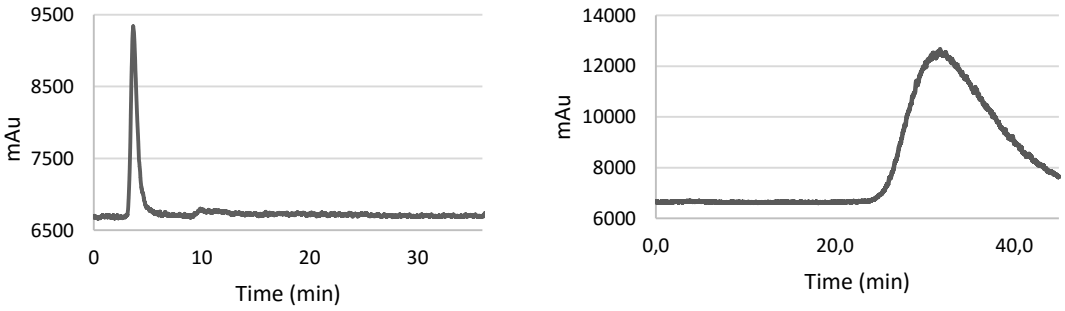

Figure 4: radioHPLC chromatograms of labelled purified micelles (left) and ^{68}Ga-oxine (right).

3.4 *In vitro* stability

After administration, polymer therapeutics are exposed to biological media like blood, which may influence and alter their physicochemical properties due to interactions with proteins or serum components [17]. The release of radioactivity was measured as an indicator for the micelle stability both in NaCl 0.9% solution and in fresh human serum. Random polymeric micelles showed to be the less stable micelles releasing half of the loaded activity after 30 minutes of incubation. After 120 min of incubation at 37°C in NaCl 0.9% solution, random, block and PEGylated-block presented 66% ± 5, 77% ± 3 and 89% ± 2 of stable radioactive micelles respectively.

In human serum media, only 56 % ± 3 of random micelles were still intact after 30 minutes of incubation (Fig.5) while block and PEGylated-block micelles showed 63 % ± 2 and 91 % ± 3 respectively at the same time point. After 1 hour incubation, block micelles had released 48 % ± 1 of the radioactive ^{68}Ga complex while for the PEGylated-block micelles, only 14 % ± 4 of the activity was released from the micelle core (Fig. 5). Additional stability analysis after 1 day incubation were performed in the PEGylated micelles labelled with ^{111} In-oxine prior to *in vivo* injection, >80 % micelles were still intact.

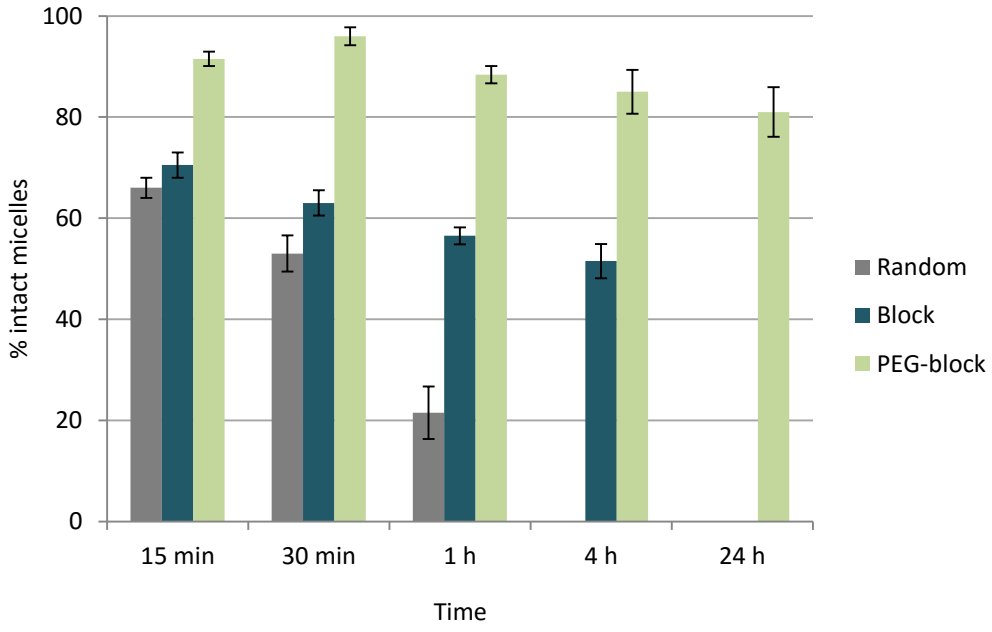

Figure 5: Stability of radiolabelled micelles in fresh human serum (n=3).

3.5 *Ex vivo* biodistribution

The favorable loading capacity and stability presented by the PEGylated block-copolymer micelles claimed for *in vivo* evaluation to gain knowledge of their biodistribution and whether the stability presented *in vitro* would persist.

The biodistribution of labelled micelles did not show specific uptake in any organ and values remained quite constant for each organ during the three time points analyzed (Fig. 6). High uptake was observed in the lungs (31.2 % ± 2.9), spleen (17.8 % ± 2.3) and kidneys (21.7 % ± 1.6) after 1 h p.i, and it barely changed after 4 and 24 h p.i. High accumulation was also observed in blood after 1 h (25.9 % ± 2.8) and 4 h (26.4 % ± 0.7) p.i however it decreased to 18.3 % ± 1.3 after 24 h p.i. Uptake in liver and heart did not show remarkable variations in the 3 points, with a mean value of 9.3 % ± 1.2 and 8.9 % ± 0.7 respectively. Remarkable is the high uptake (11.9 %) in urine after 1 h p.i. Slight bone accumulation is also observed.

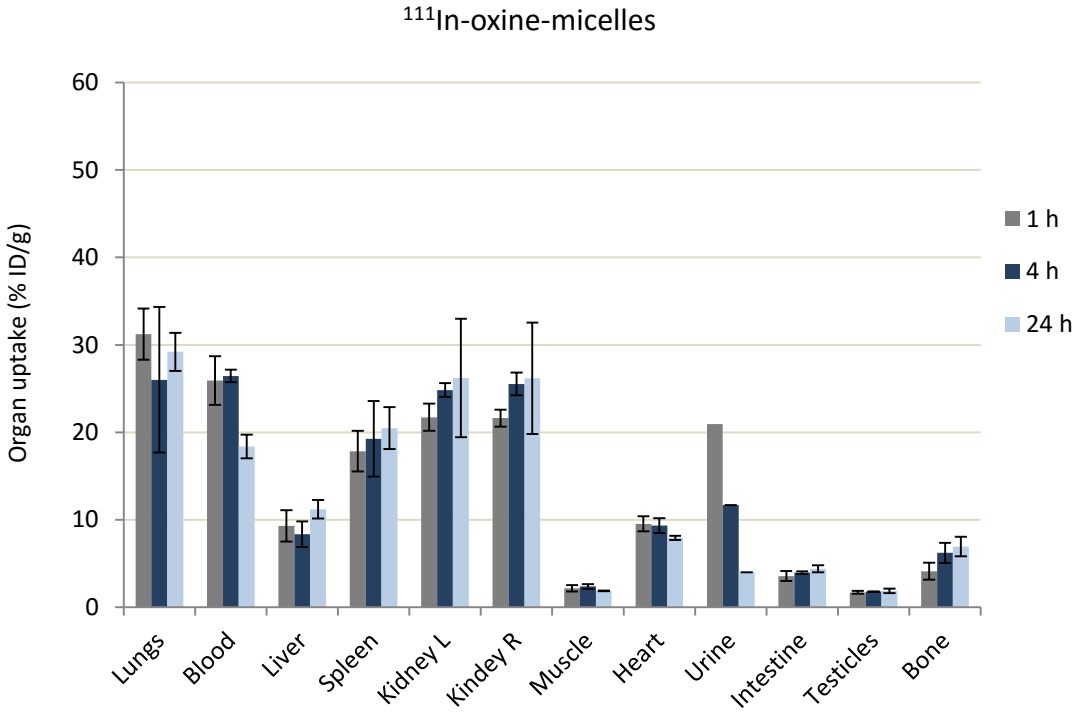

Figure 6: *Ex vivo* biodistribution of radiolabeled micelles in healthy mice (n=3) after 1 h, 4 h and 24 h p.i.

Control experiments were performed with ^{111}In-oxine (Fig.7). High retention in the lungs was detected at all time points (>40 % ID/g). High uptake of c.a 28 % was observed in the blood after 1 and 4 h p.i, which decreased to c.a 18 % after 24 h p.i. Uptake of c.a 20% in the kidneys remained constant during the three time points analyzed. Slight increase of activity over time

was observed in spleen, liver and heart, with maximum values of 14.8 % ± 1.9, 6.1 % ± 0.4 and 12.0 % ± 0.4 respectively, after 24 h p.i.

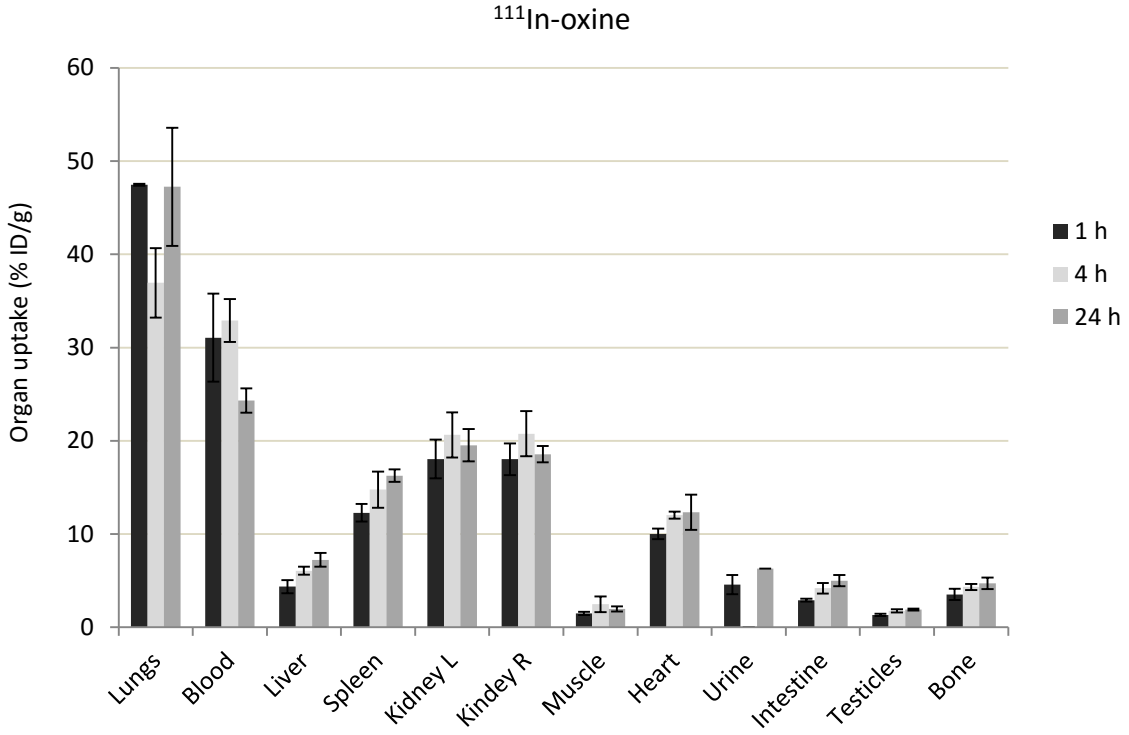

Figure 7: *Ex vivo* biodistribution of ^{111}In-oxine in healthy mice (n=3) after 1 h, 4 h and 24 h p.i

Comparing the two graphics a similar patern of both substances can be observed in some organs: a small uptake increase over time in spleen and kindneys, a high retention in lungs and a decrease in blood uptake after 24 h p.i. Urine uptake after 1 h p.i of micelles showed higher values when compared to ^{111}In-oxine.

3.6 *Ex vivo* metabolism

In order to investigate the *in vivo* stability of the labelled micelles and ^{111}In-oxine, the blood samples obtained during biodistribution were separated into different fractions: a) blood cells, b) polymer + proteins and c) plasma water. Figures 8a and 8b show the amount of radioactivity in the different fractions with reference to the total amount of radioactivity in the blood samples of ^{111}In-oxine and ^{111}In-oxine-labelled micelles. ^{111}In-oxine remains constantly concentrated in the blood cell fraction at all time points with values >90 %. 67.4 % ± 2.4 of the radiolabelled micelles are found after 1 h p.i in the blood cells fraction and only 30.1 % ± 1.9 in the fraction

containing proteins and micelles, which decreased to 21.1 % ± 1.4 and 15.1 % ± 1.5 after 4 and 24 h p.i respectively, while it increased in the blood cells fraction up to 77.4 % ± 1.4 and 82.4 % ± 1.5 after 4 and 24 h. The concentration on plasma water remained constant at low values below 2.5 % during the complete observation period of 24 h.

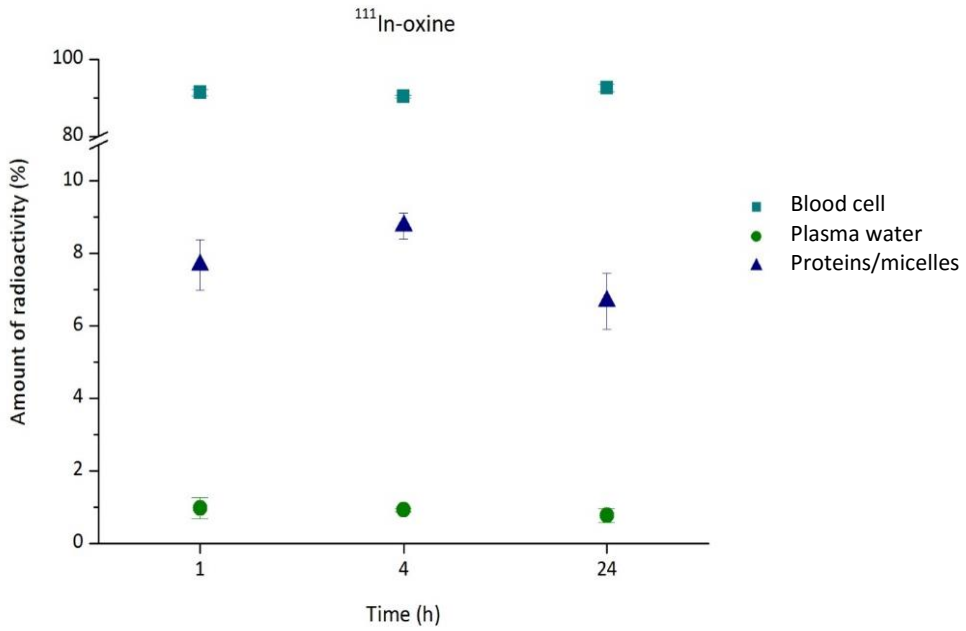

Figure 8a: Distribution of ^{111}In-oxine in the blood for up to 24 h (n=3). Data is expressed as percentage of the amount of radioactivity that was present in the whole blood sample (mean ± SEM).

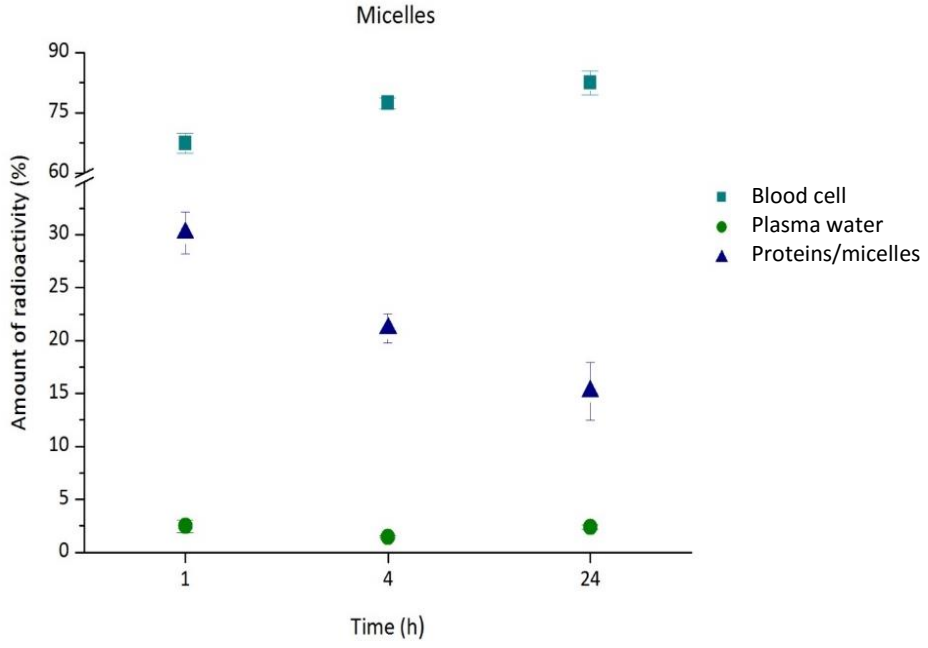

Figure 8b: Distribution of labelled micelles in the blood for up to 24 h (n=3). Data is expressed as percentage of the amount of radioactivity that was present in the whole blood sample (mean ± SEM).

4 DISCUSSION

The different structures of the polymers chosen were of interest as previous reports have demonstrate the capacity of those HPMA micellar structures as drug delivery systems [9, 18].
The encapsulation of ^{68}Ga-oxine into the micellar core showed different values depending on the structure of the polymer used. The lowest capability to incorporate the hydrophobic drug ^{68}Ga into the micellar core was observed for the random copolymer structure. Its nature leads to conformations where hydrophobic LMA can be close to the surface of the core-shell of the micelles leading to a micellar aggregation formation, which promotes the alteration of the micellar structure, and consequently the release of the incorporated drug [4]. This phenomenon is also observed in the lower stability of the radioactive micelles in human serum. It can be assumed that the hydrophobic moieties closer to the surface facilitate hydrophobic interactions [19] with serum proteins and therefore ^{68}Ga is released from the micellar core.

HPMA block copolymer micelles, having a well-defined structure, facilitate the incorporation of the hydrophobic complex into the core. Moreover, as the presence of hydrophobic LMA moieties in the micellar surface is minor when compared to random structures, the interactions between LMA and proteins present in human serum decrease. This fact is translated in a higher *in vitro* stability. However, the results were not as satisfactory as expected, in particular concerning the stability in human serum. As the core and shell of the micelles are clearly differentiated and the addition of the hydrophobic excipient, Ga-oxine, should help to induce more extensive micelle formation, besides stabilization of the hydrophobic regions, higher stability of the amphiphilic block copolymer was expected.
In order to increase stability, PEG moieties were incorporated to the corona of the block copolymer. The high hydrophilicity and flexibility of the PEG chains form a protective layer that will reduce the interactions between micelles and serum components. This fact is due to PEG is only an acceptor for H-bonding whereas poly(HPMA) is both a donor and an acceptor [11]. Finally, such micelles revealed higher loading capacity of ^{68}Ga-oxine, with quantitative incorporation and improved stability over time.

After successful results of loading capacity and stability of the PEGylated micelles, further *ex vivo* biodistribution studies were performed in healthy mice to evaluate their *in vivo* behaviour. Do to the short half-life of ^{68}Ga,^{111}In was employed instead to allow longer time frame evaluation e.g. 24 h.

The analysis of the three different blood fractions revealed low *in vivo* stability of the micelles. Only 30% of the total activity of the blood sample was found after 1 hour p.i in the pellet containing proteins and polymer, and it decreased after 4 and 24 hours to c.a 21% and 15% respectively. These results indicate release of the ^{111}In-oxine from the micellar core, consequently the amount of radioactivity in the blood cell fraction increased proportionally. ^{111}In-oxine was found to remain in high amounts in the blood cell fraction (>95%) from 1 h to 24 hours, this fact could be explained as a consequence of the high hydrophobicity of the complex, which is able to penetrate the blood cells [20]. ^{111}In-oxine is known to diffuse into red and white blood cells serving as an imaging agent of e.g. infection or inflammation *in vivo* [21-22]. Values below 2.5 % in the water plasma indicate that ^{111}In-oxine complex remained stable; there was almost no release of free ^{111}In.

These results are in concordance with the biodistribution analysis. Assuming that the micelles are not stable and only approximately 30% remained intact after 1 h p.i, the organ uptake values do not provide information on the micelles distribution, as around 70% of the activity measured belongs to free ^{111}In-oxine. This fact gets worse after 4 and 24 h post injetcion as more ^{111}In-oxine was released from the micelles. The only remarkable difference observed after 1 h p.i is the much higher uptake in the urine and lower uptake in liver 40% *vs* 30%. We could especulate that labelled micelles are rapid excreeted through the kidneys, however only one valueof urine was obtained.

5 CONCLUSIONS

Three different structures of amphiphilic HPMA-LMA based copolymers that self-assemble into micelles were studied to apply a novel radiolabelling technique. Spontaneous incorporation of hydrophobic ^{68}Ga-oxine or ^{111}In-oxine complexes in the micellar core was quantitative after one minute. The strategy does not require of previous modification of the polymer in order to be labelled with a radiometal and therefore the biological characteristics of the polymer will be totally preserved. The incorporation efficiency as well as *in vitro* stability in human serum and saline clearly depends on the polymer morphology. The optimum results were achieved for those polymers with a well-defined structure, in particular for the polymer that contains PEG moieties in the corona. Further *ex vivo* evaluation in healthy mice did not correlate with the *in vitro* stability values. Only c.a 30% of the micelles remained stable after 1 h p.i and this number decreased to c.a 15 % after 24 h p.i. This study shows an efficient labelling technique, but further investigations are needed in order to ensure *in vivo* stability.

REFERENCES

[1] Kataoka K, Kwon GS, Yokoyama M, Okano T, Sakurai Y. Block copolymer micelles as vehicles for drug delivery. *J Control Release* **1993;** 24: 1*19- 132*.

[2] Bader H, Ringsdorf H, Schmidt B. Watersoluble polymers in medicine. *Ang. Macromol. Chem* **1984;** 123: 457-485.

[3] Talelli M, Rijcken CJF, van Nostrum CF, Storm G, Hennink WE. Micelles based on HPMA copolymers. *Adv Drug Deliv Rev* **2010;** 62: 231–239.

[4] Hemmelmann M, Kurzbach D, Koynov K, Hinderberger D, Zentel R. Aggregation Behavior of Amphiphilic p(HPMA)-co p(LMA) Copolymers Studied by FCS and EPR Spectroscopy *Biomacromolecules* **2012**; 13: 4065−4074.

[5] Willmann JK, van Bruggen N, Dinkelborg LM, Gambhir SS. Molecular imaging in drug development. *Nat Rev Drug Discov* **2008**; 7: 591-607.

[6] van Dongen GA, Visser GWM, Lub-de Hooge MN, de Vries EG, Perk LR. Immuno-PET: A Navigator in Monoclonal Antibody Development and Applications. *The Oncologist* **2007**; 12: 1379–1389.

[7] Moderegger D. Radiolabeling of Defined Polymer Architectures with Fluorine-18 and Iodine-131 for Ex Vivo and in Vivo Evaluation: Visualization of Structure Property Relationships. Ph.D. Thesis, Institute of Nuclear Chemistry, Johannes Gutenberg-University, Mainz 2012.

[8] Herth M, Barz M, Moderegger D, Allmeroth M, Jahn M, Thews O, Zentel Z, Rösch F. Radioactive Labeling of Defined HPMA-Based Polymeric Structures Using [18F]FETos for *In Vivo* Imaging by Positron Emission Tomography. *Biomacromolecules* **2009**, 10: 1697–1703.

[9] Hemmelmann M, Knoth C, Schmitt U, Allmeroth M, Moderegger D, Barz M, Koynov K, Hiemke C, F. Rösch F, Zentel R .HPMA Based Amphiphilic Copolymers Mediate Central Nervous Effects of Domperidone. *Macromol Rapid Commun* **2011**; 32, 712–717.

[10] Duncan R. Development of HPMA copolymer–anticancer conjugates: Clinical experience and lessons learnt. *Adv Drug Deliv Rev* **2009;** 61: 1131–1148.

[11] Allmeroth M, Moderegger D, Gündel D, Buchholz HG, Mohr N, Koynov K, Rösch F, Thews O, Zentel R. PEGylation of HPMA-based block copolymers enhances tumor accumulation in vivo: A quantitative study using radiolabeling and positron emission tomography. *J Control Release* **2013;** 172: 77–85.

[12] Gaucher G, Dufresne MH, Sant VP, Kang N, Maysinger D, Leroux JC. Block copolymer micelles: preparation, characterization and application in drug delivery. *J Control Release* **2005;** 109; 169–188.

[13] Zhernosekov KP, Filosofov DV, Baum RP, Aschoff P, Bihl H, Razbash AA, Jahn M, Jennewein M, Rösch F. Processing of Generator-Produced ^{68}Ga for Medical Application. *J Nucl Med* **2007;** 48: 1741-1748.

[14] Mueller D, Klette I, Baum RP, Gottschaldt M, Schultz MK, Breeman WAP. Simplified NaCl Based ^{68}Ga Concentration and Labeling Procedure for Rapid Synthesis of ^{68}Ga Radiopharmaceuticals in High Radiochemical Purity. *Bioconjugate Chem* **2012;** 23: 1772-1717.

[15] Yano Y, Budinger TF, Ebbe SN, Mathis CA, Singh M, Brennan KM, Moyer BR. Gallium-68 Lipophilic Complexes for Labeling Platelets. *J Nucl Med* **1985;** 26: 1429-1437.

[16] Workman P, et al. Guidelines for the welfare and use of animals in cancer research. *Br J Cancer* **2010**; 102: 1555-1577.

[17] Hemmelmann M, Mohr N, Fischer K, Zentel R, Schmidt M. Interaction of pHPMA−pLMA Copolymers with Human Blood Serum and Its Components. Mol Pharmaceutics 2013; 10, 3769−3775.

[18] Hemmelmann M, Metz VV, Koynov K, Blank K, Postina R, Zentel R. Amphiphilic HPMA–LMA copolymers increase the transport of Rhodamine 123 across a BBB model without harming its barrier integrity. *J Control Release* **2012;** 163: 170–177.

[19] Winzelberg GG, Castronovo FP, Callahan RJ, McKusick KA, Strauss HW. ^{111}In oxine labeled red cells for detection of simulated lower gastrointestinal bleeding in an animal model. *Radiology* **1980**; 135: 455-61.

[20] Ebbe S, Taylor S, Maurer H, Kullgren B. Uptake of Indium-111-Labeled Platelets and Indium-111 Oxine by Murine Kidneys after Total-Body Irradiation. *Radiation Research* **1996;** 146: 216-222.

[21] Heyns AP, MG Lotter MG, Kotze HF, Wessels P, Pieters H, Badenhorst PN. Kinetics, distribution, and sites of destruction of indium-111 oxine labelled red cells in haemolytic anaemia. *J Clin Pathol* **1985**; 38:128-132.

[22] Becker W, Fischbach W, Jenett M, Reiners C, Börner W. ^{111}In-oxine-labelled white blood cells in the diagnosis and follow-up of crohn's disease. *Int J Mol Imaging* **1986;** 64: 141-148.

Supporting Information

^{68}Ga-, ^{111}In- oxine: A novel strategy of in situ radiolabelling of HPMA-based micelles

A. de la Fuente, S. Kramer, N. Mohr, S. Pektor, N. Bausbacher, R. Zentel, F. Rösch

Contents

I Synthesis of 4-cyano-4-((thiobenzoyl)sulfanyl)pentanoic acid

The 4-cyano-4-((thiobenzoyl)sulfanyl)pentanoic acid was used as the chain transfer agent (CTA) and synthesized according to the literature in a three step reaction [1].

II Synthesis of Pentafluorophenylmethacrylate (PFPMA)

PFPMA was prepared according to the literature [2].

III Synthesis of the reactive ester random copolymer

RAFT polymerization of pentafluorophenylmethacrylate (PFPMA) and lauryl methacrylate (LMA) with 4-cyano-4-((thiobenzoyl)sulfanyl)pentanoic acid (CTA) was carried out in a schlenk tube [1,2]. For this purpose , 4 g of PFPMA and 1.2 g of LMA were dissolved in 5 ml of absolute dioxane and 8.5 mg of CTA and 1.9 mg of 2,2´-Azobis-(4-methoxy)-2,4-dimethyl)valeronitrile (ABNDM) were added. After three-freeze-vacuum-thaw cycles, the mixture was immersed in an oil bath at 40 °C and stirred overnight. Afterwards the polymer solution was precipitated three times in n-hexane, centrifuged und dried under vacuum at 40 °C over night. A slightly pink powder was obtained. ^{1}H NMR (300 MHz, $CDCl_3$): δ [ppm] 4.00 (br, 2H), 2.48-0.83 (m, 5H). ^{19} F NMR (400 MHz, $CDCl_3$): δ [ppm] -151.5 - -153.1 (br, 2F), -157.9 - -158.2 (br, 1F), -162,9 - -163.4 (br, 2F).

IV Synthesis of the reactive ester block copolymer

- Synthesis of the reactive ester homopolymer (macro-CTA):

The PFPMA-macro-CTA was synthesized by RAFT polymerization of PFPMA with CTA under schlenk conditions. The reaction vessel was loaded with 4 g of PFPMA, 40 mg of CTA, 4 mg of ABNDM and 5 ml of absolute dioxane. Following three freeze-vacuum-thaw cycles, the tube was immersed into an oil bath at 40 °C and stirred overnight. After the polymerization the polymer solution was precipitated three times in n-hexane, isolated by centrifugation and dried overnight under vacuum at 40 °C. In the end a slightly pink powder was obtained. ^{1}H NMR (300 MHz, $CDCl_3$): δ [ppm] 2.1 – 2.5 (br, 2H), 1.3 – 1.6 (m, 3H). ^{19} F NMR (400 MHz, $CDCl_3$): δ [ppm] -151.5 - -153.1 (br, 2F), -157.9 - -158.2 (br, 1F), -162,9 - -163.4 (br, 2F).

- Synthesis of the reactive ester block copolymer:

0.5 g of the macro-CTA obtained after homo polymerization of PFPMA was dissolved in 4 ml of absolute dioxane. Afterwards 0.3 g of LMA and 1.4 mg of ABNDM were added and mixed. After three freeze-vacuum-thaw cycles, the tube was immersed into an oil bath at 40 °C and stirred for three days. Afterwards poly(PFPMA)-b-poly(LMA) was precipitated three times from dioxane into ethanol, isolated by centrifugation and dried overnight under vacuum at 40 °C. In the end a slightly pink powder was obtained. ^{1}H NMR (300 MHz, $CDCl_3$): δ [ppm] 3.9 (br, 2H), 2.4 – 0.9 (m, 5H). ^{19}F NMR (400 MHz, $CDCl_3$): δ [ppm] -151.5 - -153.1 (br, 2F), -157.9 - -158.2 (br, 1F), -162,9 - -163.4 (br, 2F).

V Removal of the dithioester end groups

The copolymer was precipitated in ethanol and collected by centrifugation. The copolymer was dried under vacuum at 40 °C overnight and a colourless powder was obtained. Yield: 380-390 mg (95-98 weight %). The absence of the dithiobenzoate end group was confirmed by UV/Vis spectroscopy by the absence of the peak at 302 nm.

VI Polymer analogous reactions

- Synthesis of poly(HPMA)-*random*-poly(LMA)

A total of 40 mg of the poly(PFPMA)-*ran*-poly(LMA) precursor polymer without dithioester end groups, was dissolved in 4 ml absolute dioxane and 1.5 ml absolute dimethylsulfoxide under argon atmosphere. 121 µL of 2-hydroxypropylamine and the equivalent molar amount of triethylamine were added. The mixture was stirred at 50 °C for three days. Afterwards the solution was diluted with Milli-Q water and dialysed for 3 days using Spectra/Por membranes (MWCO 3500 g/mol) and changing the water every 12 hours. The resulting solution was freeze dried to obtain a colourless powder. Yield: (90%). ^{1}H NMR (400 MHz, DMSO-d_6): δ [ppm] 7.4 – 7.2 (br, -NH), 4.7 (br, 1H), 3.7 – 3.4 (br, 2H), 2.9 (br, 2H), 2.3 – 0.8 (br, 5H).

- Synthesis of poly(HPMA)-*block*-poly(LMA).

A total of 100 mg of the poly(PFPMA)-*b*-poly(LMA) precursor polymer without dithioester end groups, was dissolved in 4 ml absolute dioxane and 1.5 ml absolute dimethylsulfoxide under argon atmosphere. 262 µL of 2-hydroxypropylamine and the equivalent molar amount of triethylamine were added. The mixture was stirred at 50 °C for three days. Afterwards the solution was diluted with Milli-Q water and dialysed for 3 days using Spectra/Por membranes

(MWCO 3500 g/mol) and changing the water every 12 hours. The resulting solution was freeze dried to obtain a colourless powder. Yield: (90%). ^{1}H NMR (400 MHz, DMSO-d_6): δ [ppm] 7.4 – 7.2 (br, -NH), 4.7 (br, 1H), 3.7 – 3.4 (br, 2H), 2.9 (br, 2H), 2.3 – 0.8 (br, 5H).

- Synthesis of PEGylated poly(HPMA)-*block*-poly(LMA)

A total of 100 mg of the poly(PFPMA)-*b*-poly(LMA) precursor polymer without dithioester end groups, was dissolved in 4 ml absolute dioxane and 1.5 ml absolute dimethylsulfoxide under argon atmosphere. 53 mg of PEG_{2kDa} with amine functionality and an equivalent amount of triethylamine was added. The colourless solution was stirred at 50 °C for 24 hours. Afterwards 120 µL of 2-hydroxypropylamine and the equivalent molar amount of triethylamine were added and stirred at 50 °C for another three days. The polymer solution was diluted with Milli-Q water and dialysed for 3 days using Spectra/Por membranes (MWCO 3500 g/mol) and changing the water every 12 hours. The resulting solution was freeze dried to obtain a colourless powder. Yield: (93%). ^{1}H NMR (400 MHz, DMSO-d_6): δ [ppm] 7.4 – 7.2 (br, -NH), 4.7 (br, 1H), 3.7 – 3.4 (br, 2H, 4H PEG), 3.3 (s, 2H PEG), 2.9 (br, 2H), 2.3 – 0.8 (br, 5H).

REFERENCES

[1] Chong YK, Moad G, Rizzardo E, Tang SH. A More Versatile Route to Block Copolymers and Other Polymers of Complex Architecture by Living Radical Polymerization: The RAFT Process. *Macromolecules* **1999**; 32: 2071–2074.

[2] Eberhardt M, Mruk R, Zentel R, Theato P. Synthesis of pentafluorophenyl(meth)acrylate polymers: New precursor polymers for the synthesis of multifunctional materials. *Eur Polym J* **2005**; 41: 1569–1575.

3.3 ^{44}Sc labelling of PSMA-617 for dosimetry of prostate cancer

^{44}Sc-PSMA-617 for dosimetry of prostate cancer

A. de la Fuente[1*], E. Eppard[2*], M. Benesova[3], F. Rösch[1], M. Essler[2], K. Kopka[3]

[1]Institute of Nuclear Chemistry, Johannes Gutenberg University,
55128 Mainz, Germany

[2]Department of Nuclear Medicine, University Hospital Bonn,
53127 Bonn, Germany

[3]Division of radiopharmaceutical chemistry, German Cancer Research Center, 69120
Heidelberg, Germany

*contributed equally

ABSTRACT

A broad pool of radionuclides becomes available for labelling of the prostate-specific membrane antigen (PSMA) inhibitor, Glu-NH-CO-NH-Lys (Ahx), when using DOTA as chelator. Recently the novel DOTA based PSMA-617 has shown great results in prostate cancer therapy and PET imaging when labelled with ^{177}Lu and ^{68}Ga. Do to the short half-life of ^{68}Ga, long acquisition periods cannot be carried out. In this context, ^{44}Sc with a half-life of 3.97 h and suitable decay characteristics for PET imaging, it is an alternative to ^{68}Ga. In this study, ^{44}Sc-labelled PSMA-617 was investigated and evaluated as a prostate cancer PET imaging agent.

Methods:
PSMA-617 was labelled with ^{44}Sc produced *via* ^{44}Ti/^{44}Sc generator. The stability of the radiopharmaceutical was examined in physiological conditions and in presence of competing relevant cations and chelates. Internalization and affinity constant was evaluated in LNCaP cells. First human *in vivo* investigation was carried out.

Results:
Labelling yield of 98% was achieved with 18 nmol of PSMA-617 after 20 min at 95 °C. After purification, product of 100% RCY was obtained, which presented high stability (>95%) in all solutions analysed. Affinity constant in LNCaP cells was of 4.72 ± 0.7 nM and internalization of 15.78 ± 2.14 % injected activity/10^6 LNCaP cells. ^{44}Sc-PSMA-617 PET/CT imaging of PSMA receptor positive metastases in a 77-year old patient showed successful detection of the lesions even after 19 h p.i.

Conclusions:
Efficient synthesis of DKFZ-617 with ^{44}Sc was achieved within 20 min. Stability as well as affinity and internalization values in LNCaP cells led to the first human evaluation with ^{44}Sc-PSMA-617. *In vivo* results confirmed the suitability of ^{44}Sc-PSMA-617 as a promising radiotracer for PET imaging of prostate cancer lesions

Keywords: prostate cancer, PSMA-617, ^{44}Sc, PET, dosimetry, theranostics

1 INTRODUCTION

Prostate cancer (PC) is the second most common cancer and the sixth leading cause of cancer death in men worldwide despite of the significant decrease in mortality in recent years due to early detection [1].

Current diagnosis is typically through digital rectal exam and blood prostate specific antigen (PSA) testing. Nevertheless, around 25% of the men with prostate cancer have serum PSA levels within the normal range, resulting in false negatives, while others have elevated serum PSA levels due to other reasons than prostate cancer resulting in false positives and unnecessary biopsies [2,3].

Since elevated serum PSA levels do not always correlate with disease, the prostate-specific membrane antigen (PSMA) has recently focused the attention for PC identification. PSMA, is an integral transmembrane protein significantly overexpressed (>95%) in prostate cancer, including metastatic disease, conceiving PSMA as a very attractive target for prostate cancer on the way to a personalized medicine, in which nuclear medicine offers both diagnostic and therapeutic tools using different radioisotopes [2-5].

Different radiopharmaceuticals have been in clinics for detection and treatment of prostate cancer but those with low molecular weight presented better results [6-9]. This fact gave rise to development of low-molecular-weight urea-based inhibitors pepidomimetics with high affinity to the catalytic domain of PSMA [9,11]. Among them, a DOTA derivative of the Glu-urea-Lys motif (PSMA-617) has been recently developed, the chelator is conjugated *via* an aromatic linker that improves tumor accumulation while simultaneously reducing kidney uptake. The novel compound has shown successful *in vivo* results not only with ^{177}Lu but also with ^{68}Ga, being nowadays powerful theranostic tracers for prostate cancer [12-15].

The treatment of identified lesions with therapeutic radionuclides needs of dosimetric calculations on tumor site and nearby organs to assess safety and efficacy of treatment as well as the pre-selection of patients. The analogue imaging probe quantifies the absorbed dose delivered in a specific site, offering accurate monitoring and planning of the patient's response to therapy and final response to the treatment in a post-therapeutic control [16].

^{68}Ga has been to date, the isotope used for imaging with the novel PSMA radiopharmaceutical [10, 11]. In spite its suitable decay characteristics ideal for PET imaging (β^+ = 89%, $\bar{E}$ = 0.74 MeV) and its availability *via* a ^{68}Ge/^{68}Ga generator, its short half-life of 68 min limits its application as it

only covers imaging periods of few hours. In this sense, the longer-lived positron-emitter ^{44}Sc is an alternative to ^{68}Ga.

^{44}Sc (β^+ = 94%, $\bar{E}$ = 0.597 MeV) has a half-life of 3.97 h and it is both generator and cyclotron produced [17, 18]. As ^{68}Ga is a trivalent cation but its half-life is 4 times longer thus providing a longer imaging frame-time. Another advantage of Sc^{III} in nuclear medicine, is the possibility of using the isotope ^{47}Sc (β^-, primary γ-ray of 159 keV and t ½ = 3.3 d) for therapy, constituting together a match for imaging and therapy $^{44/47}$Sc representing a real theranostic [19,20].

The aim of this work was to determine optimal conditions for radiolabeling PSMA-617 with ^{44}Sc to be used as prostate cancer imaging agent allowing for dosimetry calculation of the therapeutic ^{177}Lu analogue (Fig.1). Parameters that influence reaction kinetics, like incubation time, influence of organic solvent, temperature and amount of chelate-peptide of the reaction were investigated. Stability of the formed conjugate was checked in 0.9% NaCl, phosphate buffered-saline (PBS, pH 7.4), human serum and in presence of different metal cations as well as other competing chelators, like EDTA and DTPA. Affinity and internalization of ^{44}Sc-PSMA-617 were studied in LnCaP cells and the results were compared with ^{177}Lu and ^{68}Ga analogues. ^{44}Sc-PSMA-617 was finally evaluated in a 77-year old patient suffering from prostate cancer.

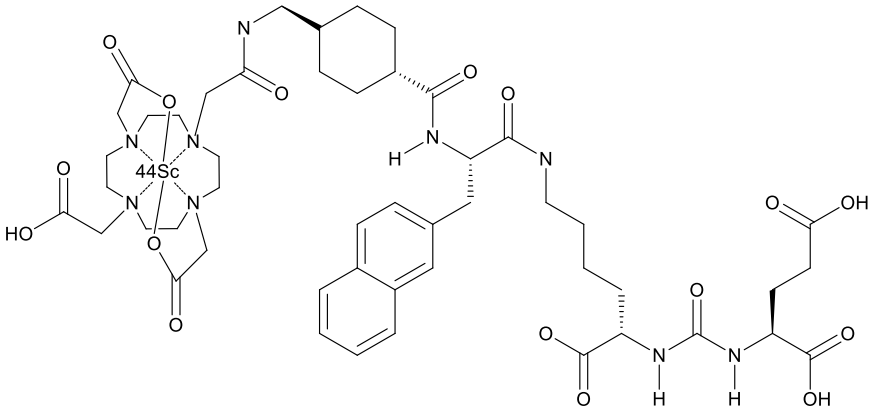

Figure 1: Structure of ^{44}Sc-PSMA-617

2 MATERIALS AND METHODS

Reagents were purchased from Sigma-Aldrich (Germany) and used without further purification, unless otherwise stated. Deionized water (18 MΩ cm^{-1}) was used in all reactions. No further special measures were taken regarding working under strict metal-free conditions. PSMA-617 was obtained as GMP-grade from ABX (Radeberg, Germany).

^{44}Sc was obtained from ^{44}Ti/^{44}Sc -generator. ^{44}Sc was eluted with 20 mL of 0.005 M $H_2C_2O_4$/0.07 M HCl mixture which were directly post-processed onto a miniaturized column filled with cation-exchange resin AG50W–X8 (200–400 mesh, H^+ form, 60 mg) where ^{44}Sc was quantitatively adsorbed online and successively eluted using 2–3 mL of 0.25 M ammonium acetate buffer (pH 4.0) [17]. This ^{44}Sc solution of small volume and free of competing oxalates was used for labelling.

2.1 Labelling of PSMA-617 with ^{44}Sc

Labelling of PSMA-617 with ^{44}Sc was performed by mixing different volumes of PSMA-617 stock solution (1 mg/mL) with post-processed ^{44}Sc eluate in 0.25 M ammonium acetate buffer pH 4.0. Effect of PSMA-617 concentration on labelling yields was evaluated with quantity of peptide varying from 14 to 26 nmol. Solutions were heated for 20 min at 95°C.

2.2 Solid phase extraction (SPE)

^{44}Sc-PSMA-617 was purified from unreacted ^{44}Sc species by reversed-phase chromatography with mini C–18 cartridges (Phenomenex Strata–X Tube, 30 mg). Final product was obtained in 1 mL of EtOH.

2.3 Quality control

Analysis of ^{44}Sc-PSMA-617 formation was monitored by thin-layer chromatography (TLC) (Silica-gel 60, Merck) using 0.1 M sodium citrate pH 4.0 as eluent, by iTLC (Instant thin layer chromatography) with a mixture 1:1 of ammonium acetate 1 M and ethanol, and by HPLC using Lichrosphere 100–RP18 EC column (5 mm, 250mm x 4 mm) (phenomenex). The gradient elution system utilized mobile phase A (deionized H_2O with 0.01% TFA) and mobile phase B (100% acetonitrile) at a flow rate of 1 mL/min, starting with 82% A/18% B for 30 min, after which gradient parameters returned to the initial conditions during next 2 min.

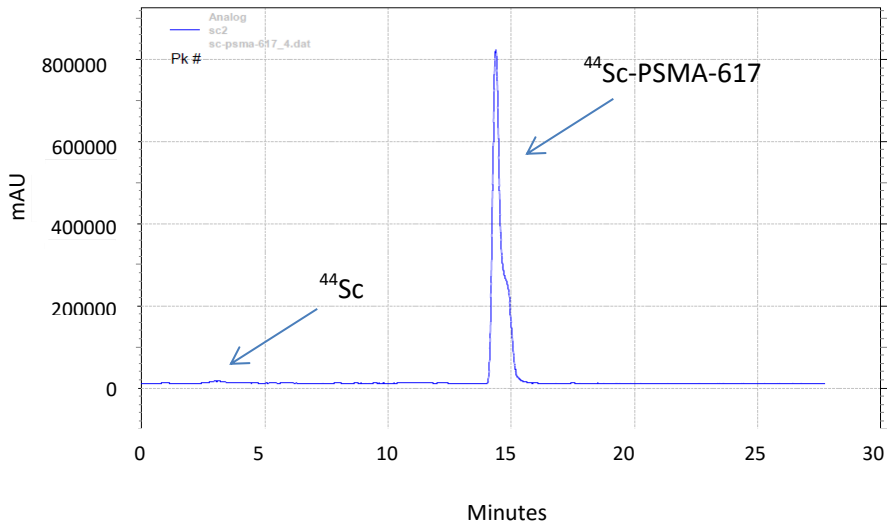

Figure 2: HPLC chromatogram of ^{44}Sc-PSMA-617

2.4 *In vitro* stability

Stability was performed by addition 20 µL of purified ^{44}Sc-PSMA-617 conjugate to 500 µL of 0.9% NaCl, human serum and solutions containing different metal cations (Fe^{3+}, Ca^{2+} and Mg^{2+}) at concentration levels of 10^{-2} M. Solutions were incubated for 24 h at 37°C.

Studies with DTPA and EDTA were also performed to check the stability of synthesized ^{44}Sc-PSMA-617 in the presence of competing chelating ligands. The appropriate aliquots of purified ^{44}Sc-PSMA-617 were added to DTPA or EDTA solutions in 0.9% NaCl in such a way that the final molar ratio of DTPA or EDTA to conjugate was equal to 100:1. The final volume of all solutions was 500 µL.

2.5 Binding affinity and internalization.

Competitive binding and internalization experiments were performed using the PSMA+ LNCaP cell line (European Collection of Cell Cultures, Salisbury, UK) derived from an androgen-sensitive human lymph node metastatic lesion of prostatic adenocarcinoma (ATCC CRL-1740). The cells were grown in RPMI 1640 medium (PAN-Biotech, Aidenbach, Germany) supplemented with 10% fetal calf serum (FCS) and 1% L-glutamine. Cell cultures were maintained in an atmosphere of 5% CO_2 at 37 °C in a humidified incubator.

The binding affinity was determined using a cell-based competitive assay with ^{68}Ga-labelled Glu-urea-Lys-(Ahx)-HBED-CC dimer (^{68}Ga-PSMA-10) and expressed as K_i values. ^{nat}Sc-PSMA-617 at twelve different concentrations (0–5000 nM) was incubated with 0.75 nM of ^{68}Ga-PSMA-10 together with LNCaP cells (10^5 LNCaP cells/well). After 45 min incubation at 37 °C, the cells were washed three times with ice-cold PBS. A gamma counter measured radioactivity accumulated in the cells and the data fitted using a nonlinear regression algorithm (GraphPad Software) to calculate 50% inhibitory concentrations (IC_{50} values).

For the determination of internalization, LNCaP cells (10^5 LNCaP cells/well) were seeded in poly-L-lysine coated plates 24 h before the experiment. The cells were incubated for 45 min at 37 °C with 32 nM of ^{44}Sc-labelled PSMA-617 in 250 μL Opti-MEM. Additionally, for confirmation of specific cellular uptake, the second set of compounds was also treated with 500 μM/well of PSMA-inhibitor 2-PMPA (2-(phosphonomethyl)pentane-1,5-dioic acid). The cells were washed four times with ice-cold PBS and the surface-bound radioactivity was removed by washing twice with 50 mM glycine (pH 2.8). After washing the cells with PBS, the internalized fraction was determined by lysis of the LNCaP cells using 0.3 M NaOH. The radioactivity collected from the glycine and hydroxide fractions was measured in a gamma counter and calculated as %IA/10^6 LNCaP cells.

2.6 Human evaluation

Labelling was performed with 40 nmol of PSMA-617 for 20 min at 95 °C. After purification with a C-18 column, the final product was formulated in isotonic NaCl 0.9 % solution with subsequent sterile filtration with a 94% recovery (decay corrected). A 77-year old man suffereing from prostate cancer was injected with 55.76 MBq of ^{44}Sc-PSMA-617 in the Nuclear Medicine department of University Klinikum Bonn, and the protocol for dosimetry studies was followed:

1) withdrawal of blood samples in heparinized syringe ofr determining of blood haematocrit value. 2) Acquisition of low dose CT scan for patient positioning and attenation correction. 3) 30 min dynamic PET scan under PET/CT camera. 6 images x 10 sec, 10 images x 30 sec and 8 images x 180 sec. 4) Static whole body scans (proximal femur to base of skull) preceded by low dose CT scan at: a) 30 min p.i with 2 min acquisition per bed position, b) 2 h p.i with 4 mn acquisition per bed position and c) 19 h p.i with 5 min acquisition per bed position. 4) Collection of 3 mL venous samples after 30 min, 2 h and 19 h whole body scan. 5) Collection of all urine voided during dynamic scan as well as during the entire length of acquisition up to 3 h p.i in separate

containers. Images were acquired using Siemens Biograph 2 PET/CT scanner and images were reconstructed with software Synchro.

3 RESULTS AND DISCUSSION

The formation of the ^{44}Sc-DOTA complex formation requires heating at elevated temperatures therefore the reaction was carried out at 95 °C. The radiochemical yield was evaluated with different amounts of PSMA-617 and after 20 minutes was of 98% when 18 nmol of PSMA-617 were added to c.a 110 MBq of post-processed ^{44}Sc eluate (pH 4.0). Increasing amount of compound did not influence the reaction yield by that time but amounts >20 nmol presents quantitative yields after 10 minutes of reaction (Fig.3).

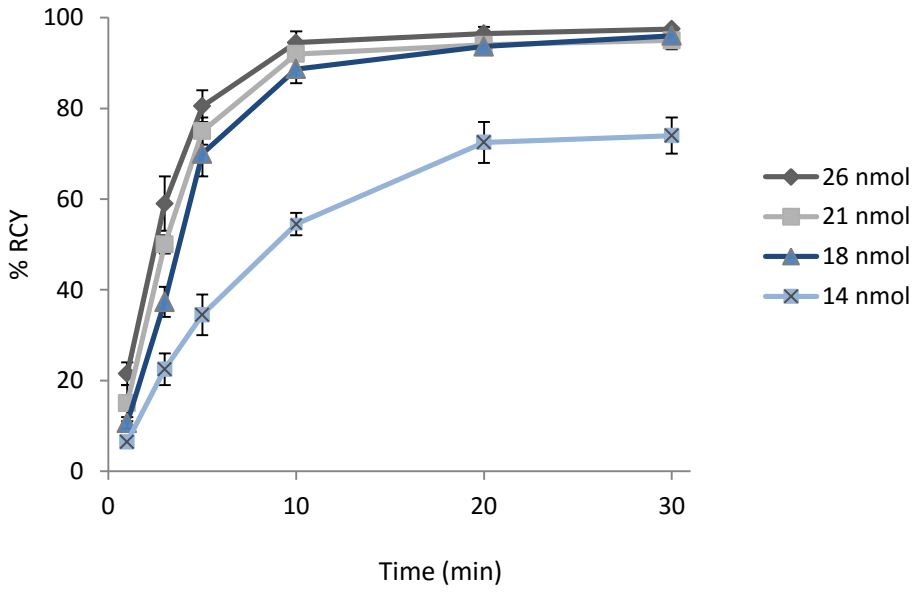

Figure 3: Time course of ^{44}Sc complexation reaction forming ^{44}Sc-PSMA-617 with different amounts of PSMA-617 at pH 4.0 (T= 95 ^{o}C, n = 3).

Purification for further *in vitro and in vivo* studies was performed on cation exchange and the conjugate was recovered in 500 mL fraction of ethanol with a 91% efficacy and containing 0.8% free ^{44}Sc. After administration, polymer therapeutics are exposed to biological media like blood which may influence and alter their physicochemical properties due to interactions with proteins or serum components [18]. Therefore stability at physiological conditions must be proved.

Stability of ^{44}Sc-PSMA-617 was analysed in 0.9% NaCl and human serum albumin at 37°C simulating physiological conditions. After 24 h incubation >95% of labelled compound remained still intact (Fig. 4).

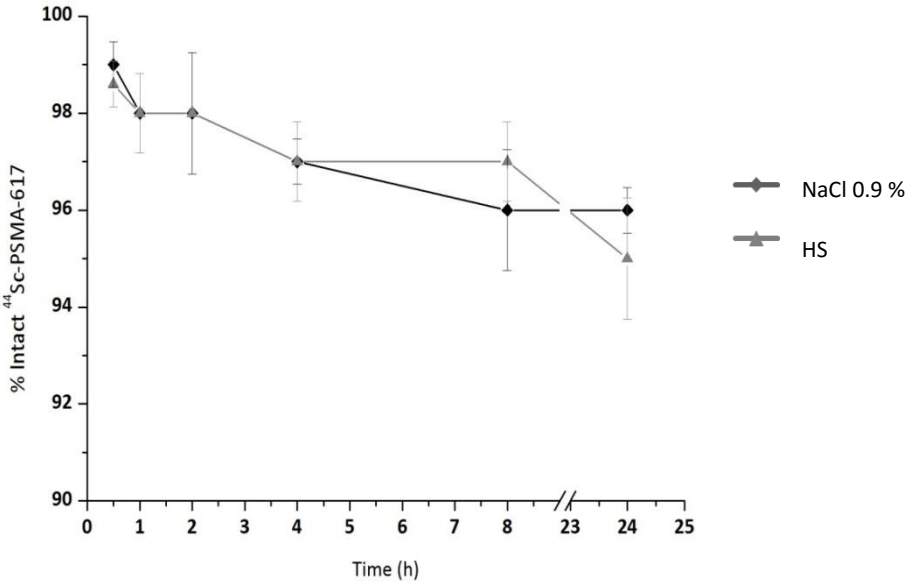

Figure 4: Stability of ^{44}Sc-PSMA-617 in NaCl 0.9% and human serum at 37 ^{O}C (n = 3).

Presence of different metal cations in final solution can cause transmetallation of radionuclide-conjugate and finally induce a release of ^{44}Sc into solution. Therefore, it is interesting to determine whether ^{44}Sc-PSMA-617 is stable in presence of relevant metal cations. The addition of Ca^{2+}, Mg^{2+} and Fe^{3+} did not induce decomplexation of ^{44}Sc. ^{44}Sc-PSMA-617 presented high stability values even after 24 h incubation at rather high metal concentration levels of 10^{-2} M (Tab. 1).

To calculate the affinity (K_i) of ^{44}Sc-PSMA-617, natural Sc was used instead. The affinity of ^{nat}Sc-PSMA-617 for the receptor was determined indirectly by measuring its ability to compete with dimeric PSMA inhibitor (PSMA-7) labelled with ^{68}Ga. Various concentrations of ^{nat}Sc-PSMA-617 were allowed to compete with a fixed concentration of ^{68}Ga-dimer (0.75 nM) for a receptor and while the concentration of unlabelled ligand increases, the amount of radioligand bound to the receptor decreases. A nanomolar affinity of 4.72 ± 0.7 nM was revealed for ^{nat}Sc-PSMA-617 on LNCaP cells, such results are directly comparable to the ^{nat}Ga- and ^{nat}Lu-labelled PSMA-617 values from the literature (Tab. 2).

Table 1: Stability of ^{44} Sc-PSMA-617 at 37 ^{o}C in presence of different metal cations and in presence of DTPA and EDTA at 10^{-2} M concentration (n = 3)

Time (h)	% Intact ^{44}Sc-PSMA-617 ± SD				
	Ca^{2+}	Mg^{2+}	Fe^{3+}	EDTA	DTPA
0.5	98.0 ± 0.0	98.7 ± 0.5	97.3 ± 0.9	96.7 ± 0.1	96.7 ± 1.2
1	98.3 ± 0.5	98.3 ± 0.5	98.0 ± 0.8	97.3 ± 0.1	97.7 ± 0.5
2	97.0 ± 0.1	98.0 ± 0.8	98.0 ± 0.8	97.3 ± 0.1	97.0 ± 0.8
4	97.0 ± 1.4	97.7 ± 0.5	96.7 ± 0.5	97.3 ± 0.1	96.7 ± 0.5
24	96.7 ± 0.8	97.2 ± 0.8	95.0 ± 1.4	95.9 ± 1.2	95.1 ± 0.8

^{44}Sc-PSMA-617 was specifically internalized into human prostate carcinoma (LNCaP) cells, up to 15.78 ± 2.14 percentage injected activity/10^6 LNCaP cells (n = 4). The results of the three radiopharmaceuticals do not present remarkable differences. The internalization values are slightly below the ^{68}Ga and ^{177}Lu analogues, but in contrast, ^{44}Sc-PSMA-617 showed reduced unspecific binding values. (Tab.2, Fig.5).

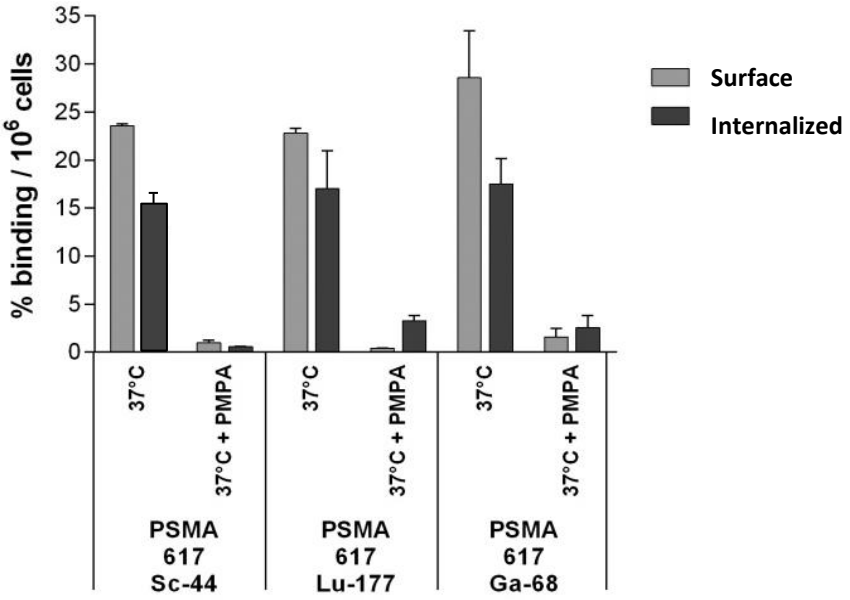

Figure 5: Internalization values of ^{44}Sc-, ^{68}Ga and ^{177}Lu-labelled PSMA-617 in LNCaP cells

Table 2: Affinity constant and internalization values of ^{44}Sc- ^{68}Ga- ^{177}Lu-labelled PSMA-617 compounds. Same set up was used for the three compounds [15].

	K_i ± SD	Internalization ± SD
^{44}Sc	4.72 ± 0.78	15.78 ± 2.14
^{68}Ga	6.40 ± 1.02	17.67 ± 4.35
^{177}Lu	6.91 ± 1.32	17.51 ± 3.10

The labelling efficiency as well as *in vitro* stability, affinity and internalization results brought ^{44}Sc-PSMA-617 to a first evaluation in humans in the Nuclear Medicine department of University Klinikum Bonn.

^{44}Sc-PSMA-617 PET/CT imaging of PSMA receptor positive metastases in a 77-year old man was clearly successful (Fig. 6). Even at low activity of c.a 3 MBq, at a late time-point of 19 h post injection, lesions are still detectable. In that case all activity is in the lesions with no uptake in urin or kidneys.

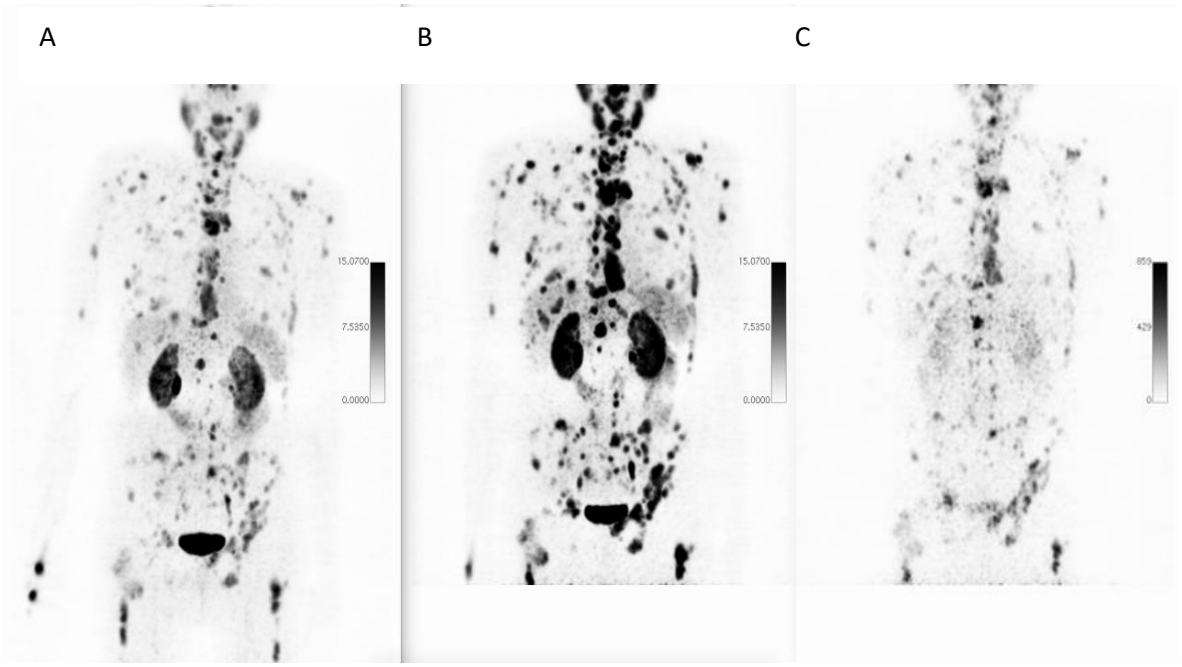

Figure 6: ^{44}Sc-PSMA-617 PET/CT imaging (55.76 MBq Injected) of PSMA receptor positive metastases after A) 30 min p.i, B) 2 h p.i and C) 19 h p.i (Department of Nuclear Medicine, Uniklinikum Bonn, Germany)

In addition to the detection of the prostate lesions, the purpose of such *in vivo* evaluation, is to measure the uptake kinetics of ^{44}Sc-PSMA-617 in metastatic tumors in order to estimate the optimum radiation dose the individual patient will receive in a subsequent therapeutic application of the biologically and chemically analogous compound ^{177}Lu-PSMA-617. Such calculations are still ongoing.

4 CONCLUSIONS

Radiolabelling of PSMA-617 with the generator derived PET radionuclide ^{44}Sc was investigated in detail for its application as a PET imaging agent of prostate cancer lesions. Incorporation of ^{44}Sc into PSMA was almost quantitative at pH 4.0 after 20 min with 18 nmol of PSMA-617.
The radiopharmaceutical presented high stability in physiological conditions as well as against competing cations and chelates that could induce transmetallation. Affinity and internalization results showed reduced unspecific binding and higher specific internalization in LNCaP cells with similar values than those for ^{68}Ga and ^{177}Lu. Such promising results were translated into the clinics and evaluated for a first time in a patient suffering from prostate cancer.

^{44}Sc-PSMA-617 showed successful PSMA receptor localization even after 19 hours post injection. This study confirms that the novel radiopharmaceutical ^{44}Sc-PSMA-617 can be considered as an ideal tracer for PET imaging prostate cancer lesions.

REFERENCES

[1] Jemal A, Bray F, Center MM, Ferlay J, Ward E, Forman D. Global cancer statistics. CA *Cancer J Clin* **2011**; 61: 69–90.

[2] Hillier SM, et al. Preclinical Evaluation of Novel Glutamate-Urea-Lysine Analogs that Target Prostate Specific Membrane Antigen as Molecular Imaging Pharmaceuticals for Prostate Cancer. *Cancer Res.* **2009**; 69: 6932-6940.

[3] Wright GL Jr, Haley C, Beckett ML, Schellhammer PF. Expression of Prostate-Specific Membrane Antigen in Normal, Benign, and Malignant Prostate Tissues. *Urol Oncol* **1995**; 1: 18-28.

[4] Davis MI, Bennett MJ, Thomas LM, Bjorkman PJ. *Proc Natl Acad Sci U S A.* **2005**; 102: 5981-5986. Crystal structure of prostate-specific membrane antigen, a tumor marker and peptidase.

[5] Eder M, Eisenhut M, Babich J, Haberkorn U. PSMA as a target for radiolabelled small molecules. *Eur J Nucl Med Mol Imaging*. **2013;** 40: 819–823.

[6] Small EJ. Monoclonal Antibody Therapy for Prostate Cancer: Finally a Reality? *J Clin Oncol* **2004**; 22: 2515-2516.

[7] Ali Afshar-Oromieh, et al. Comparison of PET imaging with a ^{68}Ga-labelled PSMA ligand and ^{18}F-choline-based PET/CT for the diagnosis of recurrent prostate cancer. *Eur J Nucl Med Mol Imaging* **2014**; 41: 11–20.

[8] Rinnab L, et al. [(11)C]choline PET/CT in prostate cancer patients with biochemical recurrence after radical prostatectomy. *World J Urol* 2009; 27: 619–25.

[9] Lütje S, et al. PSMA Ligands for Radionuclide Imaging and Therapy of Prostate Cancer: Clinical Status. *Theranostics* **2015**; 5: 1388-1401.

[10] Martin Schäfer M. A dimerized urea-based inhibitor of the prostate-specific membrane antigen for ^{68}Ga-PET imaging of prostate cancer EJNMMI Res. 2012; 2: 23.

[11] Eder M, Schäfer M, Bauder-Wüst U, Hull WE, Wä C. ^{68}Ga-Complex Lipophilicity and the Targeting Property of a Urea-Based PSMA Inhibitor for PET Imaging. *Bioconjug Chem* **2012**: 23:688-697.

[12] Baum RP, et al. Lutetium-177 PSMA Radioligand Therapy of Metastatic Castration-Resistant Prostate Cancer: Safety and Efficacy. *J Nucl Med*. **2016;** [Epub ahead of print]

[13] Kabasakal L, AbuQbeitah M, Aygün A, Yeyin N, Ocak M, Demirci E, Toklu T. Pre-therapeutic dosimetry of normal organs and tissues of (177)Lu-PSMA-617 prostate-specific membrane antigen (PSMA) inhibitor in patients with castration-resistant prostate cancer. *Eur J Nucl Med Mol Imaging* **2015;** 42: 1976-83.

[14] Delker A. Dosimetry for (177)Lu-DKFZ-PSMA-617: a new radiopharmaceutical for the treatment of metastatic prostate cancer. *Eur J Nucl Med Mol Imaging* **2016**; 43: 42-51.

[15] Benesova M, et al. Preclinical Evaluation of a Tailor-Made DOTA-Conjugated PSMA Inhibitor with Optimized Linker Moiety for Imaging and Endoradiotherapy of Prostate Cancer. J *Nucl Med* **2015**; 56: 914-920.

[16] Zechmann CM, et al. Radiation dosimetry and first therapy results with a $^{124/131}$ I. *Eur J Nucl Med Mol Imaging*. **2014**; 41: 1280-92.

[17] Roesch F. Scandium-44: Benefits of a Long-Lived PET Radionuclide Available from the ^{44}Ti/^{44}Sc Generator System. *Current Radiopharmaceuticals*, 2012, *5,* 187-201.

[18] Alliot C, Kerdjoudj R, Michel N, Hadad F, Huclier S. Cyclotron production of high purity $^{44m/44}$Sc with deuterons from $^{44}CaCO_3$ targets. *Nucl Med Biol* **2015;** 42: 524-529.

[19] Rösch F, Baum RP. Generator-based PET radiopharmaceuticals for molecular imaging of tumours: on the way to THERANOSTICS. *Dalton Trans* **2011**; 40, 6104-6011.

[20] Marek Pruszynski M, Majkowska-Pilip A, Loktionova N, Eppard E, Rösch F. Radiolabeling of DOTATOC with the long-lived positron emitter ^{44}Sc. *Appl. Radiat. Isotopes* **2012;** 70: 974–979.

[21] Hemmelmann M, Mohr K, Fischer K, Zentel R, Schmidt M. Interaction of pHPMA−pLMA Copolymers with Human Blood Serum and Its Components. *Mol. Pharmaceutics* **2013**; 10: 3769−3775

3.4 Labeling and preliminary *in vivo* assessment of niobium-labeled radioactive species: A proof-of-concept study

Labeling and preliminary *in vivo* assessment of niobium-labeled radioactive species: A proof-of-concept study

V. Radchenko[a], P. Bouziotis[b], T. Tsotakos[b], M. Paravatou-Petsotas[b], A. de la Fuente[a], G. Loudos[b,c], A.L. Harris[d], S. Xanthopoulos[b], D. Filosofov[e], H. Hauser[f], M. Eisenhut[f], B. Ponsard[g], F. Roesch[a].

[a]Institute of Nuclear Chemistry, Johannes Gutenberg University, Mainz, Germany

[b]Institute of Nuclear & Radiological Sciences & Technology, Energy & Safety, N.C.S.R. "Demokritos", Athens, Greece

[c]Department of Biomedical Engineering, Technological Educational Institute of Athens, Athens, Greece

d [d]Weatherall Institute of Molecular Medicine, University of Oxford, Oxford, UK

[e]Dzhelepov Laboratory of Nuclear Problems, Joint Institute of Nuclear Research, Dubna, Moscow region, Russian Federation

[f]Radiopharmaceutical Chemistry, German Cancer Research Center, Heidelberg, Germany

[g]Institute of Nuclear Materials Science, BR2 Reactor, Radioisotopes and NTD Silicon Production, Belgian Nuclear Research Centre, SCKCEN, Mol, Belgium

ABSTRACT

The application of radionuclide-labeled biomolecules such as monoclonal antibodies or antibody fragments for imaging purposes is called immunoscintigraphy. More specifically, when the nuclides used are positron emitters, such as zirconium-89, the technique is referred to as immuno-PET. Currently, there is an urgent need for radionuclides with a half-life which correlates well with the biological kinetics of the biomolecules under question and which can be attached to the proteins by robust labeling chemistry. ^{90}Nb is a promising candidate for *in vivo immuno*-PET, due its half-life of 14.6 h and low β^+ energy of E_{mean} = 0.35 MeV per decay. ^{95}Nb on the other hand, is a convenient alternative for longer-term *ex vivo* biodistribution studies, due to its longer half-life of (t ½ = 35 days) and its convenient, lower-cost production (reactor-based production). In this proof-of-principle work, the monoclonal antibody bevacizumab (Avastin®) was labeled with $^{95/90}$Nb and *in vitro* and *in vivo* stability was evaluated in normal Swiss mice and in tumor-bearing SCID mice.

Initial *ex vivo* experiments with ^{95}Nb -bevacizumab showed adequate tumor uptake, however at the same time high uptake in the liver, spleen and kidneys was observed. In order to investigate whether this behaviour is due to instability of *Nb-bevacizumab or to the creation of other *Nb species *in vivo*, we performed biodistribution studies of ^{95}Nb-oxalate, ^{95}Nb-chloride and ^{95}Nb-Df. These potential metabolite species did not show any specific uptake, apart from bone accumulation for ^{95}Nb-oxalate and ^{95}Nb-chloride, which, interestingly, may serve as an "indicator" for the release of ^{90}Nb from labeled biomolecules. Concerning the initial uptake of ^{95}Nb-bevacizumab in non-tumor tissue, biodistribution of a higher specific activity radiolabeled antibody sample did show only negligible uptake in the liver, spleen, kidneys or bones.

Keywords: $^{95/90}$Nb Bevacizumab, Labeling, VEGF, PET, Biodistribution

1 INTRODUCTION

Targeted imaging of cancer is crucial to modern-day cancer management, and radionuclides attached to biomolecules are an exciting strategy for tumor diagnosis and therapy [1]. An attractive feature, but also the key challenge of this strategy is to select radionuclides and targeting vehicles with characteristics which are best suited for a particular application. Angiogenesis is the development of new blood vessels from pre-existing ones. It is regulated by chemical signals of the organism, which function as an "angiogenesis switch", regulating the formation of new vasculature. Bevacizumab is a humanized monoclonal antibody (mAb) which binds all VEGF-A isoforms [2]. Currently many studies focus on labeling of bevacizumab with radionuclides for *in vivo* evaluation [3–7]. An important criterion for selecting of radionuclides for mAb is the half-life of the radionuclide which should favourably correlate to the biological kinetic of large-size biomolecules. Due to the long circulation of intact antibodies, optimal tumor-to-non tumor ratios can be reached from approximately 2 to 5 days post-injection, therefore radionuclides with an appropriate half-life should be chosen. Positron-emitting radionuclides with long and medium-long half-life of interest for PET-imaging with antibodies and antibody fragments are, for example, ^{89}Zr (t ½ = 78.4 h) [8,9], ^{64}Cu (t ½ = 12.7 h) [10,11], ^{86}Y (t ½ = 14.7 h) [12], ^{76}Br (t ½ = 16.0 h) [13].

Several factors and characteristics apply to radionuclide candidates for *immuno*-PET, the most important ones are: i) a physical half-life paralleling the biological half-life of the mAb or antibody fragment; ii) a high positron branching with no or weak accompanying other radiation (β^-, γ) to offer high-sensitivity PET imaging while reducing the radiation burden of the patient; iii) a preferably low β^+-energy to allow for high-resolution PET imaging; and iv) the availability of the radionuclide, i.e., an efficient production and radiochemical separation route. In previous works we have reported a convenient way for production of ^{90}Nb–labeled biomolecules and proposed ^{90}Nb as a promising candidate for application in *immuno*-PET [14–17]. Its intermediate half-life of 14.6 h and a high positron branching of 53% may make ^{90}Nb an ideal candidate for application with antibody fragments, monoclonal antibodies, drug delivery systems and nanoparticles. Moreover, the chelate desferrioxamine (Df) has been identified as an excellent moiety to label *Nb to proteins [17,18]. In this work we report on the *in vitro* stability and *in vivo* behaviour of $^{95/90}$Nb radiolabeled bevacizumab. Biodistribution studies of ^{95}Nb-oxalate, ^{95}Nb-chloride and ^{95}Nb-Df were performed in healthy mice, to provide more information on the fate of *Nb-labeled species *in vivo*.

2 MATERIALS AND METHODS

2.1 Materials

Reagents were purchased from Sigma-Aldrich (Germany) and used without further purification, unless otherwise stated. Deionized water (18 MΩ cm−1) and ultra-pure HCl solution were used. No further special measures were taken regarding working under strict metal-free conditions. The mAb bevacizumab (Avastin®, Roche) directed against the VEGF-A family of isoforms was bought from Roche Ellas S. A. (Greece). For the purification of conjugated and labeled antibodies, PD-10 columns (GE Healthcare Life Science) were applied, for ion exchange separation Aminex A27, 15±2 μm and AG1 x 8, 200–400 mesh anionic exchange resins and DOWEX 50x8, 200–400 mesh (BioRad) were used. For solid phase extraction, UTEVA® resin (Triskem Int., France) was applied. The production yield, radionuclidic purity, radiochemical purity and separation yield of $^{95/90}$Nb were determined by γ-ray spectroscopy using an Ortec HPGe detector system and Canberra Genie 2000 software.

The dead time of the detector was always kept below 10%. The detector was calibrated for efficiency at all positions with the certified standard solution QCY48, R6/50/38 (Amersham, UK). VEGF 165-transfected MDA MB 213 cells (M165) were kindly provided by Cancer Research UK. MDAMB 231 breast cancer cells were infected with virus expressing VEGF 165. The virus was made in Pheonix cells using the plasmid pLXRSpBMN-IRES-GFP. The VEGF clone is human. The cells are cultured at safety level I in minimum essential medium (Eagle) with 2mML-glutamine in the presence of 10% fetal bovine serum, at 37 °C in a humidified 5% CO_2 incubator. Labeling efficiency and stability of the $^{95/90}$Nb labeled mAb was monitored by instant thin layer chromatography (iTLC) and high performance liquid chromatography (HPLC). ITLC was performed on chromatography strips (Biodex, NY). As mobile phase, 0.02 M citrate buffer (pH 5.0) was used. HPLC monitoring was performed on a Waters HPLC system using a TSK gel G3000SWXL size exclusion column (TOSOH Bioscience, Germany). As eluent, a mixture of 0.05 M sodium phosphate and 0.15 M sodium chloride (pH 6.8) solution was used at a flow rate of 0.8 mL/min. Formation of ^{95}Nb-Df was measured via ITLC at conditions described above. All numerical data were expressed as the mean of the values ± the standard error of the mean. Statistical analysis was performed using the t-test. A p value less than 0.05 was considered statistically significant.

2.2 Production of ^{90}Nb and ^{95}Nb

^{90}Nb was produced via the ^{90}Zr(p,n)^{90}Nb reaction at the cyclotron MC32NI of the German Cancer Research Center, Heidelberg. For irradiation, a stack of three disks of natural zirconium (natural abundance: 51.45% ^{90}Zr) foils of 10 mm diameter and a thickness of 0.25 mm each was used. Irradiation was performed at 20 MeV proton energy and a current of 5 μA for 1 h. This initial proton energy decreased, by using an aluminium holder cover of 0.5 mm thickness, to 17.5 MeV while entering the first foil of Zr. Twenty-four hours after end of bombardment (EOB), production yield and impurities were measured by gamma ray spectroscopy. The absolute activity of ^{90}Nb was calculated as average of its two gamma-lines at 141.2 keV (66.8% abundance) and 1129.2 keV (92.7%). ^{95}Nb (t ½ = 35 days) was employed for the ex vitro biodistribution experiments. ^{95}Nb was produced *via* the ^{94}Zr(n,γ) → ^{95}Zr (β^-, t ½ = 64 days) → ^{95}Nb reaction from natural zirconium granules (1–3 mm, 99.8% ChemPur, Germany). Neutron irradiations were performed at the BR2 reactor at the Belgian Nuclear Research Centre, Belgium and at BERII reactor at Helmholtz Centre in Berlin, Germany.

The production of the radionuclides ^{95}Zr/^{95}Nb and ^{90}Nb was monitored by gamma ray spectroscopy, via emissions at 724.2 keV (44.2%) and 756.7 keV (54.0%) for ^{95}Zr, and at 765.8 keV (100%) for ^{95}Nb and 1129 KeV (92%) for ^{90}Nb.

2.3 Separation and purification of n.c.a. $^{95/90}$Nb

2.3.1 First separation strategy

The first separation strategy was applied for biodistribution studies in tumor-bearing mice. The separation procedure was modified following the procedure described by Busse *et al*. [14]. In short, the zirconium metal target (260 ± 3 mg) was transferred into a 50 mL vial and 2 mL of water was added. Under ice-cooling, 48% HF (0.63 mL) was added in small portions. After complete dissolution, 10 M HCl (6mL) and saturated boric acid (3.4 mL) were added. The $^{95/90}$Nb fraction was extracted with 0.02 M N-benzoyl-N-phenylhydroxylamine (BPHA) in $CHCl_3$ (5 mL) by vigorous stirring of the two phases in a 50 mL vial for 20 min. The aqueous phase was additionally washed with $CHCl_3$ (3mL). The organic phases were combined and washed with a mixture of 9 M HCl/0.001 M HF (2 mL) and with 9 M HCl (2 mL) and finally extracted with aqua regia (5 mL). For a final purification of $^{95/90}$Nb from remaining trace amounts of zirconium, an anionic exchange method was employed. After the aforementioned back extraction, the aqueous phase was evaporated to dryness. The residue was dissolved in a mixture of 0.25 M

HCl/0.1 M oxalic acid (0.5 mL) and adsorbed onto a small Aminex A27 (15±2 µm) anionic exchange column (20 × 1.5 mm). Elution was performed under slight overpressure of 0.3 bars. After loading, the column was washed with 10 M HCl (100 µL). Residues of Zr were removed by washing with a mixture of 9 M HCl/0.001 M HF (200 µL). $^{95/90}$Nb was eluted by a mixture of 6 M HCl/0.01 M oxalic acid (200 µL).

2.3.2 Alternative separation strategy

A second separation strategy was applied to provide a sample of ^{95}Nb with a higher radioactive concentration, for use in consequent biodistribution studies. Crude separation from the Zr target was performed following a published protocol [16]. In short, 2 mL of 21 M hydrofluoric acid containing the irradiated zirconium target was passed through the cation exchange resin (DOWEX 50 × 8, 100 mg, 200–400 mesh, 10 × 5 mm) resin in F^- form for the removal of colloids, unsolved target particles and possible trace contamination of 2^+ and 3^+ charged metals, such as for example Cu^{2+} or $Fe3^+$, from the target holder. The column was additionally washed with concentrated hydrofluoric acid (1 mL). The solution (3 mL) which passed through the cation exchange resin was transferred to an anion exchange column (300 mg, 25 × 5 mm) filled with AG 1 × 8 resin (200–400 mesh) in the F^- form. Nb^V remained on this resin and the bulk amount of Zr^{IV} passed through. The column was washed with concentrated HF (4.5 mL) to elute traces of Zr^{IV}, while *Nb stays on the column. A small plastic column was filled with UTEVA resin (150 µm, 100 mg, 10 × 5 mm). The aforementioned anion exchange column was directly connected with the UTEVA column and 7 mL of 0.3 M oxalic acid/ 7.5 M HCl were passed through both columns. The UTEVA column was next washed with 5 M HCl (5 mL). Traces of Zr^{IV} passed through the UTEVA, while $*Nb^V$ remains absorbed on the column. For elution of *Nb 0.1 M oxalic acid was applied. The column was washed with 200 µL and *Nb eluted with another 400 µL of 0.1 M oxalic acid.

2.4 Preparation of ^{95}Nb-oxalate, ^{95}Nb-chloride, and ^{95}Nb-desferrioxamine

^{95}Nb-Df-oxalate (10 mM) was prepared by dilution of the aliquot of the purified ^{95}Nb (5 ± 1 MBq) fraction with saline. ^{95}Nb-chloride was prepared by evaporation of an aliquot (50 µL) of the oxalate fraction obtained after ^{95}Nb (5 ± 1 MBq) purification and addition of several portions (3 × 100 µL) of 30 % HCl, after which the mixture was the dried again at 100 °C. The resulting preparation was dissolved in saline. For the preparation of ^{95}Nb-Df, 50 mM of Df in saline (1.45

mL) was mixed with ^{95}Nb-oxalate (50 µL) and incubated for 30 min at room temperature. The formation of ^{95}Nb-Df was monitored by thin layer chromatography.

2.5 Monoclonal antibody modification with Df-Bz-NCS.

The labeling of bevacizumab with ^{95}Nb was performed after the coupling of Df to bevacizumab. Coupling was performed by use of the novel bifunctional chelator p-isothiocyanato-benzyl-desferroxiamine (Df-Bz-NCS) from Macrocyclics (Dallas, USA). In short, while gently shaking, a threefold molar excess of Df-Bz-NCS (in 25 µL DMSO) was added to the mAb (2–3 mg in 1 mL 0.1 M $NaHCO_3$ buffer, pH 9.0), and incubated for 30 min at 37 °C. Non-conjugated chelate was removed by size-exclusion chromatography using a PD-10 column and 0.9% sodium chloride (pH 6.5) as the eluent. The number of chelates per antibody was assumed to be 1.5 according to our previous work [16] and the report from Perk *et al* [18].

2.6. Labeling of bevacizumab with $^{95/90}$Nb

Df-Bz-NCS-bevacizumab (abbreviated up to now as Df-bevacizumab) was labeled with $^{95/90}$Nb following two different labeling protocols. For the first protocol, to a $^{95/90}$Nb solution (10 ± 2 MBq for ^{95}Nb) in 6 M HCl/0.01 M oxalic acid solution (200 µL), 6 M NaOH (180 µL) and 1 M NaOH (230 µL) were added. After 3 min, 0.5 M HEPES buffer (pH 7.0) (390 µL) and Df-mAb (1.5mg/mL) (1.0mL) were added. The total volume of the mixture was 2 mL. For the second labeling protocol, a purified $^{95/90}$Nb fraction (10 ± 2 MBq for ^{95}Nb) in 0.1 M oxalic acid (20 µL) was mixed with 300 µL of normal saline and then the mixture was adjusted to pH 6–7 with 0.1 M Na_2CO_3 (50–60 µL). The modified mAb (300 µg, 2 nmol, 120 µL) was then added to this mixture and then the volume of the mixture was adjusted to 1mL saline. Both mixtures were incubated at room temperature for 60 min. Analysis of product formation was monitored by ITLC (0.02 M citric acid/MeCN, 90/10) at 10, 30 and 60 min and by HPLC at 60 min post-incubation. Finally, $^{95/90}$Nb-Df-Bz-NCS-bevacizumab was purified by using a PD-10 column, with 0.9% sodium chloride solution as the mobile phase. Figure 1 schematically represents the mAb modification with Df and further labelling with ^{90}Nb.

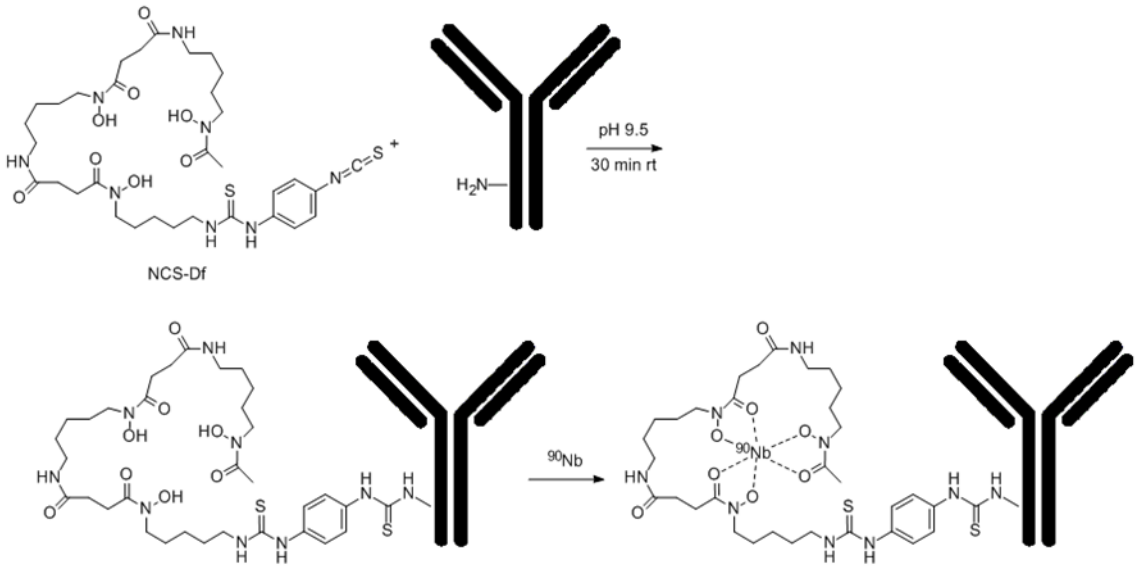

Figure 1: Df-conjugation of the mAb *via* NCS-Bz-Df and labeling with $^{95/90}$Nb (not proven by crystal structure)

2.7 *In vitro* stability

Stability of $^{95/90}$Nb-Df-bevacizumab was studied in two setups, first in normal saline at room temperature and in fresh human plasma at 37 °C. For preparation of human plasma, human blood was collected in heparinized polypropylene tubes and centrifuged at 5000 rpm at 4 °C for 5 min. The plasma was collected and three fold excess (300 µL) was incubated with $^{95/90}$Nb-Df-bevacizumab (100 µL) at 37 °C. Aliquots of the sample were withdrawn at 60 min, 3 h, 3 days, 5 days and 7 days, and analysed by ITLC and HPLC.

2.8 Biodistribution studies

All animal experiments were carried out in compliance to European and Greek regulations. Female athymic SCID (Severe Combined Immunodeficiency) mice (average weight 20 g, 5 weeks) as well as normal Swiss mice were obtained from the breeding facilities of the NCSR 'Demokritos'. The animals were kept under aseptic conditions until the day of biodistribution. The SCID mice were inoculated subcutaneously into the right front leg with M165 cells (1×10^7 cells/animal) in 100 µL fetal bovine serum-free medium. When tumors reached a size of 0.2 to 1 g (i.e., 10 to 15 days), biodistribution studies were performed. Tumor-bearing mice were injected via the tail vein with 100 µL of radiotracer [270 kBq/100 µg or 0.4 TBq/mmol (10.94 Ci/mmol)]. Groups of three animals were sacrificed at 4, 24, 48 and 168 h after injection of radiolabeled antibody. To determine VEGF-specificity, an excess of unlabelled bevacizumab

(100-fold) was injected 24 h prior to the injection of the ^{95}Nb-Df-bevacizumab. Blocking studies were performed at 24 and 48 h p.i. Biodistribution studies of ^{95}Nb-Df, ^{95}Nb-chloride and ^{95}Nb-oxalate were performed in healthy mice. Each animal received an injection of 100 µL of radiotracer [300 kBq/~10 µg or 4.5 TBq/mmol (121,56 Ci/ mmol)]. Groups of three animals were sacrificed at 4, 24, 48 and 168 h after injection of the compounds. Tumors (in the case of SCID mice), tissues and organs (blood, heart, liver, stomach, intestines, spleen, muscle, lungs, pancreas, muscle and bones) were excised, blotted dry and weighed. Samples were counted in a gamma counter (NaI gamma counter, Packard). Standards were prepared from the injected material and were counted each time simultaneously with the tissues excised, allowing for calculations to be corrected for physical decay of the radioisotope. Radiolabeled antibody distribution over time was expressed as injected dose per gram (%ID/g).

3 RESULTS

3.1 Production of *Nb

3.1.1 Production of ^{90}Nb

The overall irradiation yield of ^{90}Nb for three 1 h and 5 µA irradiations was 720 ± 50 MBq, i.e., 145 ± 10 MBq/µAh under given irradiation parameters. The radionuclidic purity of 90Nb after EOB was more than 97%. Minor isotopic impurities found were: ^{92m}Nb (t ½ = 10.2 days) = 1.64%, ^{95}Nb (t ½ = 35.0 days) = 0.08%, ^{95m}Nb (t ½ = 3.6 days) = 0.29% and ^{96}Nb (t ½ = 23.4 h) = 0.88%. The calculated theoretical specific activity for ^{90}Nb is 8.9 x 10^{7} GBq/g.

3.1.2 Production of ^{95}Nb

At a neutron flux of $2 \cdot 10^{14}$ $s^{-1} \cdot cm^{-2}$ (BER II), a 50-day irradiation of 300 mg target produced more than 1.5 GBq of ^{95}Zr. The maximum daughter activity of ^{95}Nb generated from ^{95}Zr was obtained at ~67 days, EOB. The calculated theoretical specific activity for ^{95}Nb is 1.4 x 10^{6} GBq/g.

3.2 Separation and purification of no-carrier added $^{95/90}$Nb

3.2.1 First separation strategy

The extraction steps provided crude separation of $^{95/90}$Nb from the target material with the organic phase collecting more than 99% of $^{95/90}$Nb. After the back extraction procedure, the 5 mL aqueous phase contained 90–95% of the $^{95/90}$Nb activity. After both extractions this corresponds

to a high reduction of the Zr target mass by a factor of 10^4. Subsequent anionic exchange separation further removes those traces of Zr. The final separation yield of $^{95/90}$Nb was 60–65% and the decontamination factor for Zr/Nb was ≥10^7, representing ≤26 ng of Zr present in the final $^{95/90}$Nb fraction. The separation was performed for each niobium isotope separately.

3.2.2 Second separation strategy

The overall separation proceeds with a yield of 93–95% of $^{95/90}$Nb, collected in 400 µL 0.1 M oxalic acid. The whole separation procedure takes less than one hour, which is almost 4 times faster than the first separation method. The decontamination after UTEVA purification is 3×10^8. This decontamination factor equals 0.77 ng of zirconium present in the final fraction for a 260 mg zirconium target.

3.3 Preparation of $^{95/90}$Nb-labeled Df-Bz-NCS-mAb

The ^{90}Nb labeling yield was > 90 % (96% ITLC, 95 % HPLC) after 1 h. Labeling kinetics indicate that the labeling yields reached ≥ 80 % already at 15 min and increased to more than 90 % after 50 min. After SEC separation on a PD-10 column, the ^{90}Nb-Df-mAb derivative had 99.0 % purity. The specific activity of $^{95/90}$Nb-bevacizumab labeled with the ^{95}Nb from the first separation strategy was 0.4 TBq/mmol (10.94 Ci/mmol), while from the alternative separation strategy, the specific activity of the radiotracer was 4.5 TBq/mmol (121.56 Ci/mmol).

3.4 *In vitro* stability

After 3 days of incubation in saline at room temperature, more than 99% (≥ 99 % HPLC, ≥ 99 % ITLC) and after 7 days ≥ 95 % (99 % HPLC, 97 % ITLC) of $^{95/90}$Nb-Df-bevacizumab were detected. Stability testing in fresh human plasma at 37 °C showed only slightly higher product degradation (Fig. 2). After 3 days of incubation ≥ 94 % (97 % HPLC, 94 % ITLC) of labeled product was available, while at 7 days ≥ 86 % (89 % HPLC, 86 % ITLC) of the product was still intact.

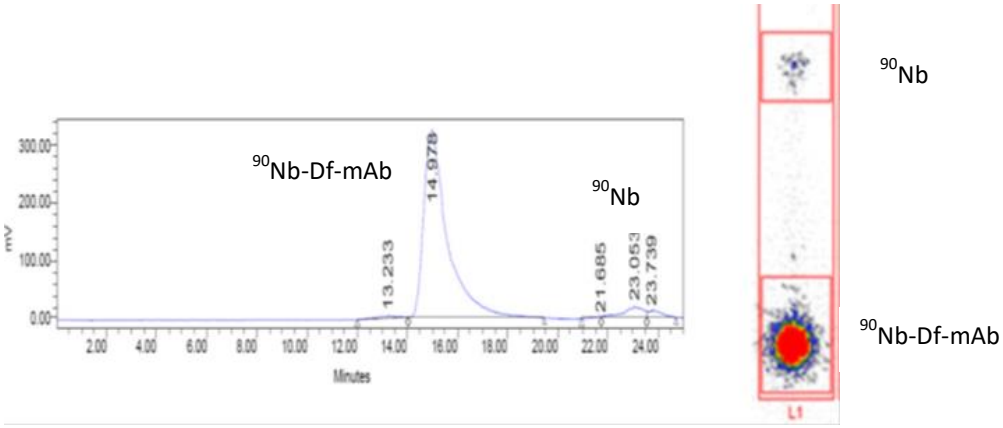

Figure 2: ITLC image (right) and HPLC chromatogram (left) of *in vitro* stability ^{90}Nb-Df-bevacizumab after 7 days in saline at room temperature

3.5 Biodistribution experiments

3.5.1 Biodistribution of ^{95}Nb-oxalate, ^{95}Nb-chloride and ^{95}Nb-Df in healthy mice

The biodistribution of ^{95}Nb-oxalate and ^{95}Nb-chloride showed similar results, with no specific organ uptake observed (Fig. 3). However, for ^{95}Nb-chloride the uptake in all organs was higher in comparison to ^{95}Nb-oxalate. The main uptake was in the blood, lungs and bones. Slight bone accumulation was measured for both substances. Uptake for liver, kidneys and spleen was approximately 1% at 24 h p.i. for oxalate and below 3 % for the chloro species. After 168 h (7 days) p.i, all organs uptakes except for bone were below 1 % and 2 % respectively, for both ^{95}Nb-oxalate and ^{95}Nb-chloride, apart from the bone uptake, which was ≥ 2 % for the oxalate and ≥ 4 % for the chloride species. ^{95}Nb-Df showed a very fast clearance from the body (Fig. 3). At 24 h p.i., no single organ uptake above 0.5 % was observed. After 4 h, uptake in kidneys, stomach and intestines was still detected, while uptake in all other organs was almost negligible. After 168 h p.i. the radiolabeled products had almost completely cleared from the organism.

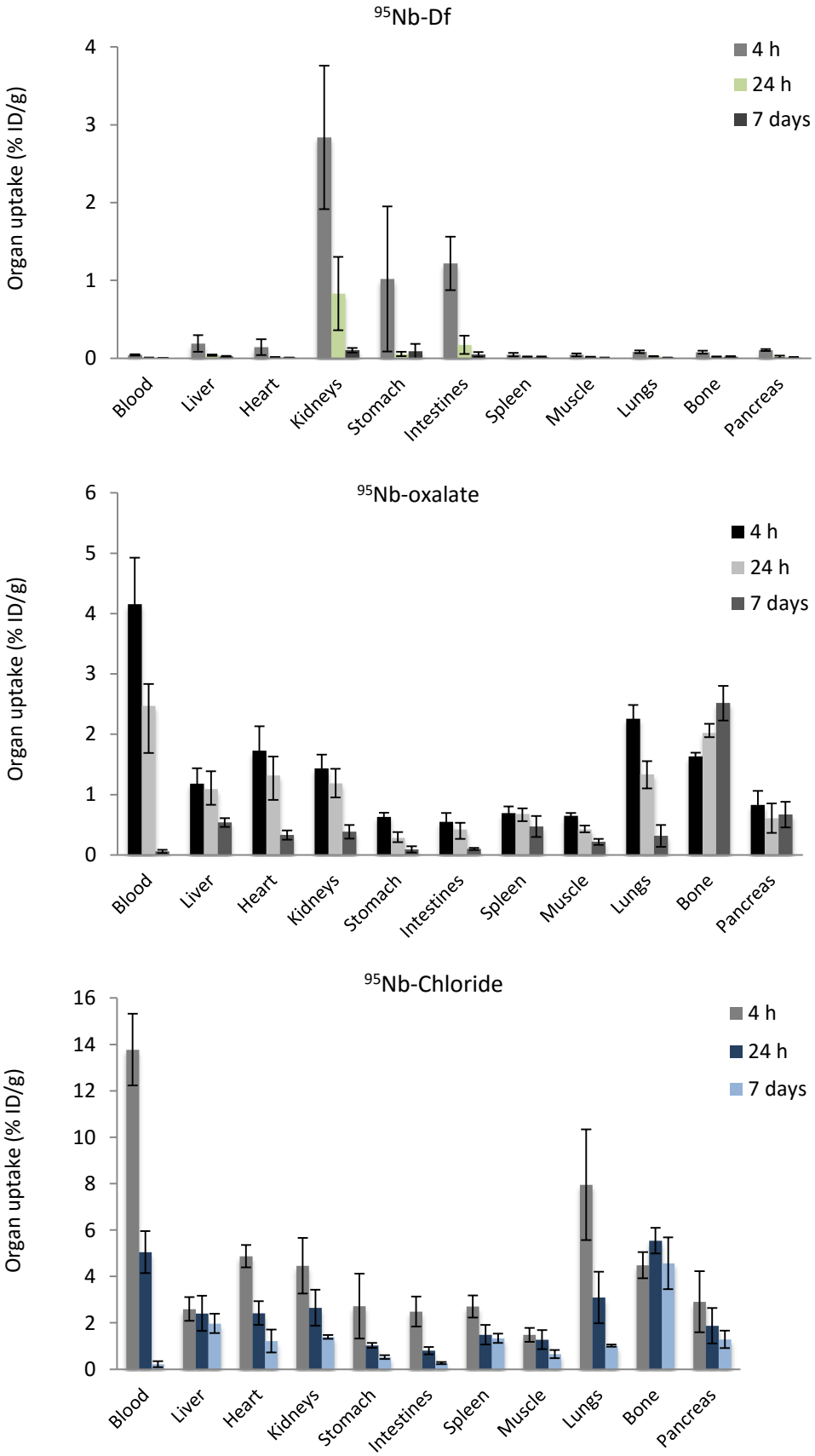

Figure 3: Biodistribution of ^{95}Nb-oxalate, ^{95}Nb-chloride and ^{95}Nb-Df in healthy mice

3.5.2 Biodistribution of ^{95}Nb-Df-bevacizumab of two different specific activities in tumor-bearing and healthy mice

Biodistribution of ^{95}Nb-Df-bevacizumab at an injected dose of 270 kBq/100 µg/mouse showed a relatively low accumulation in the tumor (≤ 3 %) at 24 h p.i., which decreased in time (Fig. 4). On the other hand, high accumulation in the liver (> 30 %), spleen (> 10 %) and kidneys (> 5 %) was detected. Indicative blocking studies performed at two time-points (24 and 48 h p.i.) showed that VEGF was significantly blocked when an excess amount of bevacizumab (100-fold) was injected 24 h prior to the injection of the radiotracer, thus showing the specificity of ^{95}Nb-bevacizumab binding to the VEGF-positive tumor (24 h p.i.: 2.8 % ± 1.1 ID/g *vs* 1.1 % ± 0.4 ID/g, $p < 0.01$; 48 h p.i.: 1.6 % ± 0.6 ID/g *vs* 0.6 % ± 0.3 ID/g, $p < 0.03$).

To prove that the previous biodistribution data, i.e., high liver, lung and spleen uptake, were a consequence of the antibody concentration, i.e., the specific activity of the ^{95}Nb-Df-bevacizumab batch injected and not of the instability of the labeled product, another biodistribution study was conducted, where normal Swiss mice were injected with a higher specific activity product [4.5 TBq/mmol (121.56 Ci/mmol)].

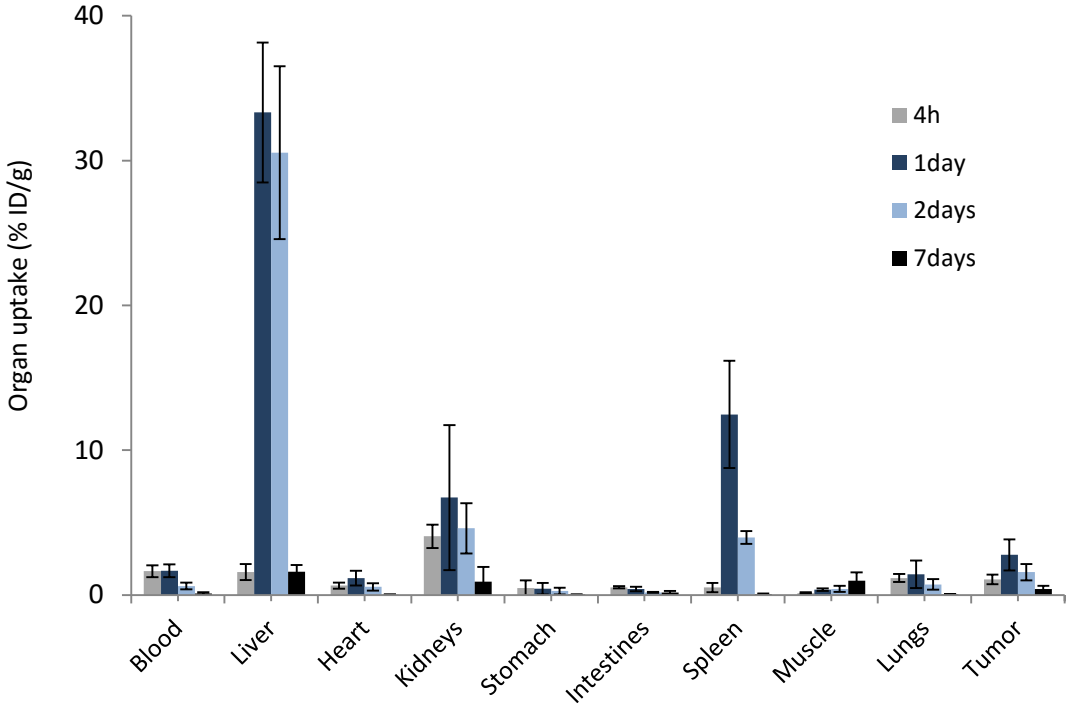

Figure 4: Biodistribution of low specific activity 0.4 TBq/mmol (10.94 Ci/mmol) of ^{95}Nb-Df-bevacizumab in tumor-bearing mice

The results presented in figure 5 show a different kinetic behaviour for the higher specific activity of ^{95}Nb-Df-bevacizumab. Significantly less uptake in the liver (3.3 ± 0.3 % ID/g vs 33.3 % ± 4.8 ID/g, $p < 0.0002$), as well as in the spleen (2.2 % ± 0.3 ID/g vs 12.5 % ± 3.7 ID/g, $p < 0.004$) was observed at 24 h p.i. for the higher-specific activity radiotracer, which further rapidly decreased over time. After 168 h, the uptake in these organs was less than 2 %. On the other hand, a much higher initial uptake in blood (13.0 % ± 1.1 ID/g vs 1.7 % ± 0.4ID/g,) and lungs (5.9 % ± 0.1 ID/g vs 1.43 ± 0.95 % ID/g, $p < 0.0006$) was detected. At 168 h p.i., the uptake in these organs is significantly decreased as well (6.9 % ± 1.5 ID/g vs 13.0 % ± 1.1 ID/g, $p < 0.003$ and 2.7 % ± 0.8 ID/g vs 6.0 % ± 0.1 ID/g, $p < 0.001$ for blood and lung at 168 h and 24 h p.i., respectively). High tracer uptake was observed in the heart, which can be attributed to high blood uptake levels. A constant bone uptake (c.a 2 % ID/g) was observed over the range of 4 to 168 h, thus allowing us to conclude that no release of ^{95}Nb from the labeled monoclonal antibody occurs.

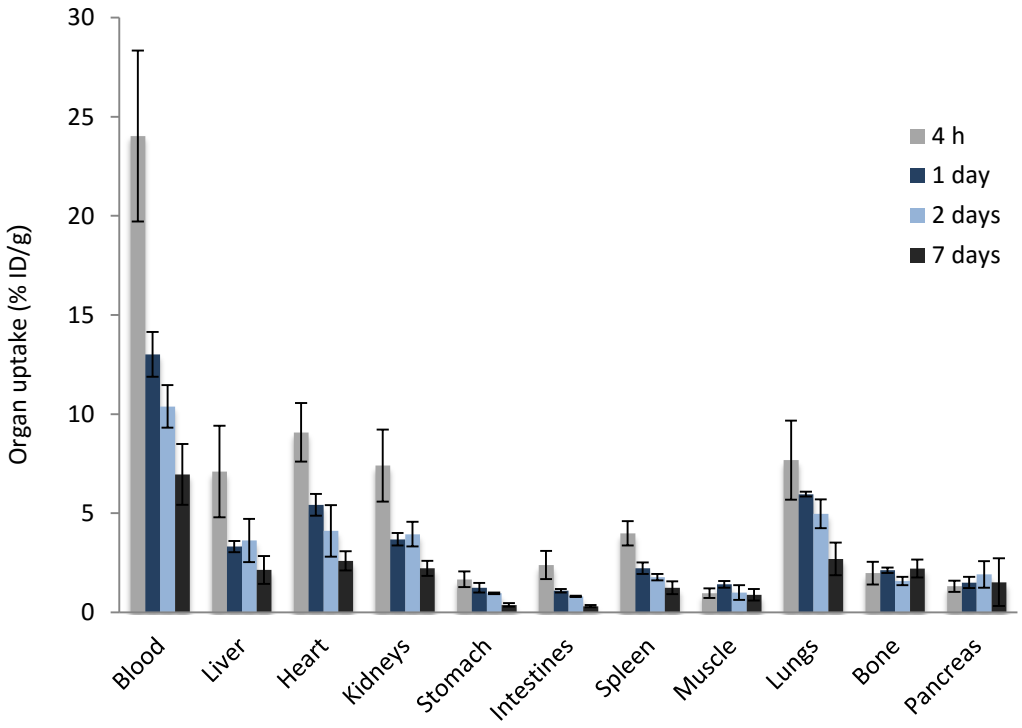

Figure 5: Biodistribution of high specific activity 4.5 TBq/mmol (121.56 mCi/mmol) of ^{95}Nb-Df-bevacizumab in normal Swiss mice

4 DISCUSSION

The radiolabeled monoclonal antibody ^{95}Nb-Df-bevacizumab, with a maximal specific activity of 0.4 TBq/mmol (10.94 Ci/mmol) was synthesized during the first separation strategy which is described herein. Our alternative separation strategy provided more than 10 times higher specific activity [4.5 TBq/mmol (121,56 Ci/mmol)] for ^{95}Nb and even higher for ^{90}Nb (~45 TBq/mmol (1216 Ci/mmol).

This study aimed at first evaluations of a ^{90}Nb-labeled monoclonal antibody. While both isotope productions and labeling appear to be established, the data on the *in vitro* stability of the proof-of-principle ^{95}Nb-Df-bevacizumab have been obtained for the first time. It can be concluded, that the Df-mediated label is stable *in vitro*. *In vivo* experiments showed the same result, where ^{90}Nb-data *in vivo* match ^{95}Nb data from *in vitro* studies. However, the pharmacology of the two radiotracers clearly depended on the specific activity of the ^{90}Nb-labeled monoclonal antibody, revealing significant accumulation in non-tumor organs.

Consequently, the separation chemistry of radio-niobium from both nuclear reactor (^{95}Nb) and cyclotron (^{90}Nb) irradiated zirconium targets was improved. This allowed the synthesis of ^{90}Nb-Df-bevacizumab batches of significantly increased specific activity, which is comparable to the specific activity of bevacizumab radiolabeled with other isotopes, as shown by various groups e.g. Nagengast *et al*. [3] reported specific activities of 8.7 TBq/mmol (235.14 Ci/mmol) and 7.5 TBq/mmol (202.7 Ci/mmol) for ^{89}Zr-bevacizumab and ^{111}In-bevacizumab, respectively, while Paudyal et al [4] acquired specific activities of 0.38–0.6 TBq/mmol (10.2–16.2 Ci/mmol) for ^{64}Cu-bevacizumab.

Biodistribution of 100 µg of bevacizumab with our lower specific activity of ^{95}Nb-Df-bevacizumab (0.4 TBq/mmol) showed adequate tumor uptake (3%), with tumor-to-blood ratios of 1.65 and 3.64 at 24 and 168 h p.i. respectively, which are comparable to the results of Nagengast *et al*., for ^{89}Zr-bevacizumab (T/B ratios of 0.51 and 1.86 at 24 and 168 h p.i. respectively), and other groups [3,4]. The significant difference which was observed was the unusually high uptake in liver, spleen and kidneys at 24 h p.i. The first image of a ^{90}Nb-labeled antibody was also acquired on an experimental small animal PET camera, which was in good agreement to our *ex vivo* biodistribution studies, i.e., even though the acquired images need refining, satisfactory tumor and enhanced liver uptake can be observed. To prove that liver and spleen uptake is the result of low specific activity radiolabeled antibody, an *in vivo* evaluation of ^{95}Nb-oxalate, ^{95}Nb-chloride and ^{95}Nb-Df was initially conducted. These compounds can be formed by destruction of the

labeled product. They biodistribution values in healthy mice did not show specific uptake in any organs.

The concentration of ^{95}Nb-chloride and ^{95}Nb-oxalate in the blood remained high up to 24 h p.i., which can probably be attributed to the formation of metal complexes with plasma proteins [19,20]. A relatively high uptake in the heart and lung, both highly-vascularized organs, is also observed up to 24 h p.i. This activity was rapidly cleared in favour of uptake in the bone. The bone uptake for both ^{95}Nb-chloride and ^{95}Nb-oxalate demonstrates the high affinity of Nb(V) to phosphonate, which is so strong that, in the case of ^{95}Nb-oxalate it shows a slow but steady increase in percentage of bone uptake, while for ^{95}Nb-chloride a small decrease in bone uptake is observed. ^{95}Nb-Df was immediately cleared from the system, without any sign of bone uptake. The final step in this work was to evaluate a higher specific activity sample of ^{95}Nb-bevacizumab in healthy mice. These results showed pronounced uptake in the blood, heart and lungs, which diminished at 24 h p.i., while uptake in the liver, spleen and kidneys, as well as in bone, was low. These data clearly prove the high *in vivo* stability of *Nb-Df-conjugated biomolecules.

5 CONCLUSIONS

The obtained results provide a very important proof of stability of $^{95/90}$Nb labeled biomolecules *in vivo*. The radiolabeled monoclonal antibody ^{95}Nb-Df-bevacizumab with a relatively high specific activity (4.5 TBq/mmol (121.56 Ci/mmol) was obtained, which allowed us to conduct biodistribution studies upon injection of a low concentration of bevacizumab (~10 μg/100 μL). The continuation of this project is well justified, as our results show that there is great promise for the application of ^{90}Nb in *immuno*-PET.

ACKNOWLEDGMENTS

The authors gratefully acknowledge financial support from the COST Action TD1004 (Theranostics Imaging and Therapy: An Action to Develop Novel Nanosized Systems for Imaging-Guided Drug Delivery), the Program for the Promotion of the Exchange and Scientific Cooperation between Greece and Germany IKYDA, scientific project titled “Targeted Immuno-PET imaging of neoangiogenesis with biomolecules labeled with the positron-emitter Niobium-90” (Contract number 205), the German Research Foundation under DFO Ro 985/40-1 and

Russian Foundation for Fundamental Research grant (RFBR 15-53-12372). We <would also like to thank the teams of BR2 Berlin and TRIGAMainz reactors for production of the Niobium isotopes.

REFERENCES

[1] Rösch F, Baum RP. Generator-based PET radiopharmaceuticals for molecular imaging of tumours: on the way to THERANOSTICS. Dalton Trans 2011;40(23):6104–11.

[2] Ellis LM, Hicklin DJ. VEGF-targeted therapy: mechanisms of anti-tumour activity. Nat Rev Cancer 2008; 8 :579–91.

[3] Nagengast WB, de Vries EG, Hospers GA, Mulder NH, de Jong JR, Hollema H, et al. In vivo VEGF imaging with radiolabeled bevacizumab in a human ovarian tumor xenograft. J Nucl Med 2007; 48: 1313–9.

[4] Paudyal B, Paudyal P, Noboru O, Hanaoka H, Tominaga H, Endo K. Positron emission tomography and biodistribution of vascular endothelial growth factor with 64Cu-labeled bevacizumab in colorectal cancer xenografts. Cancer Sci 2011;201(1):117–21.

[5] Nagengast WB, de Korte MA, Oude Munnink TH, Timmer-Bosscha H, den Dunnen WF, Hollema H, et al. ^{89}Zr-bevacizumab PET of early antiangiogenic tumor response to treatment with HSP90 inhibitor NVP-AUY922. J Nucl Med 2010;51:761–7.

[6] Nayak TK, Garmestani K, Baidoo KE, Milenic DE, Brechbiel MW. PET imaging of tumor angiogenesis in mice with VEGF-A-targeted 86Y-chx-a”-dtpa-bevacizumab. Int J Cancer 2011;128:920–6.

[7] Chang AJ, Sohn R, Lu ZH, Arbeit JM, Lapi SE. Detection of rapalog-mediated therapeutic response in renal cancer xenografts using ^{64}Cu-bevacizumab immunoPET. 2013; 8(3):e58949.

[8] Vugts DJ, Visser GW, van Dongen GA. ^{89}Zr-PET radiochemistry in the development and application of therapeutic monoclonal antibodies and other biologicals. Curr Top Med Chem 2013;13(4):446–57.

[9] Severin GW, Engle JW, Barnhart TE, Nickles RJ. ^{89}Zr radiochemistry for positron emission tomography. Med Chem 2011;7(5):389–94.

[10] Anderson CJ, Ferdani R. Copper-64 radiopharmaceuticals for PET imaging of cancer: advances in preclinical and clinical research. Cancer Biother Radiopharm 2009; 24(4):379–93.

[11] Rösch F, Herzog H, Stolz B, Brockmann J, Kohle M, Muhlensiepen H, et al. Uptake kinetics of the somatostatin receptor ligand [86Y]DOTA-DPHE1-TYR3-octreotide ([^{86}Y]smt487) using positron emission tomography in non-human primates and calculation of. Med Mol Imag 2003;30:510–8.

[12] Nayak TK, Brechbiel MW. ^{86}Y based PET radiopharmaceuticals: radiochemistry and biological applications. Med Chem 2011 Sep;7(5):380–8.

[13] Tolmachev V. Radiobromine-labelled tracers for positron emission tomography: possibilities and pitfalls. Curr Radiopharm 2011;4(2):76–89.

[14] Busse S, Brockmann J, Roesch F. Radiochemical separation of no-carrier-added radioniobium from zirconium targets for application of 90Nb-labelled compounds. Radiochim Acta 2002; 90: 411–5.

[15] Radchenko V, Filosofov DV, Bochko OK, Lebedev NA, Rakhimov A, Aksenov NV, et al. Separation of 90Nb from zirconium target for application in immuno-PET. Radiochim Acta 2014;102(5):433–43.

[16] Radchenko V, Hauser H, Eisenhut M, Vugts JD, van Dongen GAMS, Roesch F. ^{90}Nb— a potential PET nuclide: production and labeling of monoclonal antibodies. Radiochim Acta 2012;100(11):857–63.

[17] Radchenko V, Busse S, Roesch F. Desferrioxamine as an appropriate chelator for ^{90}Nb: comparison of its complexation properties for M-Df-octreotide (M = Nb, Fe, Ga, Zr). Nucl Med Biol 2014;41(9):721–7.

[18] Perk LR, Vosjan MJ, Visser GW, Budde M, Jurek P, Kiefer GE, et al. psothiocyanatobenzyl-desferrioxamine: a new bifunctional chelate for facile radiolabeling of monoclonal antibodies with zirconium-89 for immuno-PET imaging. Eur J Nucl Med Mol Imaging 2009;37:250–9.

[19] Mealy J. Turn-over of carrier-free zirconium in man. *Nature* 1957; 179: 673–674.

[20] Backstrom J, Hammarstrom L, Nelson A. Distribution of zirconium and niobium in mice: autoradiographic study. Acta Radiol Diagn 1967;6(2):122–8.

3.5 Conjugation, labelling and *in vitro / in vivo* assessment of an anti-VEGF monoclonal antibody labelled with niobium isotopes

Conjugation, labelling and *in vitro / in vivo* assessment of an anti-VEGF monoclonal antibody labelled with niobium isotopes.

A. de la Fuente[1], V. Radchenko[1], T. Tsotakos[2], C. Tsoukalas[2], M. Paravatou-Petsotas[2], A. L. Harris[3], U. Köster[4], F. Rösch*[1], P. Bouziotis[2]

[1]Institute of Nuclear Chemistry, Johannes Gutenberg University, Mainz, Germany

[2]Institute of Nuclear & Radiological Sciences & Technology, Energy & Safety, N.C.S.R. "Demokritos", Athens, Greece

[3]Weatherall Institute of Molecular Medicine, University of Oxford, Oxford, U.K.

[4] Institut Laue-Langevin, Grenoble, France.

ABSTRACT

^{90}Nb is a positron-emitting radionuclide that exhibits attractive characteristics for use in the design and synthesis of radioimmunoconjugates. In the current study we investigated ^{90}Nb as a possible future isotope for *immuno*-PET. Prior to ^{90}Nb *in vivo* evaluatios, this paper describes *in vitro* and *ex vivo* studies using a ^{95}Nb-monoclonal antibody analogue. ^{95}Nb has a half-life of 35 days and is convenient for long-term studies. ^{95}Nb-labelled bevacizumab was evaluated for early antiangiogenic tumor response assessment and the results were compared with other well established PET nuclides for *immuno*-PET.

Methods:

Bevacizumab was modified with Df-Bz-NCS (Df) and labelled with ^{95}Nb which was previously separated from irradiated natural Zr in a multistep procedure. Stability of ^{95}Nb-Df-bevacizumab was evaluated in saline and in human plasma over 7 days. Biodistribution *ex vivo* studies were performed in M165 tumor-bearing mice.

Results:

^{95}Nb was obtained in high purity and high specific activity in 200 µL oxalic acid (0.1 M), ready for labelling**.** Df-bevacizumab labelling was efficient (>95%) and *in vitro* stability of ^{95}Nb-Df-bevacizumab was high. *Ex vivo* studies displayed good tumor-to-background ratios, optimum after 2 d p.i., when 20 µg of antibody per mouse were injected.

Conclusions:

^{95}Nb was successfully produced, purified and labelled to a pre-modified desferrioxamine-bevacizumab. After *in vitro* stability of ^{95}Nb-Df-bevacizumab has been demonstrated, *ex vivo* biodistribution studies showed specific tumor uptake in M165 tumor-bearing mice. Consequently, *in vivo* studies with ^{90}Nb-Df-bevacizumab and small animal PET are in preparation, and we expect, that ^{90}Nb-Df-conjugated antibodies will show potential for *immuno*-PET.

Keywords: $^{90/95}$Nb / bevacizumab / labelling / VEGF / biodistribution/ *immuno*-PET

1 INTRODUCTION

The application of radionuclide-labelled biomolecules such as monoclonal antibodies or antibody fragments for imaging purposes is named *immunoscintigraphy*. More specifically, when the nuclides used are positron emitters, the technique is referred to as *immuno-PET*, which combines the high sensitivity and resolution of a PET camera with the specificity of a monoclonal antibody (mAb). In personalized therapeutic strategy, *immuno*-PET provides the confirmation of both tumor expression and verification of the mAb accumulation, thus being a key tool in treatment evaluation [1].

Currently, there is an urgent need for radionuclides with a half-life (t ½) which correlates with the biological kinetics of biomolecules under question. Radionuclide candidates have to match some features to be used for *immuno*-PET. The most important ones are: i) a half-life paralleling the biological half-life of the mAb, ii) a high positron branching with no or weak accompanying radiation (β^-, γ), iii) a preferably low β^+-energy to allow high-resolution PET imaging, iv) the availability of the radionuclide, i. e. an efficient production and radiochemical separation route and v) a facile, efficient and stable coupling to mAbs as well as maintenance of the *in vivo* biological characteristics of the antibody. Nowadays the following positron emitters are under investigation for *immuno*-PET: ^{76}Br (t ½ = 16.2 h) [2], ^{86}Y (t ½ = 14.7 h) [3], ^{64}Cu (t ½ = 14 h) [4], ^{89}Zr (t ½ = 78.4 h) [5-7] and ^{124}I (t ½ = 100.3 h) [8] (Tab.1).

Table 1. Main characteristics of the most commonly-used PET nuclides [1].

Positron emitter	Half-life (hours)	Main β^+ energies	
		(keV)	(%)
^{68}Ga	1.13	1.899	87.9
^{18}F	1.83	634	100.0
^{64}Cu	12.7	653	17.4
^{86}Y	14.7	1.221	11.9
		1.545	5.6
^{76}Br	16.3	990	5.2
		3.382	25.8
		3.941	6.0
^{89}Zr	78.4	897	22.7
^{124}I	100.3	1.535	11.8
		2.138	10.9

Due to the slow pharmacokinetics of intact antibodies, positron-emitting radionuclides with long and medium-long half-life are of interest for PET-imaging with antibodies; therefore ^{68}Ga and ^{18}F, which are common nuclides in routine PET imaging applications, are not suitable. ^{90}Nb is a promising candidate due its half-life of 14.6 hours, rather high positron branching of 53% and low β^+ energy of E_{mean} = 0.35 MeV [2]. In previous reports, we have proposed ^{90}Nb as a promising candidate for application in *immuno*-PET [9-12]. Moreover, among the group of niobium isotopes we find the beta-emitter ^{95}Nb, which could be exploited as a therapeutic isotope for molecules presenting slower pharmacokinetics, such as monoclonal antibodies. These two isotopes of niobium could constitute the theranostic pair ^{90}Nb/^{95}Nb, where the same biomolecule will be labeled with two different radioisotopes of the same element, thus affording both an imaging and a therapeutic agent with identical *in vivo* properties.

The humanized monoclonal antibody (mAb) bevacizumab was the antibody chosen for the experiments as currently many studies are concentrating on the labelling of bevacizumab with radionuclides for analyzing its *in vivo* behavior [4, 10, 13-16]. Bevacizumab plays a key role in angiogenesis, as it binds all vascular endothelial growth factor-A (VEGF-A) isoforms, preventing them from binding to receptors, thus blocking the biologic pathways induced after VEGF binding [17]. By blocking the receptors, the growth of vascular endothelial cells derived from arteries and veins, which are necessary to supply solid tumors with oxygen and nutrients, is highly diminished. Because of the great variability of response to bevacizumab and lack of any predictive biomarkers [18], search for sensitive technologies to monitor anti-angiogenic response *in vivo* is an ongoing one. It has previously been shown that radiolabelled bevacizumab can be used for *in vivo* VEGF visualization and quantification, due to its interaction with the larger isoforms of VEGF-A that are associated with the surface and/or the extracellular matrix [19]. Our research efforts are focused on the development of ^{90}Nb-bevacizumab as an alternative PET imaging agent for *in vivo* monitoring of VEGF-A levels within tumors.

In order to introduce ^{90}Nb as a novel positron emitter for immuno-PET, we have assessed the *in vitro* stability of ^{95}Nb-radiolabelled bevacizumab, as well as its cell binding capacity to breast cancer cells transfected with the VEGF-165 isoform. Furthermore, *ex vivo* biodistribution studies on tumor-bearing SCID mice were performed.

2 MATERIALS AND METHODS

2.1 Materials

Reagents were purchased from Sigma-Aldrich (Germany) and used without further purification, unless otherwise stated. Deionized water (18 MΩ cm^{-1}) and ultra-pure HCl solution were used. No further special measures were taken regarding working under strict metal-free conditions. Bevacizumab (Avastin®, Roche) was bought from Roche Ellas S. A. (Greece). For the purification of conjugated and labeled antibodies, PD-10 columns (GE Healthcare Life Science) were applied, for ion exchange separation Aminex A27, 15 ± 2 μm and AG1x8, 200-400 mesh anionic exchange resins and DOWEX 50x8, 200-400 mesh (BioRad) were used. For solid extraction, UTEVA® resin (Triskem Int., France) was applied.

The production yield, radionuclidic purity, radiochemical purity and separation yield of ^{95}Nb were determined by γ-ray spectroscopy using an Ortec HPGe detector system and Canberra Genie 2000 software. The dead time of the detector was always kept below 10%. The detector was calibrated for efficiency at all positions with the certified standard solution QCY48, R6/50/38 (Amersham, UK).

VEGF165-transfected MDA MB 213 cells (M165) were cultured at safety level I in minimum essential medium (Eagle) with 2 mM L-glutamine in the presence of 10% fetal bovine serum, at 37 °C in a humidified 5% CO_2 incubator.

Labelling efficiency and stability of ^{95}Nb-bevacizumab was monitored by instant thin layer chromatography (iTLC) and high performance liquid chromatography (HPLC). ITLC was performed on chromatography strips (Biodex, NY). As mobile phase, 0.02 M citrate buffer (pH 5.0) was used. HPLC monitoring was performed on a Waters HPLC system using a TSKgel G3000SWXL size exclusion column (TOSOH Bioscience, Germany). As eluent, a mixture of 0.05 M sodium phosphate and 0.15 M sodium chloride (pH 6.8) solution was used at a flow rate of 0.8 mL/min. T-test was used for statistical analysis. A *p* value less than 0.05 was considered statistically significant.

2.2 Production of ^{95}Nb

^{95}Nb (t ½ = 35 d) was employed for biodistribution experiments to cover longer periods. It was produced via the ^{94}Zr (n, γ) → ^{95}Zr (β^-, t ½ 64 d) → ^{95}Nb reaction from 99.94% pure zirconium foil (Product No. 00417, Alfa Aesar, USA). The foil contained 0.16 ppm Nb. Neutron irradiation was

performed at the high flux reactor of Institute Laue-Langevin in Grenoble, France. The production of the radionuclides ^{95}Zr / ^{95}Nb was monitored by gamma ray spectrometry, *via* emissions at 724.2 keV (44.2%) and 756.7 keV (54.0%) for ^{95}Zr, and at 765.8 keV (100%) for ^{95}Nb.

2.3 Separation and purification of n.c.a. ^{95}Nb

The separation/purification strategy, leading to high radioactive concentration of ^{95}Nb, has been described elsewhere[9]. Briefly, the irradiated zirconium target, dissolved in 21 M HF, was passed through a cation exchange resin (DOWEX 50x8, 100 mg, 200-400 mesh, 10x5 mm) in F^- form for the removal of colloids, unsolved target particles and possible trace contamination of 2^+ and 3^+ metal cations, such as for example Cu^{2+} or Fe^{3+} from the target holder. The column was additionally washed with concentrated hydrofluoric acid (1 mL). This solution (3 mL) was transferred to an anion exchange column (300 mg, 25x5 mm) filled with AG 1x8 resin (200-400 mesh) in the F^- form. $^{95}Nb^{V}$ remained on this resin and the bulk amount of Zr^{IV} passed through. The column was washed with concentrated HF (4.5 mL) to elute traces of Zr^{IV}, while ^{95}Nb stays on the column. A small plastic column was filled with UTEVA resin (150 µm, 300 mg, 25 x 5 mm). The aforementioned anion exchange column was directly connected with the UTEVA column and 4 mL of 0.3 M oxalic acid/ 7.7 M HCl were passed through both columns. The UTEVA column was next washed with 5 M HCl (5 mL). Traces of Zr^{IV} passed through the UTEVA, while $^{95}Nb^{V}$ remains absorbed on the column. For elution of ^{95}Nb, oxalic acid 0.1 M was applied, the column was first washed with 200 µL with another 400 µL ^{95}Nb was eluted.

2.4 Monoclonal antibody modification with Df-Bz-NCS

Desferrioxamine (Df) has been shown to be an appropriate chelator for Nb [20]. Bevacizumab was pre-modified with the bifunctional chelator Df-Bz-NCS following the protocol for ^{89}Zr labelling [21]. In short, a threefold molar excess of Df-Bz-NCS (in 20 µL DMSO) was added to 5 mg of the mAb in 1 ml 0.1 M $NaHCO_3$ buffer, pH 9.0, and incubated for 30 min at 37 °C. Non-conjugated chelator was separated by size exclusion chromatography (SEC) using a PD-10 column and saline as the eluent.

2.5 Labelling of bevacizumab with ^{95}Nb

A purified ^{95}Nb fraction in 0.1 M oxalic acid (20-100 µL) was mixed with 300 µL of 0.9% sodium chloride solution and then the mixture was adjusted to pH 6-7 with 0.1 M Na_2CO_3 (50-60 µL). The

modified mAb (150-300 µg, 120 µL) was then added to this mixture and the volume of the mixture was adjusted to 1 mL with normal saline. The mixture was incubated at room temperature for 60 min. Finally, ^{95}Nb-Df-Bz-NCS-bevacizumab was purified using a PD-10 column, with 0.9% sodium chloride solution as the mobile phase. Analysis of the product was monitored by ITLC (0.02 M citric acid/ACN, 90/10) and HPLC using a TSKgel G3000SWXL size exclusion column (TOSOH Bioscience, Germany) and as eluent, a mixture of 0.05M sodium phosphate and 0.15M sodium chloride (pH 6.8) solution at a flow rate of 0.8mL/min for 60 min.

2.6 *In vitro* metabolic stability

Metabolic stability of ^{95}Nb-Df-bevacizumab was studied in normal saline at room temperature and in fresh human plasma at 37°C. For preparation of human plasma, human blood was collected in heparinized polypropylene tubes and centrifuged at 5000 rpm at 4°C for 5 min. The plasma was collected and in three fold excess (300 µL) incubated with ^{95}Nb-Df-bevacizumab (100 µL) at 37°C. Aliquots of the sample were withdrawn, treated with ethanol (2:1 EtOH/aliquot, v/v) and analyzed by ITLC and HPLC.

2.7 Immunoreactivity

The immunoreactivity of radiolabelled bevacizumab was determined using a VEGF ELISA assay, as described by Collingride *et al* [22]. Briefly, 96-well ELISA plates were coated with 100 µl human VEGF165 (5 µg/ml, R&D Systems; Oxfordshire, United Kingdom) overnight in bicarbonate coating buffer (15 mM Na_2CO_3, 35 mM $NaHCO_3$, pH 9.6) at 4°C. As a next step, wells were blocked with 100 µl of 1% BSA in PBS. The wells were then washed three times with PBS and 0.1% Tween 80. Radiolabelled bevacizumab was diluted to 10 ng/ml, added to the wells (100 µl) and allowed to bind for 2 h at room temperature. After incubation, the unbound antibody was removed, the wells were washed three times with PBS and 0.1% Tween 80, and the bound antibody was solubilized with 0.2 M NaOH. The total radioactivity added to each well and the radioactivity from bound antibody was measured on a multisample γ-counter system Packard Minaxi 5500 equipped with a 3'' NaI (Tl) crystal. Immunoreactivity of the antibody was calculated as *bound counts x 100/total counts*. Experiments were repeated three times.

2.8 Cell binding

For the cell binding experiments, MDA MB 231 human breast cancer cells stably transfected with the VEGF-165 isoform were used. These M165 cells overexpressing VEGF-165 were cultured in DMEM supplemented by 10% (v/v) fetal bovine serum (FBS) 100 U/mL penicillin and 100 μg/mL streptomycin. Cells were kept in a controlled humidified atmosphere containing 5% CO_2 at 37°C. On the previous day of the experiment, cells were seeded in 24-well plates and grown to confluency. For the binding experiment, increasing concentrations of the labelled antibody (0.4, 0.8, 2.0, 4.0, and 10.0 nM) were added to each well. Triplicates of each concentration were incubated at 37° C for 60 min. In order to assess specificity of binding, M165 cells in some of the wells were pretreated with an excess of unlabeled bevacizumab (125 μg). The supernatant was then removed, the cells were washed three times with ice-cold PBS, and the bound antibody was solubilized with 0.2 M NaOH. The total radioactivity added to each well and radioactivity from bound antibodies was measured in a gamma counter.

2.9 Biodistribution studies

All animal experiments were performed in compliance with EC Directive 86/609 and its implementation in national legislation (updated version EL 56/2013). Female athymic SCID mice (average weight 20 g, 5 weeks) were obtained from the breeding facilities of the Institute of Biology of the NCSR "Demokritos". The SCID mice were inoculated subcutaneously into the right front leg with M165 cells (1 x 10^7cells/animal) in 100 μL fetal bovine serum-free medium. When tumors reached a size of 0.2 to 1 g (i.e. 10 to 15 days), biodistribution studies were performed. Tumor-bearing mice were injected with 100 μL of ^{95}Nb-Df-bevacizumab [(270 kBq/20 μg or 2.03 TBq/mmol (54.83 mCi/mmol)] *via* the tail vein. Groups of three animals were sacrificed at 1, 2 and 4 days post-injection.

To prove specific binding of the ^{95}Nb-Df-bevacizumab to the tumor, blocking experiments were performed in the tumor-bearing mice. A group of animals was treated with 125-fold excess of the cold bevacizumab (2500 μg /100 μL) and after 24 hours, these animals were injected with 270 kBq/20 μg [2.03 TBq/mmol (54.83 mCi/mmol)] ^{95}Nb-Df-bevacizumab and sacrificed at 4 days after injection of the labelled antibody.

Tumors, tissues and organs (blood, heart, liver, stomach, intestines, spleen, muscle, lungs, pancreas, muscle and bones) were excised, blotted dry and weighed. Samples were measured in a gamma counter (NaI gamma counter, Packard). Standards were prepared from the injected

material and were counted each time simultaneously with the tissues excised, allowing calculations to be corrected for physical decay of the radioisotope. Radiolabelled antibody distribution over time was expressed as injected dose per gram (%ID/g).

3 RESULTS

3.1 Production of ^{95}Nb

^{95}Zr was produced in the ILL high flux reactor at neutron fluxes of 1.5x 10^{15} s-1·cm^{-2} and. 1.0x10^{15} s^{-1}·cm^{-2} respectively. A 7-day irradiation of 356.2 mg of natural Zr produced more than 1.5 GBq ^{95}Zr. The maximum daughter activity of 1 GBq ^{95}Nb generated from ^{95}Zr was obtained at ~67 d after end of irradiation.

3.2 Separation and purification of no-carrier-added ^{95}Nb

The overall separation proceeds with a yield of 95-98% of ^{95}Nb, collected in 400 µL 0.1 M oxalic acid with the whole separation procedure lasting less than one hour. Decontamination after UTEVA purification is 3 x 10^{8} which equals to 0.77 ng of zirconium present in the final fraction for a portion of 260 mg zirconium target.

3.3 Preparation of ^{95}Nb-labeled Df-Bz-NCS-bevacizumab

Labelling kinetics indicate a yield of ≥ 80% already at 15 min, increasing to more than 90% after 50 min. The final labelling yield with ^{95}Nb was ≥ 95% (96% ITLC, 95% HPLC) after 1 hour. After SEC separation on a PD-10 column, the ^{95}Nb-Df-bevacizumab had a radiochemical purity of 99%. The specific activity was 2.03 TBq/mmol (54.83 mCi/ mmol).

3.4 *In vitro* stability

After 7 days of incubation of ^{95}Nb-Df-bevacizumab in NaCl 0.9% solution at 37°C and RT, ≥ 95% (99% HPLC, 97% ITLC) was still detected. Stability testing in fresh human serum at 37°C showed slightly higher product degradation. After 3 days of incubation ≥ 94% (97% HPLC, 94% ITLC) of labelled product was available, while at 7 days ≥ 86% (89% HPLC, 86% ITLC) of the product was still intact.

3.5 Immunoreactivity and cell binding experiments

An immunoreactivity assay was performed to ascertain the biological integrity of the labeled ^{95}Nb-Df-bevacizumab, the result of which is shown in figure 1. For reasons of comparison, the immunoreactivity of ^{99m}Tc labeled bevacizumab is also shown.

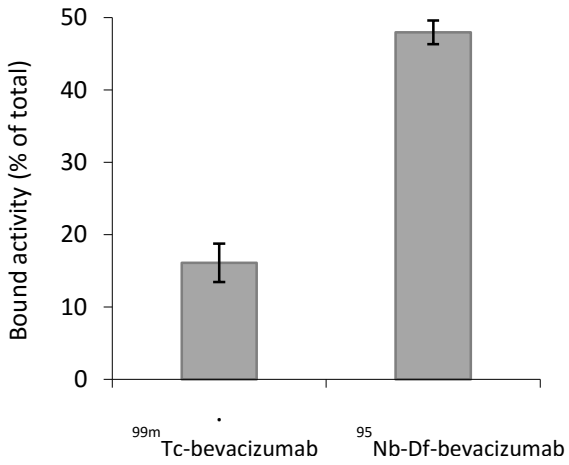

Figure 1: Immunoreactivities of radiolabelled bevacizumab: ^{99m}Tc-bevacizumab (partial reduction of disulfide bonds of antibody), ^{95}Nb-Df-Bevacizumab. Immunoreactivity of the antibody was calculated as bound counts x 100/total counts.

In vitro binding studies performed on M165 cells showed a very low overall percentage of ^{95}Nb-Df-bevacizumab binding, compared to the initially added activity (~ 2%), and the binding of the radiolabeled antibody was diminished when the cells were pretreated with an excess of cold bevacizumab (unblocked *vs* blocked cells). Thus, we are thus led to the conclusion that ^{95}Nb-Df-bevacizumab mainly bound to the secreted VEGF-165, but also showed selectivity for the cell-associated VEGF-165.

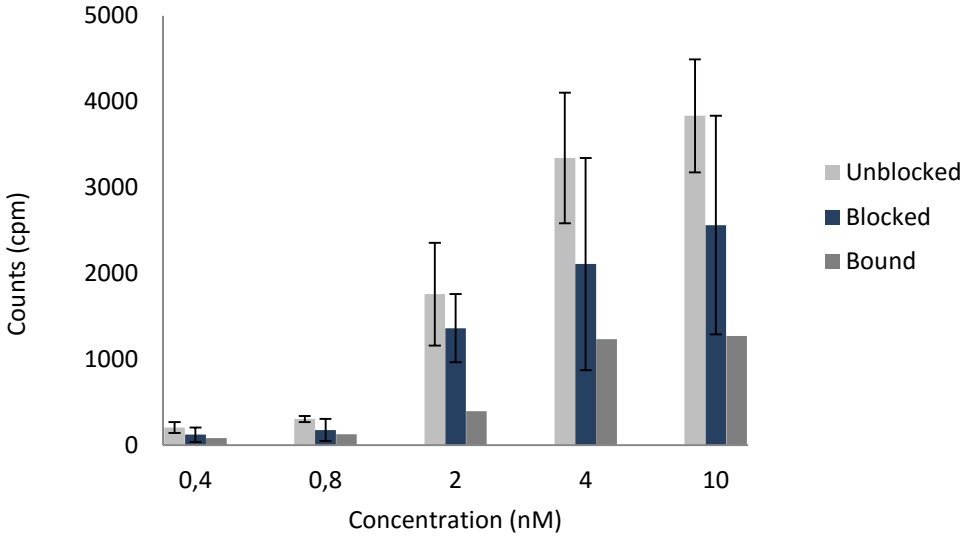

Figure 2: Cell binding studies on M165 cells incubated with increasing concentrations of ^{95}Nb-Df-bevacizumab.

3.6 Biodistribution

Biodistribution of ^{95}Nb-Df-bevacizumab, at an injected dose of 270 kBq/20 µg [2.03 TBq/mmol (54.83 mCi/mmol)] per mouse was performed in tumor-bearing mice (Figure 3). At all time-points, the levels of radiotracer in most tissues (blood, liver, spleen, lungs, heart, stomach, intestines and pancreas) were less than those in the tumor. Tumor uptake showed a decreasing pattern in time (9.42 ± 3.75 %ID/g and 1.21 ± 0.38 %ID/g at 1 and 4 days p.i., respectively), however the tumor-to-blood ratios increased from 1 to 2 days p.i. (3.58 and 5.11 respectively), showing a slight drop at 4 days p.i (4.69) (Table 2).

Table 2: Tumor-to-blood ratios of injected ^{95}Nb-Df-bevacizumab

1 day	2 days	4 days	4-day blocking
3.58	5.11	4.69	1.06

Specificity of tumor targeting was assessed by injecting tumor-bearing mice with an excess of unlabelled bevacizumab, also shown in figure 3. When mice were given unlabeled bevacizumab 1 day prior to ^{95}Nb-Df-bevacizumab and sacrificed 4 days later, the %ID/g in the tumor decreased by ~50 %, compared with unchallenged mice (0.68 ± 0.02 %ID/g *vs* 1.21 ± 0.38 %ID/g respectively). The %ID/g for the other tissues did not decrease, on the contrary, ^{95}Nb-Df-bevacizumab showed a slight increase after pretreatment with unlabelled bevacizumab.

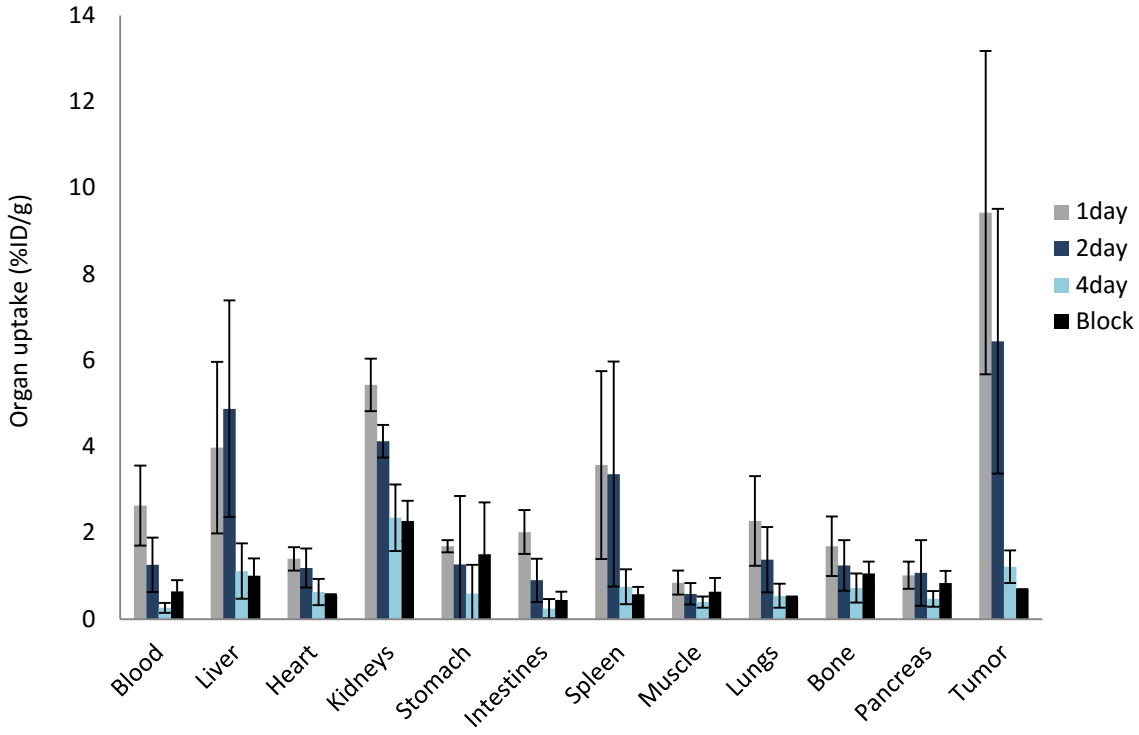

Figure 3: Biodistribution of ^{95}Nb-Df-bevacizumab (270 kBq/20 µg/mouse, [2.03 TBq/mmol (54.83 mCi/mmol) in tumor-bearing mice

4 DISCUSSION

During the past decade a number of antiangiogenic agents such as sorafenib, an inhibitor of several tyrosine protein kinases, and ranibizumab, a monoclonal antibody that inhibits VEGF-A, have been US FDA approved. An important issue that needs our attention is the careful selection of patients that are most likely to respond to a specific antiangiogenic treatment. Nuclear imaging modalities have been explored as a possible way to screen patients for antiangiogenic therapy. Previous groups have demonstrated that radiolabeled bevacizumab accumulates in VEGF-A expressing tumors, and has thus been investigated as a potential SPECT and PET imaging

agent for the selection of patients who are likely to benefit from antiangiogenic therapies [13-16]. More specifically, Nagengast *et al* were the first to report on the noninvasive measurement of VEGF-A levels in the tumor, with ^{111}In- and ^{89}Zr-labeled bevacizumab [13]. Nayak *et al* recently took a step further, by reporting on the radiolabelling of bevacizumab with ^{86}Y for PET imaging of VEGF-A tumor angiogenesis and as a surrogate marker for ^{90}Y-based radioimmunotherapy (RIT), thus introducing a true theranostic agent, with distinct advantages over bevacizumab radiolabeled with ^{111}In and ^{89}Zr, which have been proposed as surrogate markers for ^{90}Y-based RIT [15].

Our focus is on the development of a novel PET imaging agent, namely ^{90}Nb-Df-bevacizumab, by investigating the radiolabelling and *in vitro/in vivo* characteristics of bevacizumab radiolabeled with ^{95}Nb, a convenient alternative for longer-term *ex vivo* biodistribution studies, due to its longer half-life (t ½ = 35 d) and its convenient, lower-cost production (reactor-based production). Apart from its gamma emissions, ^{95}Nb decays by emitting beta particles with 43 keV average energy. Therefore, what we are actually proposing in this work is a theranostic, radioimmunodiagnostic/radioimmunotherapeutic pair, i.e. ^{90}Nb-Df-bevacizumab for PET imaging of VEGF-A tumor angiogenesis and ^{95}Nb-Df-bevacizumab for RIT.

Immunoreactivity studies showed adequate VEGF binding of ^{95}Nb-Df-bevacizumab, thus proving that bevacizumab retained its immunoreactivity post-labelling. In the case of ^{99m}Tc-bevacizumab, the direct method of reducing endogenous disulfide bonds resulted in lower biological activities of the labelled antibody (16.11 ± 2.66 binding efficiency), when compared to the labelling of the antibody with ^{95}Nb *via* the desferrioxamine chelator (47.98 ± 1.62 binding efficiency). The results acquired for ^{95}Nb-Df-bevacizumab were comparable to other reported immunoreactivity data for radiolabeled bevacizumab [13-15]. Cell binding studies on M165 cells showed that ^{95}Nb-Df-bevacizumab bound to the cells, and that binding was decreased when an excess of bevacizumab was added to the cells prior to the addition of the radiotracer.

^{95}Nb-Df-bevacizumab remains intact over a long period. A biodistribution study was performed in tumor-bearing mice injected at 1, 2 and 4 days p.i. [270 kBq/20 µg/mouse, 2.03 TBq/mmol (54.83 mCi/mmol)]. A dramatic decrease in blood pool activity was observed up to 4 days p.i. (2.63 ± 0.93% ID/g at 1 day *vs* 0.26 ± 0.11% ID/g at 4 days). Maximum tumor accumulation was observed at 1 day p.i., with ~ 68% of the radioactivity still present in the tumor at 2 days p.i (9.42 ± 3.75% ID/g *vs* 6.44 ± 3.07% ID/g). While tumor uptake further decreased at 4 days p.i., tumor-to-background ratios increased from 1 to 2 days p.i. (3.58 *vs* 5.11), showing only a slight

decrease at 4 days p.i. (4.69). In all cases, low bone uptake was observed over time, which demonstrates the stability of the ^{95}Nb-Df complex.

Tumor uptake of ^{95}Nb-Df-bevacizumab was lower than that observed with bevacizumab labelled with other isotopes [4, 13, 15, 16] and this may be due to the differences in the available target for the antibody. While bevacizumab has high binding affinity to all VEGF-A isoforms, the M165 cell line used in our experiments overexpresses the VEGF-165 isoform, which is partly cell- and extracellular matrix associated and partly secreted from the cells. This could be the reason for the observed washout from the tumor.

Finally, the use of 20 µg of ^{95}Nb-Df-bevacizumab per mouse for biodistribution studies may have resulted in accelerated and increased clearance of the radiotracer in the absence of IgG production by nude mice [23]. Nonetheless, the tumor-to-blood ratios of our experiments are higher than those that have been shown by other groups.

The pre-injection of an excess of unlabeled bevacizumab prior to ^{95}Nb-Df-Bevacizumab resulted in a significant reduction in tumor uptake (1.22 ± 0.38 %ID/g vs 0.68 ± 0.02 %ID/g), leading to the conclusion, that ^{95}Nb-Df-bevacizumab binds specifically to VEGF *in vivo*. A slight increase in radiotracer uptake in the normal tissues was also observed, which is probably attributable to the fact that unlabeled bevacizumab blocks the available VEGF binding sites in tumors, thus leading to an excess of ^{95}Nb-Df-bevacizumab in the circulation. This is also demonstrated in ^{95}Nb-Df-bevacizumab blood levels of mice injected pretreated with excess antibody, which are significantly higher than in those without excess antibody (0.64 ± 0.24 %ID/g vs 0.26 ± 0.12 %ID/g, respectively) [15, 22].

5 CONCLUSIONS

Obtained data clearly showed excellent labelling, and excellent stability of ^{95}Nb-Df- bevacizumab *in vitro* and *in vivo*. The *Nb/Zr separation chemistry developed should allow the synthesis of ^{90}Nb-Df-bevacizumab following the ^{90}Zr(p,n) production. This PET tracer will be used to reproduce the promising results shown here with ^{95}Nb-Df-bevacizumab and to further validate its potential for application in *immuno*-PET. In conclusion, we believe that ^{90}Nb-Df-bevacizumab would be a valuable tool not only for the selection of patients most likely to benefit from antiangiogenic therapies targeting VEGF-A, but also for the selection of appropriate candidates to undergo ^{95}Nb-RIT.

ACKNOWLEDGMENTS

The authors gratefully acknowledge financial support from the COST Actions TD1004 (Theranostics Imaging and Therapy: An Action to Develop Novel Nanosized Systems for Imaging-Guided Drug Delivery) and D38 (Metal-Based Systems for Molecular Imaging Applications), the Program for the Promotion of the Exchange and Scientific Cooperation between Greece and Germany IKYDA 2013 (Contract No. 205), the People Program (Marie Curie Actions) of the European Union's seventh Framework Program (FP7/2007-2013) under REA grant agreement no.PITN-GA-2012-317019 'Trace'n Treat', and the Deutsche Forschungsgemeinschaft (DFG) under grant DFG Ro 985/40 – 1. Acknowledgements are also due to Mr. Stavros Xanthopoulos, for technical assistance. We also acknowledge the reactor teams of BER2 Berlin and TRIGA Mainz where irradiations for preparatory experiments had been performed and the reactor team of ILL Grenoble for producing the ^{95}Zr/^{95}Nb activity used in the present work.

REFERENCES

[1] Van Dongen GA, Visser GWM., Lub-de Hooge MN, de Vries EG, Perk LR. Immuno-PET: A Navigator in Monoclonal Antibody Development and Applications. *Oncologist* 2007; 12: 1379–1389.

[2] Tolmachev V. Radiobromine-labelled tracers for positron emission tomography: possibilities and pitfalls. *Curr Radiopharm* 2011; 4: 76-89.

[3] Nayak TK, Brechbiel MW. ^{86}Y based PET radiopharmaceuticals: radiochemistry and biological applications. *Med Chem* 2011; 7: 380-388.

[4] Chang AJ, Sohn R, Lu ZH, Arbeit JM, Lapi SE. Detection of rapalog-mediated therapeutic response in renal cancer xenografts using ^{64}Cu-bevacizumab immunoPET. *PLoS ONE* 2013; 8:e58949

[5] Vugts DJ, Visser GW, van Dongen GA. ^{89}Zr-PET radiochemistry in the development and application of therapeutic monoclonal antibodies and other biologicals. *Curr Top Med Chem* 2013; 13: 446-457.

[6] Verel IMS, Visser GWM, Boellaard R., Stigter-van Walsum M, Snow GB, van Dongen, GA. ^{89}Zr Immuno-PET: Comprehensive procedures for the production of ^{89}Zr-labeled monoclonal antibodies. *J Nucl Med* 2013; 44: 1271–1281.

[7] Severin GW, Engle JW, Barnhart TE, Nickles RJ. ^{89}Zr radiochemistry for positron emission tomography. *Med Chem* 2011; 7: 389-394.

[8] Chacko AM, Li C, Nayak M, Mikitsh JL, Hu J, Hou C, et al. Development of ^{124}I immuno-PET targeting tumor vascular TEM1/endosialin. *J Nucl Med* 2014; 55: 500-507.

[9] Radchenko V, Hauser H, Eisenhut M., Vugts JD, van Dongen GA, Roesch F. ^{90}Nb – a Potential PET Nuclide: production and labeling of monoclonal antibodies. Radiochim Acta 2012; 100: 857-864.

[10] Radchenko V, Bouziotis P, Tsotakos T, Paravatou-Petsotas M., de la Fuente A, Loudos G, et al. Labeling and preliminary in vivo assessment of Niobium-labeled radioactive species: a proof-of-concept study. *Nucl Med Bio* 2016; 43: 280-287.

[11] Busse S, Rösch F, Qaim SM. Cross section data for the production of the positron emitting niobium isotope ^{90}Nb via the ^{90}Zr (p, n)-reaction. *Radiochim Acta* 2002; 90:1-5.

[12] Busse S, Brockmann J, Roesch F. Radiochemical separation of no-carrier-added radioniobium from zirconium targets for application of ^{90}Nb-labelled compounds. *Radiochim Acta* 2002; 90: 411-415.

[13] Nagengast WB, de Vries EG, Hospers GA, Mulder NH, de Jong JR., Hollema H, et al. In vivo VEGF imaging with radiolabeled bevacizumab in a human ovarian tumor xenograft. *J Nucl Med* 2007; 48: 1313–1319.

[14] Nagengast WB, de Korte MA, Oude Munnink TH, Timmer-Bosscha H, den Dunnen WF, Hollema H, et al. ^{89}Zr-bevacizumab PET of early antiangiogenic tumor response to treatment with HSP90 inhibitor NVP-AUY922. J Nucl Med 2010;51:761–767.

[15] Nayak TK, Garmestani K, Baidoo KE, Milenic DE, Brechbiel MW. PET imaging of tumor angiogenesis in mice with Vegf-A-targeted ^{86}Y-chx-a”-dtpa-bevacizumab. *Int J Cancer* 2011; 128: 920–926.

[16] Stollman TH, Scheer MGW, Leenders WPJ. Specific imaging of VEGF-A expression with radiolabeled anti-VEGF monoclonal antibody. *Int J Cancer* 2008; 122: 2310–2314.

[17] Ferrara N, Hillan KJ, Novotny W. Bevacizumab (Avastin), a humanized anti-VEGF monoclonal antibody for cancer therapy. *Biochem Biophy Res Commun* 2005; 333: 328–335.

[18] Jayson GC, Kerbel R, Ellis LM, Harris AL. Antiangiogenic therapy in oncology: current status and future directions. 2016 doi: 10.1016/ S0140-6736(15)01088-0.

[19] Stollman TH, Scheer MG, Franssen GM., Verrijp KN, Oyen WJ, Ruers TJ, et al. Tumor accumulation of radiolabeled bevacizumab due to targeting of cell- and matrix-associated VEGF-A isoforms. *Cancer Biother Radiopharm* 2009; 24: 195-200.

[20] Radchenko V, Busse S, Roesch F. Desferrioxamine as an appropriate chelator for ^{90}Nb: Comparison of its complexation properties for M-Df-Octreotide (M=Nb, Fe, Ga, Zr). *Nucl Med Biol* 2014; 41: 721–727.

[21] Vosjan MJ, Perk LR., Visser GW, Budde M, Jurek P, Kiefer GE, van Dongen GA. Conjugation and radiolabeling of monoclonal antibodies with zirconium-89 for PET imaging using the bifunctional chelate p-isothiocyanatobenzyl-desferrioxamine. *Nat. Protocols* 2010; 5: 739–743.

[22] Collingridge DR, Carroll VA, Glaser M, Agoagye EO, Osman S, Hutchinson, OC, Barthel H, et al. The development of [^{124}I]Iodinated-VG76e: A novel tracer for imaging vascular endothelial growth factor in vivo using positron emission tomography. *Cancer Res* 2002; 62: 5912-5919.

[23] Sharkey RM, Natale A, Goldenberg DM, Mattes MJ. Rapid blood clearance of immunoglobulin G2a and immunoglobulin G2b in nude mice. *Cancer Res* 1991; 51: 3102-3107.

4 SUMMARY, CONCLUSIONS AND FUTURE PERSPECTIVES

4.1 Optimization of HPMA based nanoparticles for theranostic applications.

One of the major problems in current chemotherapy is the lack of selectivity of the utilized anticancer drugs. The therapeutic index of a drug can be improved by increasing the accumulation at the target site. In this context, HPMA-based polymers came under focus of drug development as drug carrier systems due to their biocompatibility and possible multifunctionality as well as their capacity to accumulate in tumor tissue by means of the EPR effect [1].

To benefit of these advantages and bring them to the field of nuclear medicine, different HPMA polymers have been investigated to serve as imaging or therapeutical agents. By combining both HPMA nanoparticles and nuclear medicine a powerful theranostic tool can be accomplished.

In nuclear medicine, both metal and organic radioisotopes can be employed. Radiometals offer the advantage of providing higher radiolabelling yields in contrast to organic isotopes. In addition some radiometals with application in nuclear medicine are easy available *via* generators. However, the labelling of nanoparticles with a radiometal requires of a bifunctional chelate that is previously attached to the nanoparticle, and the modification of nanoparticles with chelates may alter their biological functions.

Part of this work aimed to achieve quantitative radiolabelling yields by modifying as less as possible different HPMA-based nanocarriers. Labelling and stability results of several synthetized HPMA-linker-DOTA systems show that: alkane chains are more suitable than alkoxy chains to serve as linker structures, shorter linker lengths provide faster labelling kinetics and only a minimum amount of 1.6 % of DOTA is enough to achieve quantitative yields after 20 minutes incubation at 95 °C (Tab.1). Stability in different media was ensured after 2 h incubation at 37 °C.

Table 1: Description of HPMA-DOTA conjugate 31c

Characteristics		Organic synthesis	
Name	31c	RCY linker	~60%
n	2		
% DOTA	1.6	Polymer-linker	~25%
Structure		^{68}Ga Radiolabelling	
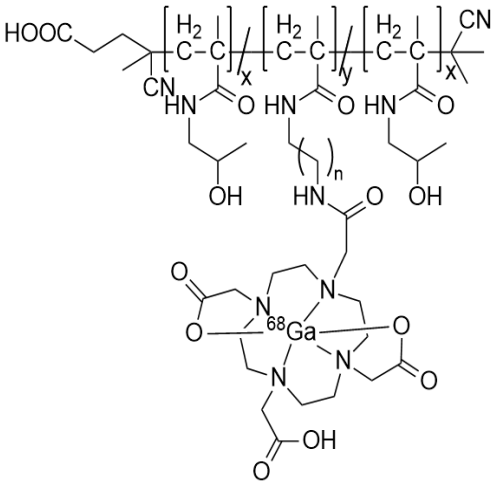		nmol	20
		time	20 min
		T	95°C
		RCY	>95%
		Stability after 2 h	
		NaCl 0.9%	98 ± 1
		HS	95 ± 2
		DTPA	83 ± 1
		EDTA	92 ± 5
		Ca^{2+}	92 ± 5
		Fe^{3+}	94 ± 3
		Mg^{2+}	92 ± 1

An initial proof-of-principle *in vivo* evaluation in tumor-bearing rat with the ^{68}Ga-labeled HPMA-DOTA conjugate 31 (11% DOTA, alkane linker of 12 carbons lengh) has been carried out (Fig. 2) [2]. Accumulation in tumor site was observed by means of EPR effect, however further *in vivo* experiments need to be performed for a better evaluation of the HPMA-based polymers modified with DOTA, particulary for the conjugate 31c (1.6% DOTA, alkane linker of 2 carbons lengh).

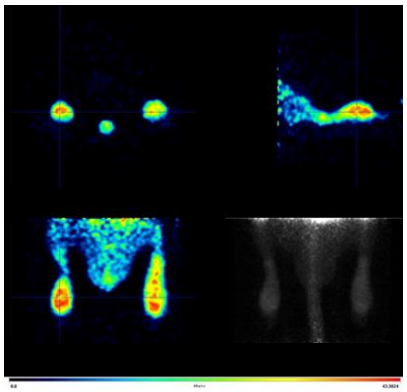

Figure 2: First PET image of ^{68}Ga-DOTA-HPMA 31 after 120 min p.i in tumor bearing rat (walker Mamma carcinoma) [2].

Another approach to minimize the modification of the carrier for its labelling with radiometals exploits the inherent ability of micelles to incorporate into their core hydrophobic substances. Hydrophobic ^{68}Ga-oxine complex was spontaneously introduced in the micellar nucleus of three different structures of HPMA-based unimers. Block architectures showed higher entrapment of ^{68}Ga-oxine and higher stability in contrast to the random architecture. Such results are attributed to a well defined structure of the block polymers that decreases the possibility to present hydrophobic moieties in the corona [3]. The values were improved when PEG moieties were added to the block copolymer. The highly hydrophilic PEG segments decrease aggregate size by increasing steric stabilization, fact that would explain their higher stability *in vitro* [4].

The successful labelling efficiency of the PEGylated-block micelles as well as their *in vitro* stability in NaCl 0.9% and serum (Fig. 2) led to their *ex vivo* evaluation in healthy mice, using ^{111}In-oxine as ^{68}Ga-oxine analogue due to its longer half-life, allowing for investigations for a longer frame-time.

In spite of the high stability *in vitro*, *in vivo* stability was not ensured. *Ex vivo* biodistribution results of the labelled micelles were quite similar to the values of the free ^{111}In-oxine injected as a control. This fact suggests a low stability of the micelles and the later blood metabolite studies confirmed such instability. After 1 h p.i only 30.1% ± 1.9 remained still intact. This value decreased after 4 h to 21.1% ± 1.4 and after 24 h p.i to 15.1% ± 1.5.

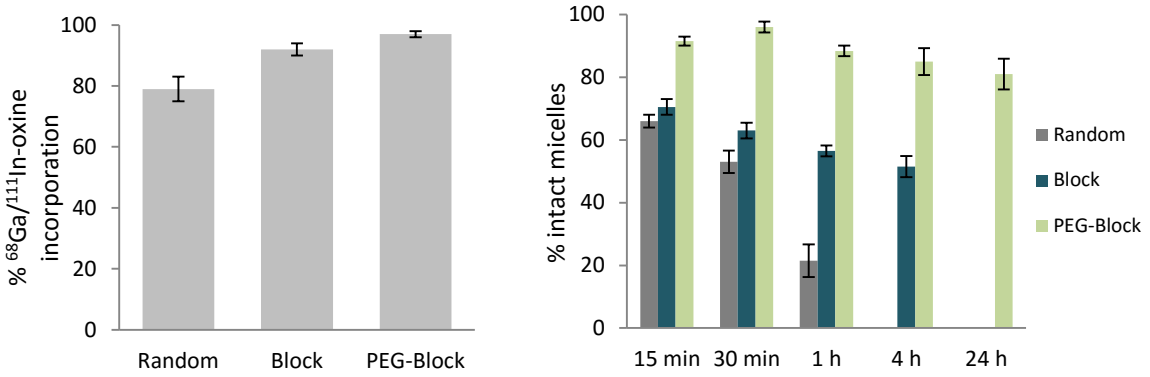

Figure 3: Left: % incorporation of ^{68}Ga/^{111}In-oxine in different polymer architecures (n=3). Right: Stability of the different labelled micelles in HS (n=3)

In order to be able to apply this efficient and fast technique for radiolabelling micelles, the *in vivo* stability needs to be imporved. An approach that could increment the stability would be to cross-link the micelles after incorporation of the hydrophobic complex. A number of core cross linked polymeric micelles have demonstrated promising efficacy in animal models preventing premature disintegration [5].

4.2 ^{44}Sc-PSMA-617 for dosimetry of prostate cancer

In the field of nuclear medicine, emerging treatments against prostate cancer have given rise to PSMA-617, a novel DOTA derivative of the Glu-urea-Lys motif. PSMA-617 has been labelled with the PET nuclide ^{68}Ga (t ½ = 68 min) and the therapeutic ^{177}Lu (t ½ = 6.7 d) showing beneficial results in the clinics. Nowadays, PSMA-617 is a powerful theranostic tracer for prostate cancer.

Besides the positive results obtained with ^{68}Ga-PSMA-617, in addition to the great interest in nuclear medicine for ^{68}Ga due to its favourable decay characteristics for PET imaging and its availability *via* generator, its short half-life limits its application. This is an important drawback on the way to personalized medicine, as dosimetry evaluation with ^{68}Ga can only be assessed during few hours post injection.

In this context, the PET nuclide ^{44}Sc with a half-life of 3.97 hours and being also generator produced is a great alternative to overcome the limitation presented by ^{68}Ga. ^{44}Sc decay characteristics (high β^+ branching of 94%, $\bar{E}$ = 0.6 MeV) provide high quality PET images and like ^{68}Ga forms stable complexes with the DOTA chelate. Such aspects have motivated the present work.

PSMA-617 has been quantitatively (>95%) labelled with ^{44}Sc obtained from ^{44}Ti/^{44}Sc generator within 20 minutes at 95^{o}C. A minimum amount of 18 nmol of precursor is needed to ensure efficient labelling, amounts <18 nmol lowered the yields. After removal of trace amounts of un-reacted ^{44}Sc by reverse-phase chromatography, *in vitro* stability evaluation was carried out with high purity product (>99 %). The radiopharmaceutical presented high stability in human serum and saline as well as in presence of an excess of competing cations and chelates that could induce transmetallation *in vivo*.

Considering that the effectiveness of a drug depends on its affinity to the substrate, a ligand binging assay on LNCaP cells was also performed. The value of the inhibitory constant obtained is in the nanomolar range, which demonstrates a high affinity of ^{44}Sc-PSMA-617 to the prostate carcinoma cells. In addition, in a parallel experiment, efficient internalization on the same cell line was revealed, the results obtained are comparable to the values of the ^{68}Ga- and ^{177}Lu-labelled PSMA-617 (Tab.2).

Table 2: Affinity constant and internalization values of ^{44}Sc-, ^{68}Ga-, ^{177}Lu-labelled PSMA-617 compounds. Same set up was used for the three compounds [6].

	K_i ± SD	Internalization ± SD
^{44}Sc	4.72 ± 0.78	15.78 ± 2.14
^{68}Ga	6.40 ± 1.02	17.67 ± 4.35
^{177}Lu	6.91 ± 1.32	17.51 ± 3.10

Finally, evaluation of ^{44}Sc-PSMA-617 in a patient suffering from prostate cancer was performed (Fig.4). ^{44}Sc-PSMA-617 revealed high *in vivo* stability and pharmacological parameters adequate to long-term (up to one day) molecular imaging. Initial human studies hold promise for a diagnostic application and dosimetric calculations.

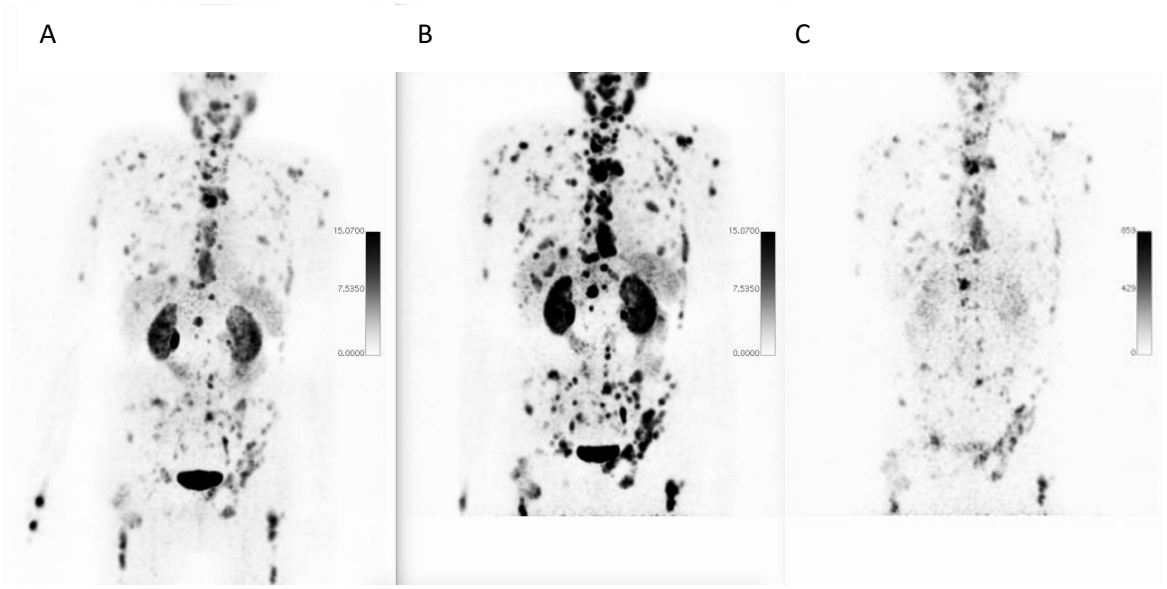

Figure 4: ^{44}Sc-PSMA-617 PET/CT imaging (55.76 MBq Injected) of PSMA receptor positive metastases after A) 30 min p.i, B) 2h p.i and C) 19 h p.i (Department of Nuclear Medicine, Uniklinikum Bonn, Germany).

4.3 Evaluation of ^{90}Nb as potential PET isotope

The advantages offered by PET over other imaging techniques have promoted the development of a big array of imaging agents. In spite of this expansion, the quantity of radionuclides with intermediate half-life, required for molecules with long pharmacokinetics such as antibodies, and with suitable decay parameters for PET imaging is small. Current options are: ^{76}Br (t ½ = 16.0 h) ^{86}Y (t ½ = 14.7 h) and ^{64}Cu (t ½ = 12.7 h). ^{86}Y and ^{64}Cu present low positron branching and low mean E_{β^+}; ^{86}Y (33% and 0.21 MeV) for ^{64}Cu (17.8%, 0.05 MeV). The proposed ^{90}Nb (t ½ = 14.6 h) has a β^+ branching of 53%, which is comparable to ^{76}Br (56 %) and a mean E_{β^+} of 0.35 MeV, which is higher than the values of ^{86}Y and ^{64}Cu, but sufficiently less than that of ^{76}Br (0.64 MeV). All these nuclides are produced by proton bombardment on low-energy cyclotrons (< 20 MeV,) and contrary to the mentioned nuclides, ^{90}Nb obtention does not requires an enriched target for irradiation.

These superior characteristics over present PET nuclides with capacity to image for several hours have motivated investigations on ^{90}Nb for its application in nuclear medicine.

Studies involving production route of ^{90}Nb, separation strategies to provide a high purity product in conditions suitable for labelling as well as its coordination chemistry have been developed in our working group [7-9]. All the above mentioned decay parameters as well as the positive results obtained in production, separation and labelling chemistry, allow to confirm that ^{90}Nb holds promise as a PET and gave reason to continue our study with *in vivo* evaluation of ^{90}Nb-labelled biomolecules for *immuno*-PET applications.

In this work, ^{95}Nb (t ½ = 35 d) has also been employed for biodistribution experiments to cover longer periods. Irradiation of a Zr natural target with neutrons afforded ^{95}Zr that *via* β^- decay to the desired ^{95}Nb.

The radiolabelling chemistry of $^*Nb^V$ appears to be quite similar to $^*Zr^{IV}$ therefore the removal of Zr of the irradiated target is essential. A high decontamination factor is crucial, because zirconium also creates very stable complexes with desferrioxamine and competes with niobium, affecting labelling efficiency. A multistep separation that includes both cation and anion exchangers and different acidic solutions afforded within 1.5 h, no carrier-added $^{90/95}$Nb in 500 µL of 1 M oxalic acid solution with a c.a 95% recovery and in high purity (decontamination factor of $3 \cdot 10^8$). Such conditions are suitable for further radiolabelling.

Desferroxamine (Df) has demonstrated to be the most apt chelate for complexation of niobium as it showed fast kinetics of complex formation and high stability, consequently the mAbs used were modified with Df. Labelling of mAb-Df was performed in PBS at pH of c.a 7, at RT and for 1 hour and >95% of radiolabelling yield was achieved. Purification through size exclusion column afforded pure *Nb-labelled antibody in NaCl 0.9 % solution (Fig.5).

$^{90/95}$Nb labelled bevacizumab presented excellent *in vitro* stability in saline as well in human serum albumin (HSA) at RT and 37°C. After 7 days incubation in saline less of 5% of product degradation was detected and more than 85% of product was detected in HSA.

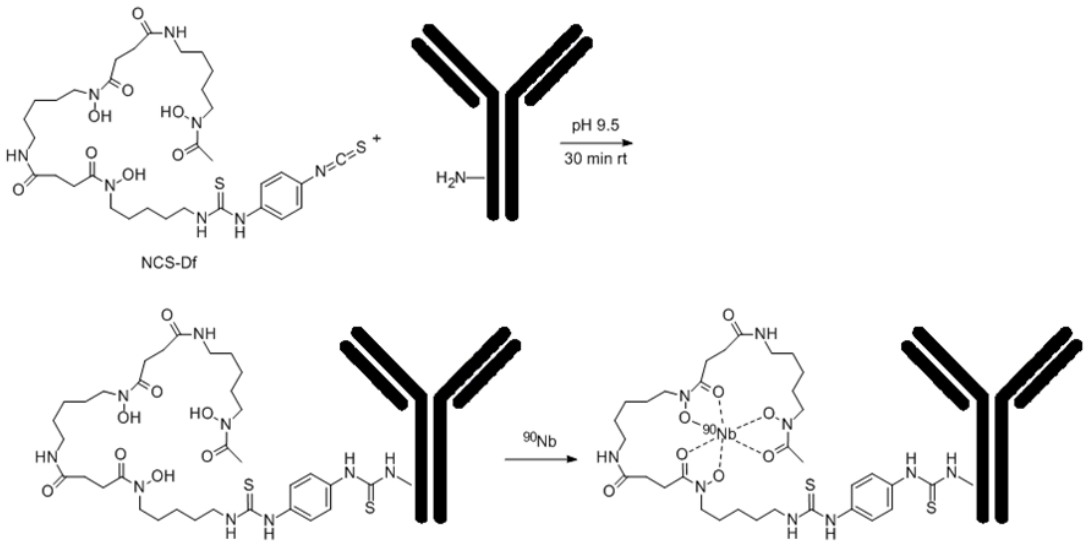

Figure 5: Df-conjugation of the mAb *via* NCS-Bz-Df and labeling with $^{95/90}$Nb

Initial *ex vivo* experiments with ^{95}Nb-Df-bevacizumab showed adequate tumor uptake, however at the same time high uptake in the liver, spleen and kidneys was observed. In order to investigate whether this behaviour is due to instability of *Nb-Df-bevacizumab and consequent creation of other *Nb species *in vivo*, biodistribution studies of ^{95}Nb-oxalate, ^{95}Nb-chloride and ^{95}Nb-Df were performed. These potential metabolite species did not show any specific uptake, apart from bone accumulation for ^{95}Nb-oxalate and ^{95}Nb-chloride, which, interestingly, may serve as an indicator for the release of *Nb from labelled biomolecules.

A second biodistribution evaluation in healthy mice was performed with a high specific activity product. Results did not show increased uptake in liver, spleen or kidneys (< 5% at 1 day p.i) and higher uptake was detected in blood and lungs.

Final *ex vivo* evaluation in tumor bearing mice presented high accumulation in tumor tissue at the same time than lower values for other organs (liver, lungs, spleen) (Fig.6). Despite that the tumor uptake showed a decreasing pattern in time, the tumor-to-blood ratios increased from 1 to 2 days p.i. expressed a slight drop at 4 days p.i.

^{90}Nb holds promise on its application in *immuno*-PET, however the popularity of ^{89}Zr, with suitable decay characteristics for PET imaging (t ½ = 3.27 d; 23 % β^+, mean E_{β^+} 0.39 MeV) and the commercially availability of GMP-compliant ^{89}Zr lowers the cost and reduces time of obtention, this fact could difficult the application of ^{90}Nb as PET nuclide.

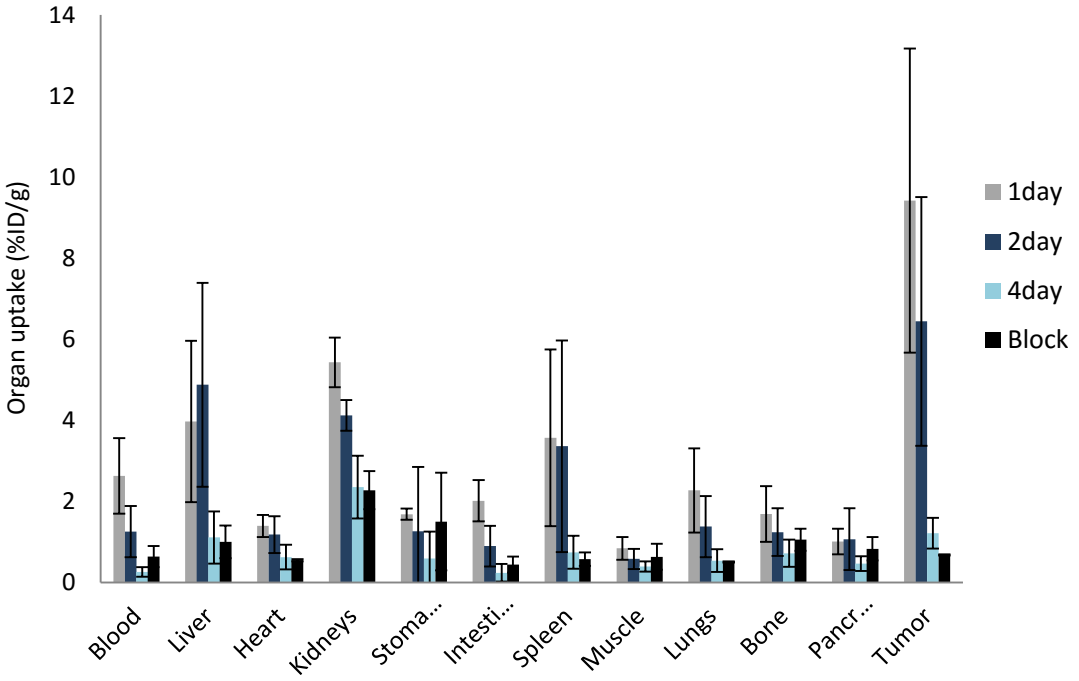

Figure 6: Biodistribution of 95Nb-Df-bevacizumab (270 kBq/20 µg/mouse, [2.03 TBq/mmol (54.83 mCi/mmol) in tumor-bearing mice

REFERENCES

[1] Tamargo J, Le Heuzey JV, Mabo P. Narrow therapeutic index drugs: a clinical pharmacological consideration to flecainide. *Eur J Clin Pharmacol* **2015**; 71: 549–567.

[2] Eppard E. PhD thesis, Johannes Gutenberg-Universität, Mainz, **2013**, 189 pp.

[3] Gaucher G, Dufresne MH, Sant VP, Kang N, Maysinger D, Leroux JC. Block copolymer micelles: preparation, characterization and application in drug delivery. *J Control Release* **2005;** 109; 169–188.

[4] Allmeroth M, Moderegger D, Gündel D, Buchholz HG, Mohr N, Koynov K, Rösch F, Thews O, Zentel R. PEGylation of HPMA-based block copolymers enhances tumor accumulation in vivo: A quantitative study using radiolabeling and positron emission tomography. *J Control Release* **2013;** 172: 77–85.

[5] Talellia M, Barz M, Rijckend CJF, Kiesslinge F, Henninka WE, Lammers T. Core-crosslinked polymeric micelles: Principles, preparation, biomedical applications and clinical translation. *Nano Today* **2015;** 10: 93—117.

[6] Benesova M, *et al*. Preclinical Evaluation of a Tailor-Made DOTA-Conjugated PSMA Inhibitor with Optimized Linker Moiety for Imaging and Endoradiotherapy of Prostate Cancer. J *Nucl Med* **2015**; 56: 914-920.

[7] Busse S, Rösch F, Qaim SM. Cross section data for the production of the positron emitting niobium isotope ^{90}Nb via the ^{90}Zr (p, n)-reaction. *Radiochim Acta* 2002; 90:1-5.

[8] Busse S, Brockmann J, Roesch F. Radiochemical separation of no-carrier-added radioniobium from zirconium targets for application of ^{90}Nb-labelled compounds. *Radiochim Acta* 2002; 90: 411-415.

[9] Radchenko V, Busse S, Roesch F. Desferrioxamine as an appropriate chelator for ^{90}Nb: Comparison of its complexation properties for M-Df-Octreotide (M = Nb, Fe, Ga, Zr). *Nucl Med Biol* 2014; 41: 721–727.

5 OUTLOOK

The application of radiometals in nuclear medicine is of growing utilization both in diagnostic and therapeutic radiopharmaceuticals due to their diversity in chemical and nuclear properties. The large amount of pathlogies and the need of personalized treatments ask for different diagnostic and therapeutic radiopharmaceuticals.

Nanomaterials have become under focus of drug development as with multiple functionalities could be used for both diagnosis and therapy. Among them, polymeric materials play a key role due to their high biocompatibility, biodegradability and structural diversity. In this work systematic studies on the influence of the linker structures and the degree of occupancy of chelator in HPMA-based unimers, as well as a novel startegy for radiolabelling HPMA-based micelles have been carried out. Such studies aimed to minimize the modification needed to achieve quantitative radiolabelling yields and consecuently diminish the alteration of the biomolecule. *In vivo* studies were performed, however further evaluations are needed.

The contineous development of new drug delivery systems for nuclear medicine have increased the demand of radioisotopes to better match the different pharmacokinetics. In this context, ^{44}Sc has been evaluated as an alternative to the short-lived ^{68}Ga for PET imaging of prostate cancer lesions showing successful results in a first human patient. Its longer half-life allows for longer-term evaluation, thus being more suitable for dosimetric calculations of therapeutic analogs of ^{177} Lu and therefore obtain a better plan for personalized medicine.

^{90}Nb has also been studied as a novel nuclide for *immuno*-PET. Its half-life of 14.6 h makes it suitable for imaging of biomolecules with intermediate and long half-lifes, such as antbodies or antibody fragments. Radiolabelling of mAb with Nb isotopes has been investigated and first *in vivo* evaluations in healthy and tumor bearing mice were performed. Reults have shown a high potential for application of ^{90}Nb in *immuno*-PET.

List of abbreviations

$^{1}_{0}\mathrm{n}$	Neutron
$^{1}_{0}\beta^{+}$	Positron
$^{1}_{1}\mathrm{p}$	Proton
µm	micrometer
$^{0}_{0}\nu_{\mathrm{e}}$	electron-neutrino
a	year *(annus)*
A	activity
AAZTA-5	6-amino-6-methylperhydro-1,4-diazepine tetraacetic acid
Bq	Bequerel
c.a	around *(circa)*
$CDCl_3$	deuterated chloroform
CEX	Cation exchange resin
d	day
DMSO	diethyl sulfoxide
DOTA	1,4,7,10-tetraazacyclododecane - 1,4,7,10-tetraacetic acid
DOTATOC	DOTA-Phe(1)-Tyr(3) octreotide
DTPA	diethylene-triamine pentaacetic acid
e.g	for example (*exempli gratia)*
g	gram
h	hour
$H_2C_2O_4$	Oxalic acid
HCl	Hydrochloric acid
HBED	N,N'-Bis(2-hydroxybenzyl) ethylenediamine
HMPAO	hexamethyl propylene amine oxime
HPLC	High Pressure Liquid Chromatography
Hz	Herz
i.e	for example (*id est*)
i.v.	intra venous
kDa	kilodalton
keV	kiloelectronvolt
mAb	monoclonal antibody
max.	maximum
M	molarity
Mn	Number average molar mass
Mw	Molecular weight
MBq	Megabequerel
mCi	milicurie
MeV	Megaelectron Volt
min	minute
NaCl	sodium chloride
NMR	Nuclear Magnetic Resonance
ran	random
PDI	polydispersity index
p.i.	post injection
Ps	Positronium
PSMA	Prostate specific membrane antigen
RCY	Radiochemical yield
TLC	Thin Layer Chromatography